Analysing the Molecular Mechanisms of Cell Migration Inhibition in Response to Honokiol

YING LEI

A thesis submitted in partial fulfilment of the requirements of Edinburgh Napier University, for the award of Master by Research.

August 2021

Declaration

I declare that:

- This thesis has not been submitted for any other degree or professional qualification.
- The thesis is the result of my own independent work.

YING LEI

Abstract

Malignant melanoma is the leading cause of skin cancer-induced death worldwide. Current therapies for treating melanoma patients are limited by rapid resistance to treatments and thus alternative anti-cancer drugs with high efficiency are urgently required. Honokiol is a natural compound isolated from the *Magnoliaceae* family with potent anti-cancer effects. However, the exact molecular mechanisms underpinning the anti-cancer effects of honokiol remain poorly defined. This study demonstrated that honokiol reduced cell viability, affected metabolic activities, inhibited cellular migration, promoted apoptotic effects and induced morphological alterations in the highly metastatic melanoma cell line, A375. Comprehensive qRT-PCR and immunoblotting analyses indicated that honokiol upregulated the expression of kisspeptin (*KISS1*) and its receptor, *KISS1R*, suggesting that KISS1 / KISS1R signalling pathway might be one of the molecular mechanisms targeted by honokiol. This study further revealed that honokiol-mediated KISS1 / KISS1R signalling pathway downregulated *VEGF-A* and *MMP-2* transcription, upregulated the mRNA expression of *MMP-9* and *TIMP-4*, but not *NF-κB*. Furthermore, treatment with kisspeptin 10, with or without honokiol has been demonstrated to alter the mRNA expression of *KISS1, KISS1R, MMP-9, MMP-2, TIMP-4* and *VEGF-A*, but not *NF-κB*. This study suggests that KISS1 / KISS1R signalling pathway may be involved in honokiol-modulated anti-metastatic effects in human A375 melanoma cells, and that honokiol could be considered as a natural agent against skin cancer.

Acknowledgement

I am very grateful that the Peter KK Lee Postgraduate Scholarships funded my oversea tuition fees to allow me to study my Master by Research degree at the Edinburgh Napier University. I am very grateful to technical staff, research students and post-doctoral staff in the Biomedical Research Laboratory (3C.16). All of you have offered me the best and the most unforgettable study experience in my overseas study life. Without all the smiley face, happiness, inspiration, support and encouragement from all of you, I would have struggled to tell myself: let's try the experiment again, after I did a lot of troubleshooting and it still did not work. Thanks to all of you, this has offered me the most fantastic Master by Research study experience at the Edinburgh Napier University. Thanks for Dr. Sharron Vass and Dr. Amy Poole, my first and second supervisors, to always encourage me when my PhD applications are rejected so many times. Thank you for all the patience to support my research study and offer reference letter to my applications. Particularly, thanks for first supervisor, Dr Sharron Vass, for spending a lot of time and efforts to teach me the research technologies and academic knowledge, help me to develop research skills, and train me as an independent research student.

Thank you so much, my mum, dad and sister for everything.

Lastly but most importantly, thank you so much for the Edinburgh Napier University to train me from naive student to be a research student, offering me this next step to closer to my academic target.

Words cannot express all my appreciations, but still:

THANK YOU SO MUCH.

Table of contents

List of tables

List of figures

List of abbreviations

Ab	Absorbance
ATP	Adenosine Triphosphate
AMP	Adenosine Monophosphate
AMPK	Adenosine Monophosphate Activated Protein Kinase
Akt	Protein kinase B
AP-1	Activator Protein 1
α-Tubulin	Alpha Tubulin
BRAF	v-Raf murine sarcoma viral oncogene homolog B
bp	Base Pair
Ca^{2+}	Calcium
cDNA	Complementary Deoxyribonucleic Acid
CD200	OX-2 Membrane Glycoprotein
CEACAM1	Carcinoembryonic Antigen Related Cell Adhesion Molecule 1
Cdc	Cell Division Cycle Protein
DMEM	Dulbecco's Modified Eagle Medium
DMSO	Dimethyl Sulfoxide
DNA	Deoxyribonucleic Acid
DTT	Dithiothreitol
ECM	Extracellular Matrix
EGFR	Epidermal Growth Factor Receptors
EGF	Epidermal Growth Factor
ERK	Extracellular Signal-Regulated Kinase
EMT	Epithelial Mesenchymal Transition
EDTA	Ethylenediaminetetraacetic Acid
E2F	E2 Transcription Factor

ERα	Estrogen Receptor Alpha
FA	Focal Adhesion
FAKs	Focal Adhesion Kinases
FASL	FAS Ligand
FBS	Fetal Bovine Serum
FGF	Fibroblast Growth Factor
FITC	Fluorescein Isothiocyanate
GPR54	G Protein-Coupled Receptor 54
GTP	Guanosine Triphosphate
GDP	Guanosine Disphosphate
GRO-α	Growth-Related Oncogene α
GFP	Green Fluorescent Protein
HNK	Honokiol
HLA	Human Leukocyte Antigen
HDAC	Histone Deacetylase
Hsp	Heat Shock Proteins
HUVEC	Human umbilical vein endothelial cell
IP3	Inositol 1,4,5-Triphosphate
IDO	Indoleamine 2, 3 Dioxygenases
IL	Interleukin
IKK	Inhibitor of Nuclear Factor kappa B Kinase
IκBα	Inhibitor of Nuclear Factor kappa B
JAK	Janus Kinase
JNK	c-Jun N-terminal kinase
Kps	Kisspeptins
kDa	Kilodalton

LKB1	Master Kinase Liver Kinases B1
MAPKs	Mitogen-Activated Protein Kinases
MKK	Mitogen-Activated Protein Kinases
MEK	Mitogen-Activated Protein Kinases
MIF	Macrophage Migration Inhibitory Factor
mTOR	Mammalian Target of Rapamycin Serine/Threonine
MCP1	Monocyte Chemoattractant Protein 1
MMP	Matrix Metallopeptidase
MW	Molecular Weight
MT1-MMP	Membrane Type 1 - Matrix Metalloproteinase
NM	Nanometre
NaCl	Sodium Chloride
NTC	Non-Treated Control
NF-κB	Nuclear Factor kappa B
NK	Natural Killer
p70S6K1	p70 kDa Ribosomal Protein S6 Kinase 1
PIP2	Phosphatidylinositol-4,5-Bisphosphate
PI3K	Phosphatidylinositol-3-Kinase
p38	Stress Activated Protein Kinases
PGE2	Prostaglandin E2
PSG	Pregnancy-Specific Glycoprotein
PIGF	Phosphatidylinositol Glycan Anchor Biosynthesis Class F
PBST	Phosphate-Buffered Saline-Tween® 20
PI	Propidium Iodide
pRB	Product of Retinoblastoma Tumour Suppressor Gene

qRT-PCR	Quantitative Reverse Transcription Polymerase Chain Reactions
RNA	Ribonucleic Acid
rRNA	Ribosomal Ribonucleic Acid
RIPA	Radioimmunoprecipitation Assay
RAS	Small Guanosine Triphosphate
RAF	Proto Oncogene Serine / Threonine Protein
RANTES	Regulated on Activation Normal T-cell Expressed Secreted
RhO	Ras Homolog
ROS	Reactive Oxygen Species
Rac1	Ras-related C3 Botulinum Toxin Substrate 1
SDS-PAGE	Sodium Dodecyl Sulfate–Polyacrylamide Gel Glectrophoresis
SCC	Squamous Cell Lung Cancer
STAT3	Signal Transducer and Activator of Transcription 3
TAE	Tris-Acetate-EDTA
TIMPs	Tissue Inhibitors of Metalloproteinase
TRAIL	TNF-related apoptosis-inducing ligand
TGF	Transforming Growth Factor
TIMP	Tissue Inhibitors of Metalloproteinase
UK	United Kingdom
uPA	Urokinase-Type Plasminogen Activator
VEGF	Vascular Endothelial Growth Factor
VM	Vasculogenic Mimicry
V600E	Valine for Glutamate at Amino Acid Position 600
Zeb1	Zinc Finger E-box-binding Homeobox Transcription Factor-1

Chapter 1. Introduction

1.1. Skin cancer

Skin cancer is one of the most common cancers in the United Kingdom (UK) and the incidence of skin cancer has increased by 38% annually in the past decade (Cancer Research UK, 2017). Around 16,200 people are diagnosed with melanoma skin cancer and approximately 152,000 new non-melanoma skin cancer cases are reported every year in the UK (Cancer Research UK, 2017). The major types of skin cancer are non-melanoma skin cancer and melanoma (Apalla et al., 2017). Non-melanoma skin cancer can be further divided into basal cell carcinoma and squamous cell carcinoma, which is based on the type of skin cells where the uncontrolled growth cells develop (Apalla et al., 2017).

Melanoma is a malignant tumour that develops from uncontrolled growth of pigment-containing cells called melanocytes, which can be found in the leptomeninges, skin, eye and inner ear (Liu and Sheikh, 2014). Malignant melanoma cancer is a highly aggressive tumour, which has been reported to be a representative cell line in studying migratory and invasive properties of tumour cells (Beaumont et al., 2013). Melanoma is the leading cause of skin cancer-induced death, the Global Cancer Observatory has estimated that approximately 55,500 people die from the disease every year worldwide (Bray et al., 2018).

Currently, there is unmet need for appropriate and sustainable therapeutics, however, some emerging advanced immunotherapies have been reported to improve survival in patients with advanced melanoma. One example is, pembrolizumab, a programmed cell death checkpoint inhibitor. In an open-label, phase one clinical trial, pembrolizumab (given at a dose of 2 mg/kg of body weight every 3 weeks, 10 mg/kg every 3 weeks, or 10 mg/kg every 2 weeks until

disease progression or intolerable toxicity) was shown to have a 5-year overall survival rate of 34% and a 5-year progression-free survival rates of 21% in 655 patients with advanced melanoma (Hamid et al., 2019). A randomised phase 3 study of pembrolizumab (10mg/kg of body weight) versus ipilimumab (3mg/kg of body weight) has also reported that pembrolizumab can prolong progression-free survival and improve overall survival rate than ipilimumab (6-month progression-free survival rates were 47.3% for pembrolizumab every 2 weeks, 46.4% for pembrolizumab every 3 weeks versus 26.5% for ipilimumab every 3 weeks; 12-month survival rates were 74.1%, 68.4%, and 58.2%, respectively) (Robert et al., 2015).

However, long-term efficiency of such therapies for melanoma patients is limited by adverse effects and rapid resistance to treatments (Flaherty et al., 2012, Mannal et al., 2011). For example, pegylated interferon α-2a, an adjuvant therapy for stage III melanomas, has been reported to generate treatment-related adverse effects in melanoma patients, such as nausea, diarrhoea and headache (Atkins et al., 2018, Eggermont et al., 2008, Eigentler et al., 2016). As to resistance to therapy, the duration of effective responses of serine / threonine-protein kinase B-raf (BRAF) inhibitor - vemurafenib and dabrafenib on melanoma patients with a mutation in *BRAF* gene has been reported to be limited between 5.1 and 6.8 months (Sosman et al., 2012, Hauschild et al., 2012). Additionally, Flaherty et al. (2012) have found that the progression-free survival of mitogen-activated protein kinase (MEK) inhibitor trametinib on patients with BRAF V600-mutant advanced melanoma was only four months, suggesting that the prognosis and treatment options for these patients then becomes more limited. Thus, alternative therapies with minimal toxicity and high efficiency are crucial to explore.

1.1.1. Mechanisms of melanoma invasion

Metastasis is the term used to describe the spread of tumour cells from the primary site of disease to surrounding tissues and to distant organs (Seyfried and Huysentruyt, 2013, Flaherty et al., 2012). Melanoma metastasis is a multistage process where melanoma cells first lose cell- to- cell adhesion capacity within the primary tumour cells, which allows the malignant melanoma cells to acquire migratory and invasive properties (Seyfried and Huysentruyt, 2013, Aladowicz et al., 2013). The migratory and invasive properties allow malignant melanoma cells to dissociate from the primary site, then change interactions between cell and extracellular matrix (ECM) and invade the surrounding tissues (Seyfried and Huysentruyt, 2013, Aladowicz et al., 2013). Subsequently, melanoma cells enter the blood vessels, in which the cells can survive in the circulation and arrest at distant organ sites (Pachmayr et al., 2017). Finally, melanoma cells interact with the endothelial cells to develop adhesions by undergoing carbohydrate-carbohydrate locking reactions, and thus penetrate the endothelium of the vessels in the secondary target organ (Valastyan and Weinberg, 2011).

1.1.1.1. Local Invasion

Local invasion is a key initial step in the metastatic spread of melanoma cells, one of the important factors in melanoma invasion is the disruption of the basement membrane integrity (Harlozinska, 2005). As shown in **Figure 1.1**, metastatic melanoma cells can overexpress some proteases, such as matrix metalloproteinase (MMP)-2 (Jiao et al., 2012) and MMP-9 (Shellman et al., 2006), in order to process the proteolytic degradation of all ECM components, and, thus, melanoma cells can migrate freely through ECM.

The ECM is a highly dynamic network of hydrated macromolecular proteins organised in a tissue-specific manner, which is predominantly composed of collagens, proteoglycans, elastin and cell-binding glycoproteins (Walker et al., 2018). ECM plays an important role to regulate the most fundamental behaviours and characteristics of cellular properties, such as migration, proliferation and adhesion (Zhu et al., 2015). Dysregulation of ECM dynamic structure has also been shown to enhance migratory properties of metastatic cancer cells (Zhu et al., 2015).

1.1.1.2. Angiogenesis

Angiogenesis is another essential step in the process of melanoma invasion. Angiogenesis is the term used to describe the formation of new blood vessels from pre-existing vessels (Jiang et al., 2015). Metastatic melanoma cells produce angiogenetic factors, such as vascular endothelial growth factors (VEGFs) to activate pro-angiogenic signalling pathways of endothelial cells in a neighbouring blood vessel (Yadav et al., 2015, Gupta and Qin, 2003). As shown in **Figure 1.1**, basement membrane of the blood vessel is degraded by the production of proteases from endothelial cells, which allows endothelial cells to move toward melanoma cells and proliferate at migrating tip. Finally, a blood vessel loop between the existing vessel and the melanoma cell is formed by endothelial cells undergoing a tubule formation phase (Yadav et al., 2015, Gupta and Qin, 2003).

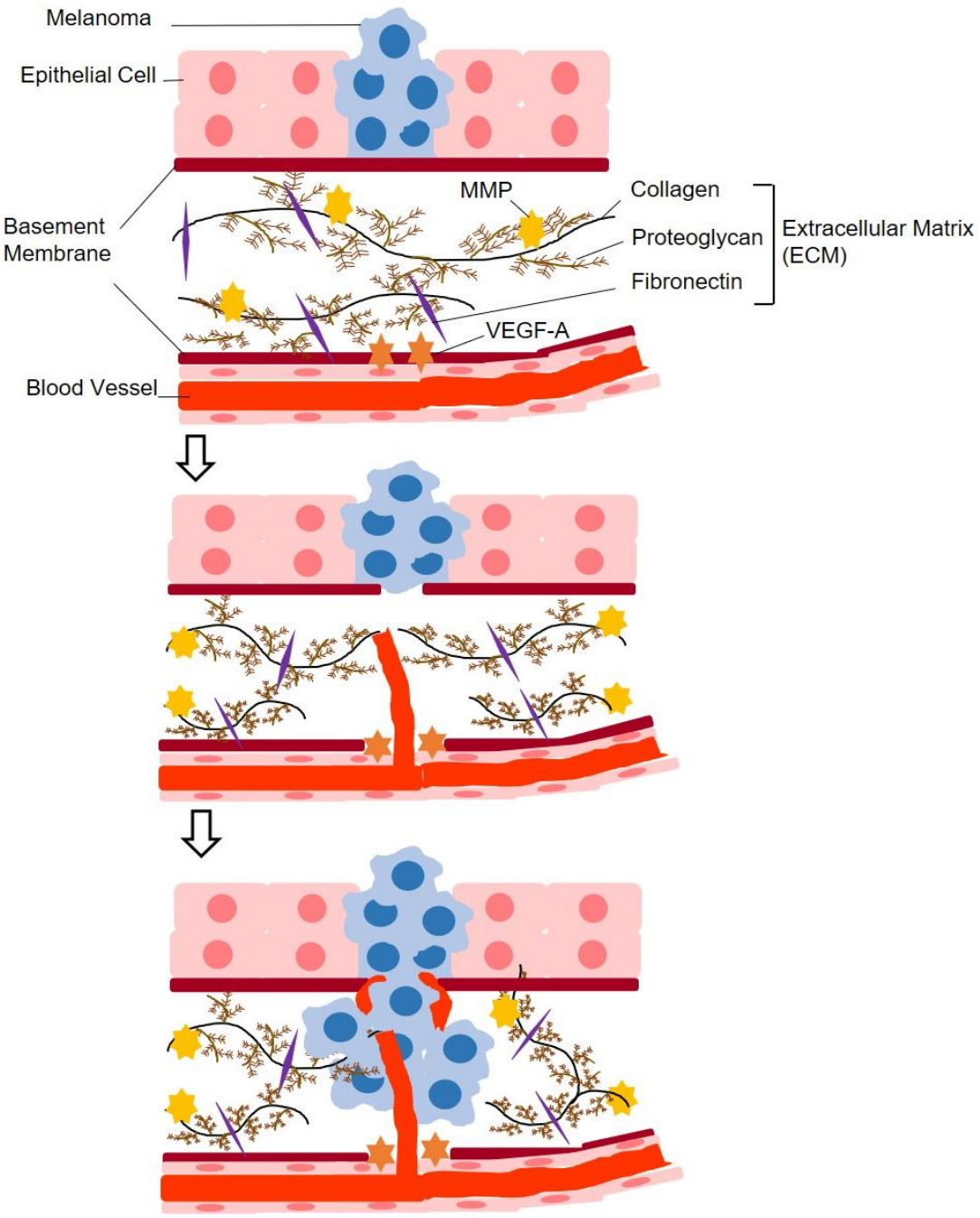

Figure 1.1. Modes of melanoma invasion and angiogenesis during melanoma metastasis. Metastatic melanoma cells can release matrix metalloproteinases (**MMPs**) to degrade extracellular matrix (**ECM**) components, and thus melanoma cells can migrate freely through ECM. Vascular endothelial growth factor – A (**VEGF-A**) is also produced by metastatic melanoma cells, to activate pro-angiogenic signalling pathways of endothelial cells in a neighbouring blood vessel. Endothelial cells release protease enzymes to degrade basement membrane and move toward melanoma cells. Finally, a new blood vessel is formed between the existing vessel and the melanoma cells (Adapted from: Jiang et al., 2015).

1.2. Melanoma metastasis and trophoblast implantation have similar mechanisms.

Early stage trophoblast implantation strongly resembles melanoma metastasis in three main ways: it is a highly invasive process; it requires the development on an independent blood supply and results in the formation of large cell mass (Soundararajan and Rao, 2004). Invading trophoblasts use similar molecular mechanisms as tumour cells to migrate and invade into the maternal uterine decidua, these similar molecular mechanisms are summarised by Holtan et al. (2009) in **Figure 1.2**.

In particular, trophoblasts from the outer layer of the blastocyst can release matrice-degrading proteases, such as MMPs (Staun-Ram et al., 2004) and plasminogen activator serine proteases (Feng et al., 2001), to invade the endometrium. This process is very similar to melanoma invasion, where for instance, malignant melanoma secretes MMPs to stromal ECM in order to migrate through basement membrane.

Another similar feature of implantation and melanoma metastasis is the acquisition of extensive vasculature. This is achieved through the secretion of VEGFs, which promote cell growth and angiogenesis (Anteby et al., 2004). However, the crucial difference is that placental trophoblast cells have the ability to tightly regulate the physiological invasion process by deploying a ‘STOP’ mechanism. Metastatic melanoma cells do not.

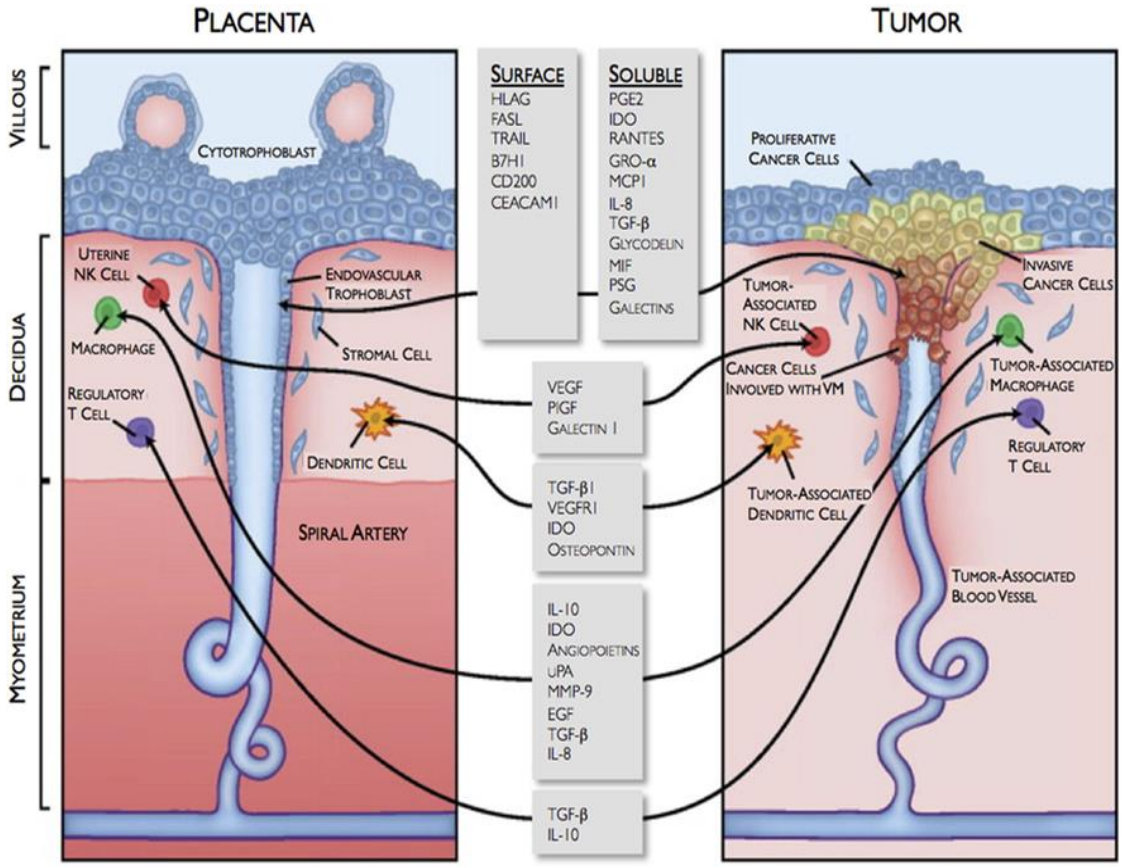

Figure 1.2. Similar characteristics between tumour microenvironment and fetomaternal interface. **FASL**: FAS ligand. **TRAIL**: TNF-related apoptosis-inducing ligand. **CD200**: OX-2 membrane glycoprotein. **CEACAM1**: carcinoembryonic antigen-related cell adhesion molecule 1 (biliary glycoprotein). **PGE2**: prostaglandin E2. **IDO**: indoleamine 2, 3 dioxygenases. **RANTES** (also known as CCL5): regulated on activation, normal T-cell expressed and secreted. **GRO-α**: growth-related oncogene α. **MCP1**: monocyte chemoattractant protein 1. **HLA**: human leukocyte antigen. **MIF**: macrophage migration inhibitory factor. **PSG**: pregnancy-specific glycoprotein. **VEGF**: vascular endothelial growth factor. **PIGF**: phosphatidylinositol glycan anchor biosynthesis class F. **uPA**: urokinase-type plasminogen activator. **MMP**: matrix metallopeptidase. **EGF**: epidermal growth factor. **TGF**: transforming growth factor. **IL**: interleukin. **VM**: vasculogenic mimicry. **NK**: natural killer (Adapted from: Holtan et al., 2009).

1.3. KISS1 / KISS1R signalling pathway is a key regulator to deploy a 'STOP' mechanism in trophoblast cellular invasion.

In 2002, it was firstly reported by Janneau et al. (2002) that kisspeptin signalling pathway plays a key role to regulate invasive and migratory capacities of trophoblast cells during the early phase of pregnancy. It was found that levels of gene expression of kisspeptin (*KISS1)* and kisspeptin receptor (*KISS1R)* were markedly increased in human placental tissue (Janneau et al., 2002). *KISS1R* expression is significantly higher in the early placenta, in which the invasive property of trophoblasts is required to be tightly regulated compared to the term placenta (Janneau et al., 2002). In 2003, Horikoshi et al. (2003) have found that concentrations of plasma immunoreactive kisspeptin 54 (Kp-54) increased in pregnant women in accordance with the progression of pregnancy. This research group also found that Kp-54 was concentrated in the syncytiotrophoblasts, which suggested that an increase concentration of plasma kisspeptin (Kp) during pregnancy was potentially derived from placenta (Horikoshi et al., 2003).

Interestingly, it was reported that only Kp-10, but not other kisspeptins (Kp-54, Kp-14 and Kp-13), induced an increase level of intracellular Ca^{2+} in the first trimester human trophoblasts, which could inhibit trophoblast migration *via* suppressing activities of MMP-2 in a dose-dependent manner (Bilban et al., 2004). This suggested that Kp-10 might be a physiological activator of KISS1R in human placenta (Bilban et al., 2004). In agreement, treatment with Kp-10 in human primary trophoblast cells have been shown to reduce the gene expression of *MMP-1, 2, 3, 7, 9, 10* and *14* as well as *VEGF-A*, and increase the gene expression of tissue inhibitors of metalloproteinases 1 (*TIMP-1*) and *TIMP-3*, which contributes to the decrease of migratory abilities in human trophoblast

cells (Francis et al., 2014). These effects were potentially mediated by KISS1 / KISS1R - activated ERK1/2 signalling pathway. Francis et al. (2014) have found that Kp-10 treatment significantly activated phosphorylation of ERK1/2, while co-treating trophoblast cells with a Kp antagonist could completely block the phosphorylation of ERK1/2. Thus, these studies suggest that KISS1 / KISS1R signalling is a key regulator in controlling migratory capability of human trophoblast cells.

1.4. KISS1 / KISS1R signalling pathway may deploy a 'STOP' mechanism in melanoma invasion.

As introduced in **section 1.2**, trophoblast invasion strongly resembles melanoma metastasis, thus, it is plausible that KISS1 / KISS1R signalling pathway might be a key regulator of melanoma metastasis through its anti-invasive effects. Indeed, KISS1 / KISS1R signalling pathway has been reported to generate anti-metastatic effects in various cancers, such as bladder (Takeda et al., 2012), ovary (Prentice et al., 2007), colorectal (Okugawa et al., 2013, Ji et al., 2014), lung (Sun and Xu, 2013, Zheng et al., 2010), prostate (Wang et al., 2012b) and pituitary (Martinez-Fuentes et al., 2011). Nevertheless, only a few studies have investigated the role of KISS1 / KISS1R signalling pathway in regulating melanoma metastasis. *KISS1* was primarily identified as a human melanoma metastasis suppressor gene by Lee et al. (1996). It was found that transfection of a full-length *KISS1* cDNA into human melanoma cell line was able to inhibit metastasis in athymic nude mice by 50% – 95% (Lee et al., 1996).

Based on this study, Lee and colleagues conducted another study in human breast carcinoma MDA-MB-435 cells, it was shown that *KISS1* also functioned as a metastatic suppressor gene in breast cancer cells (Lee and Welch, 1997). However, it has been recognised that MDA-MB-435 cells express a gene

expression pattern more closely resembling melanocytes instead of breast cancer cells, which raises the possibility that MDA-MB-435 cells are melanoma (Ellison et al., 2002, Ross et al., 2000). Although many studies have described the role of Kp and KISS1R in regulating various cancer cells, the molecular mechanism of KISS1 / KISS1R in human melanoma cells is still not clear. Thus, additional studies will be required to explore the exact mechanism underlying KISS1 / KISS1R signalling pathways of melanoma metastasis.

1.5. Introduction of KISS1 / KISS1R signalling pathways.

1.5.1. Kisspeptin

Kisspeptin is a 145-amino acid polypeptide, which is derived from the primary translation product of the *KISS1* gene (Kotani et al., 2001). *KISS1* was originally identified as a human metastasis suppressor gene, which had the ability to inhibit metastatic potential of human malignant melanoma cells (Lee et al., 1996). The human *KISS1* gene is located at chromosome 1q32 and the melanoma metastasis suppressor locus maps between chromosome 6q16.3-q23 (Miele et al., 2000).

As shown in **Figure 1.3**, human *KISS1* gene contains four exons, where the first and second exons are noncoding (Hu et al., 2017, Ciaramella et al., 2018a). Thus, only the third and fourth exons are transcribed into a *KISS1* mRNA, and subsequently translated to a 145-amino acid precursor peptide, called pre-pro-kisspeptin (Kotani et al., 2001, Stafford et al., 2002, Hu et al., 2017). The pre-pro-kisspeptin is an unstable and biologically inactive pre-pro-peptide, thus, post-translational modifications, such as proteolysis are required to cleave this pre-pro-peptide in order to generate four biologically active peptides (Kotani et al., 2001). These active peptides are distinguished by the number of amino

acids, which includes Kp-10, Kp-13, Kp-14 and Kp-54. Kp-54 was originally named as metastin (Kotani et al., 2001, Stafford et al., 2002, Ciaramella et al., 2018a).

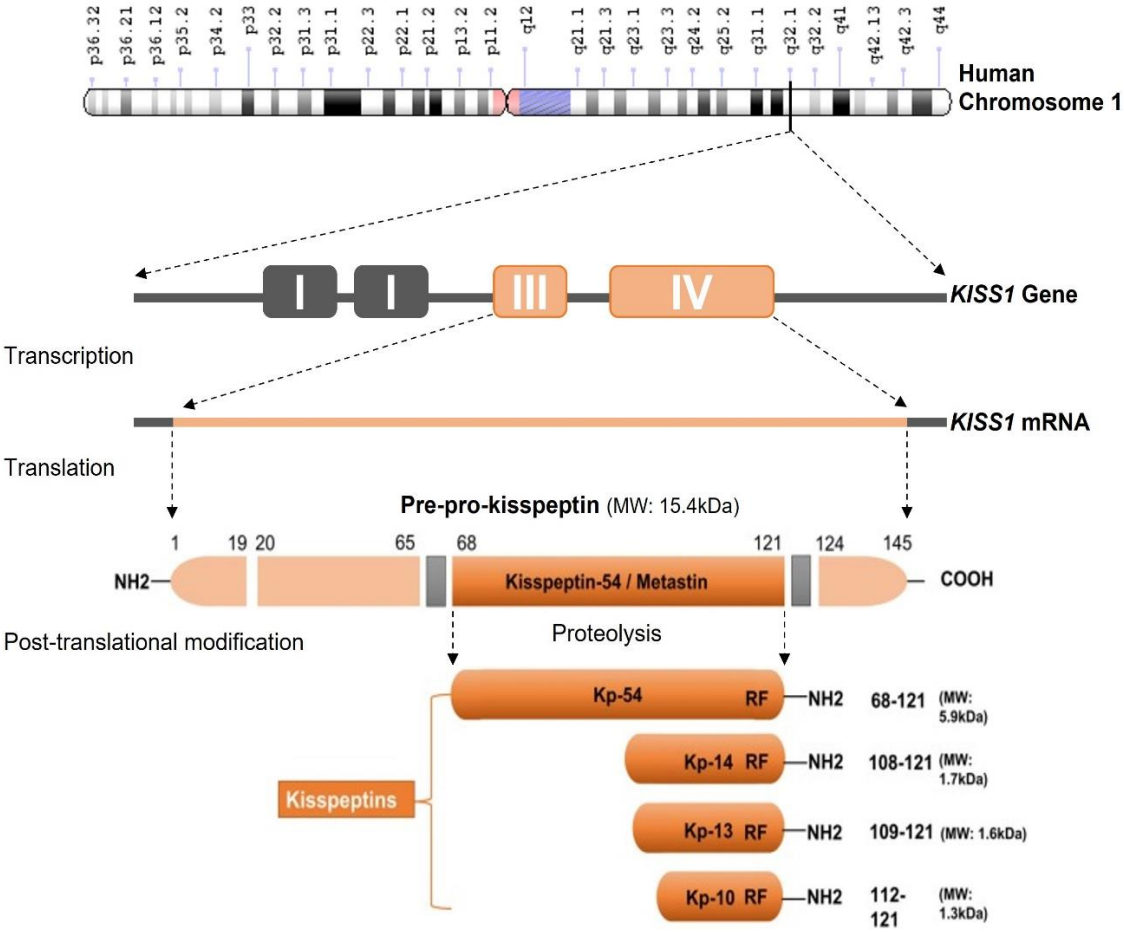

Figure 1.3. Major structural features of kisspeptin peptides encoded by the *KISS1* gene in human. The human kisspeptin (***KISS1***) gene is located at chromosome 1q32. All kisspeptins are generated by the cleavage of a common precursor, named pre-pro-kisspeptin. The pre-pro-kisspeptin contains 145 amino acids, including a 19-amino acid signal peptide and a central 54-amino acid region, kisspeptin-54 (formerly termed metastin). Kisspeptin-54 is further cleaved into the following four biologically active peptides with lower molecular weight (**MW**), which includes kisspeptin-54 (**Kp-54**), **Kp-14**, **Kp-13** and **Kp-10**. These peptides have a C-terminal region that contains an Arg–Phe–NH2 motif of the RF-amide peptide family, which allows these peptides to bind and occupy the kisspeptin receptor, thereby fully activating kisspeptin / kisspeptin receptor signalling pathway (Adapted from: Hu et al., 2017, Ciaramella et al., 2018, National Institutes of Health, 2020).

1.5.2. Kisspeptin protein processing

In 2001, three independent research groups have identified that amino acid sequences of Kp proteins have similar characteristics to neuropeptides, in that they contain a secretion signal, several dibasic cleavage sites and a cleavage amidation site (Kotani et al., 2001, Muir et al., 2001, Ohtaki et al., 2001). It has been reported that the first 19 amino acid sequences comprise a secretion signal peptide (Nash et al., 2007). The remaining amino acid sequences consist of two dibasic cleavage sites (R^{56}-K, R^{66}-R) and a cleavage amidation site (K^{123}-R), these canonical sequences are potentially cleaved by proprotein convertases (Kotani et al., 2001). A recent study has identified that Furin is the critical proprotein convertases for processing cleavage of Kp proteins (Harihar et al., 2014, Nash and Welch, 2006).

Finally, cleavage at dibasic sites R^{66}-R and K^{123}-R convert glycine to an amide by a peptidyl-glycine-α-amidating monooxygenase, which generate a 54-amino acid product term Kp-54 (Nash and Welch, 2006). Kp-54 is further processed to Kp-14, Kp-13 and Kp-10 amino acid sequence, these peptides have the C-terminally amidated region in common, in which the peptides have an Arg-Phe-NH2 motif characteristic of the RF-amide peptide family (Stafford et al., 2002, Kotani et al., 2001). All kisspeptins (Kp-54, Kp-14, Kp-13 and Kp-10) have the same affinity on KISS1 receptors, suggesting that the C-terminally amidated region of the peptides is responsible for the high-affinity binding and the activation of kisspeptin signalling pathway (Stafford et al., 2002, Kotani et al., 2001). A proposed model for Kp protein processing is shown in **Figure 1.4**.

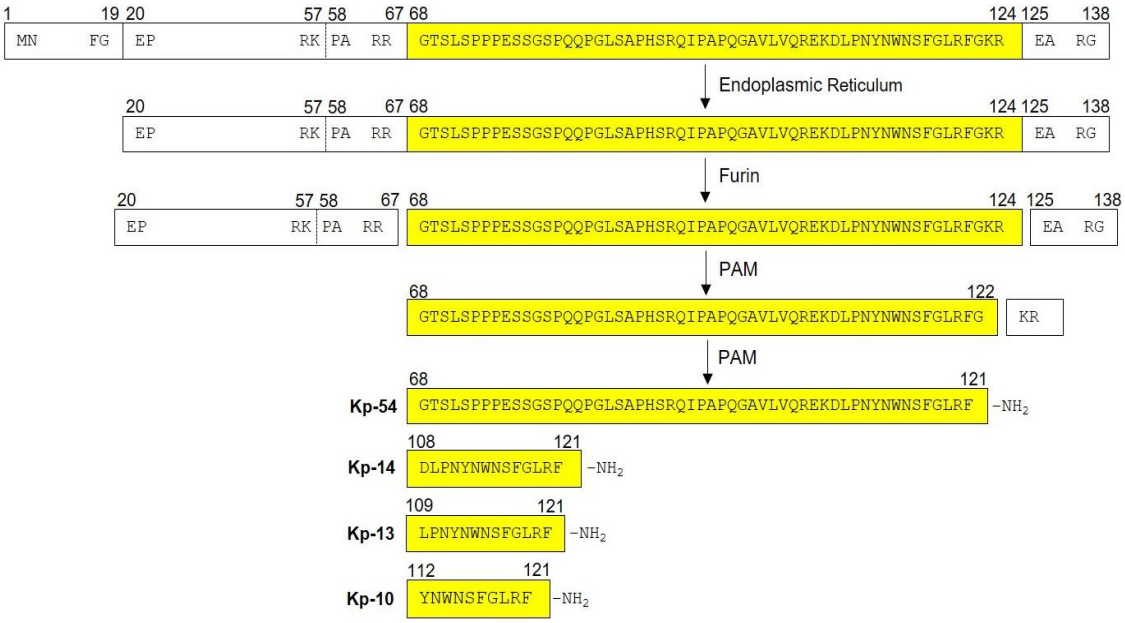

Figure 1.4. A proposed model for kisspeptin proteins processing. Kisspeptin (**Kp**) protein sequences are obtained from NP_002247.3. Kp is target to the endoplasmic reticulum by a signal secretion peptide. When Kp leaves the trans Golgi, the R^{66}-R and GK^{123}-R sites are potentially recognised by Furin and processing cleavage in acidic secretory vesicles. The C-terminal basic residues K^{123}-R is removed by peptidyl-glycine-α-amidating monooxygenase (**PAM**). Afterward, C-terminal G^{122} is converted to an amide by PAM and result in the production of a 54-amino acid product termed Kp-54. Kp-54 is further processed to Kp-14, Kp-13 and Kp-10 amino acid sequence, and the LRF-NH2 sequence at the C-terminus are critical for kisspeptin receptor binding (Adapted from: Nash and Welch, 2006).

1.5.3. Downstream signalling of kisspeptin / KISS1R activation.

The KISS1 receptor, also known as G protein-coupled receptor 54 (GPR54), hOT7T175 and AXOR12, is an orphan GPCR, which was first isolated from a rat brain in 1999 (Lee et al., 1999). The signal transduction pathways that have been reported to be activated by Kp upon KISS1R are summarised in **Figure 1.5**.

1.5.3.1. Activation of phospholipase C and mobilisation of intracellular calcium.

KISS1R belongs to the group of G-protein-coupled receptors that coupled to G proteins of the Gq/11 subfamily, which was initially identified in human embryonic kidney 293 cells in 2001 (Muir et al., 2001). The Gαq/11 protein is phosphorylated when Kp bind to KISS1R, the activated Gαq/11 protein catalyses exchange of guanosine triphosphate (GTP) for guanosine diphosphate (GDP) on a α-subunit, which leads to dissociation of α-subunit from β-subunit and γ-subunit by changing KISS1R conformation (Hu et al., 2017, Castano et al., 2009).

The α-subunit of Gq/11 activates phospholipase C-β, where the hydrolysis of phosphatidylinositol-4,5-bisphosphate (PIP2) is promoted, and thus cleave PIP2 into two potential “second messengers” inositol 1,4,5-triphosphate (IP3) and diacylglycerol (Muir et al., 2001, Kotani et al., 2001, Ohtaki et al., 2001). The activation of diacylglycerol can lead to the phosphorylation of protein kinase C. The activation of IP3 can induce intracellular calcium (Ca^{2+}) mobilisation and release from the endoplasmic reticulum (Ohtaki et al., 2001, Kotani et al., 2001).

1.5.3.2. Activation of mitogen-activated protein kinase related pathways.

In addition to the release of intracellular Ca^{2+} and the activation of protein kinase C, the action of Kp signalling upon KISS1R has been shown to stimulate the mitogen-activated protein kinases (MAPKs) – mediated extracellular signal-regulated kinase (ERK) 1 and ERK2 in various cell types, such as melanoma cells (Becker et al., 2005), pancreatic cancer cells (Masui et al., 2004) and fibrosarcoma cells (Yan et al., 2001). Furthermore, various studies have reported that Kp-induced activation of KISS1R can employ β-arrestin 1 and 2 in a co-dependent manner, in which β-arrestin 2 promote KISS1R signalling to ERK, while β-arrestin 1 inhibits the activity (Goertzen et al., 2016, Pampillo et al., 2009, Szereszewski et al., 2010).

Interestingly, previous studies have reported that some cell types show a significant activation of ERK 1/2, however, the activation of p38 MAPK is not stable in response to Kp. For example, Kp-10 treatment has been found to induce strong phosphorylation of ERK 1/2, whereas phosphorylation of p38 were very weak and no phosphorylation of stress-activated protein kinase / c-Jun NH2-terminal kinase in Chinese hamster ovary cells (Kotani et al., 2001). A similar example is observed in rat luteal cells, in which Kp effectively activate ERK1/2 but do not phosphorylate p38. This suggests that phosphorylation of ERK1/2 could be the most conserved kinase signal in many human cell types.

1.5.3.3. Phosphoinositide 3-kinases / protein kinase B pathways.

The effects of Kp in the activation of phosphatidylinositol-3-kinase (PI3K) and protein kinase B (Akt) remains controversial. For example, Kp-54 was reported to promote the phosphorylation of PI3K and Akt in KISS1R-overexpressed human thyroid cancer cells (Stathatos et al., 2005). However, Kp-54 was found not be able to induce the phosphorylation of PI3K and Akt in rat luteal cells (Peng et al., 2013). Similarly, Kp-10 has been shown to stimulate the phosphorylation of PI3K and Akt in mouse preoptic neurons (Hanchate et al., 2012), whereas the phosphorylation was inhibited in human colorectal cancer cells (Chen et al., 2016) and Chinese hamster ovary (Navenot et al., 2005). This suggested that the effect of Kp upon KISS1R in the activation of PI3K and Akt signalling pathway might be cell type specific.

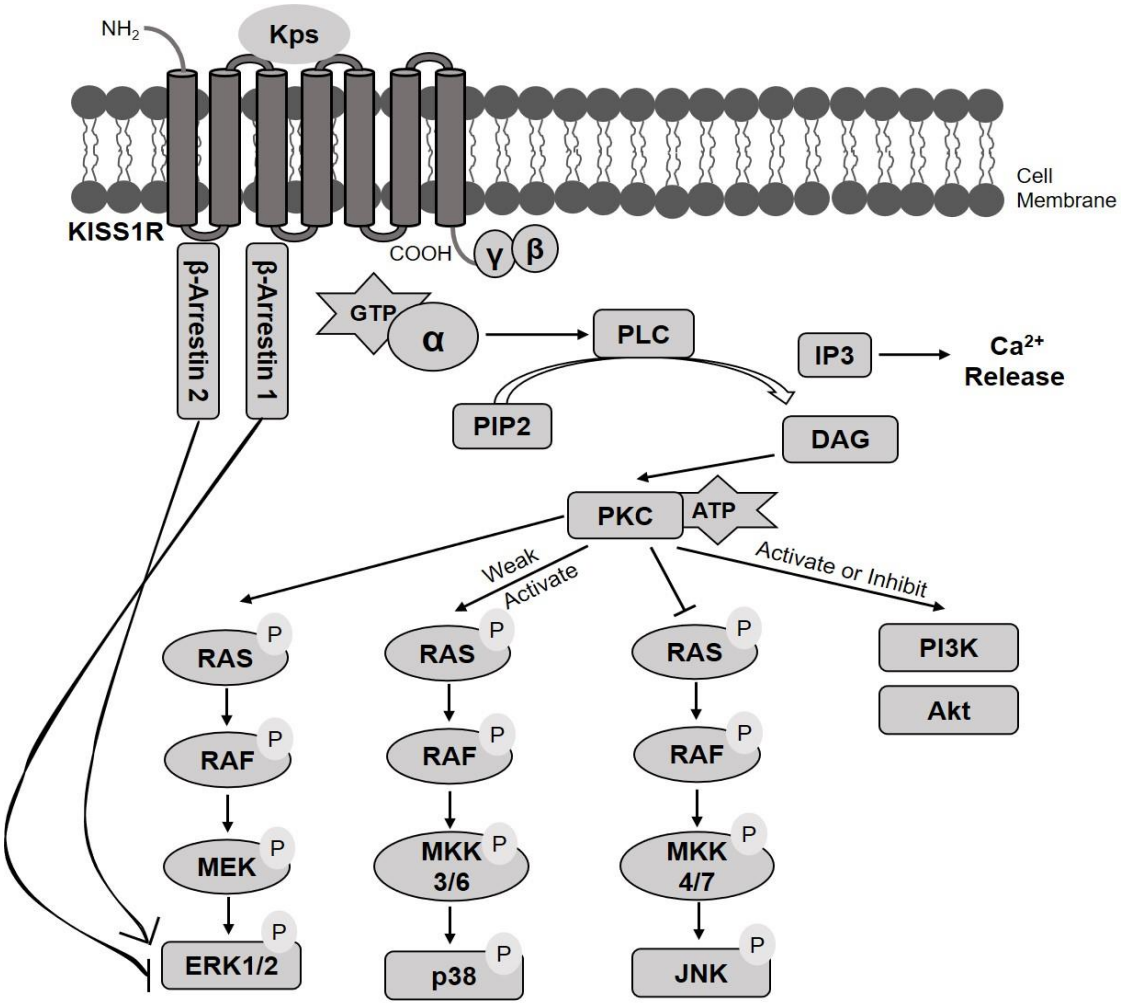

Figure 1.5. Schematic diagram illustrating the major signal transduction pathways of KISS1 / KISS1R. The Gαq/11-mediated signalling pathway is activated when kisspeptins (**Kps**) bind and occupy kisspeptin receptors (**KISS1R**). Phospholipase C (**PLC**) is activated to cleave phosphatidylinositol 4,5-bisphosphate (**PIP2**) into inositol trisphosphate (**IP3**) and diacylglycerol (**DAG**). The activation of IP3 induce intracellular calcium ion (**Ca^{2+}**) release from endoplasmic reticulum. DAG activates a signalling cascade by activating protein kinase C (**PKC**), including mitogen-activated protein kinases (**MEK** / **MKK**) and phosphatidylinositol-3-kinases (**PI3K**) / protein kinase B (**Akt**). Kp-induced activation of KISS1R recruits β-arrestin 1 and 2, where β-arrestin 2 promote KISS1R signalling to ERK but β-arrestin 1 inhibits the activity. **p38**: stress-activated protein kinases. **JNK**: c-Jun N-terminal kinases. **ERK**: extracellular signal-regulated kinase. **RAS**: small guanosine triphosphate. **RAF**: proto-oncogene serine/threonine-protein. **ATP**: adenosine triphosphate. **GTP**: guanosine triphosphate. **P**: phosphorylated. **NH_2**: azanide. **COOH**: carboxylic acid (Adapted from: Hu et al., 2017, Castano et al., 2009).

1.6. Honokiol

Honokiol (HNK) ((3',5-di-(2-propenyl)-1,1'-biphenyl-2,2'-diol) is a bioactive natural compound, which is isolated from the genus *Magnolia* of *Magnoliaceae* family (Esumi et al., 2004). The bark, cones, and leaves from *Magnolia officinalis* plants have been used in traditional Chinese medicine and is named "*houpa*". In Japan, *Magnolia obovata* has also been used in a similar manner and is known as "*koboku*" (Esumi et al., 2004).

HNK has been demonstrated to have minimal toxicity, for instance, in male Sprague-Dawley rats (intravenous administration in a dose-range of 20-80 mg/Kg of body weight, once a day for 14 days), it was observed that there were no significant differences of the body weight, haematological values, tissue pathologic changes, mean daily food intake and serum biochemical values between HNK-treated group and vehicle control group (2.5% mixture of cremophor EL and ethanol in 5% dextrose) (Wang et al., 2011). Similarly, magnolia bark extract has been shown not to generate mutagenic or genotoxic activities in Chinese hamster ovary cells (exposure for 3 hours at concentrations of 0-30 µg/ml) or Chinese hamster lung cells (treatment for 6 hours with concentrations up to 52 and 59 µg/ml) (Zhang et al., 2008). *In vitro* studies also suggested that HNK appears to have low toxicity in human healthy cells, for example, HNK did not significantly reduce cell viability of human NIH-3T3 fibroblast cell line in a concentration of 100µM (Lee et al., 2019).

In addition to the low toxicity of HNK, many studies have indicated multiple biological properties of HNK, such as, anti-inflammatory potential in rat model (Liou et al., 2003), anti-angiogenetic effects in human pancreatic islet endothelial cells, human lung cancer cells and nude mice model (Bai et al., 2003, Hu et al.,

2008). HNK has also been demonstrated to inhibit the growth of brain tumour in rat intracerebral gliosarcoma model, human xenograft glioma model (Wang et al., 2011) and to elicit anti-tumour effects in human squamous lung cancer cells (Yang et al., 2002). Furthermore, anti-neoplastic effects have been indicated in human melanoma cells and mouse models (Guillermo-Lagae et al., 2017, Mannal et al., 2011). Anti-microbial activities were shown against some species, such as *Propionibacterium acnes* and *Propionibacterium granulosum* (Park et al., 2004).

1.6.1. Molecular mechanisms underlying anti-metastatic properties of honokiol in human melanoma cells.

The molecular signalling pathways through which HNK elicits its effects in melanoma cells are beginning to be elucidated. Metastatic melanoma xenograft mouse model has indicated that HNK significantly reduces organ metastasis and peritoneal dissemination by inducing endoplasmic reticulum stress (Chiu et al., 2019). This HNK-induced endoplasmic reticulum stress can stimulate Calpain-10 and CCAAT-enhancer-binding protein regulated cascades, thereby further prevent β-catenin and microphtahalmia-associated transcription factor-induced melanoma metastasis (Chiu et al., 2019).

Additionally, *in vivo* and *in vitro* studies have shown that HNK produced anti-neoplastic effects in melanoma by significantly increased mitochondrial depolarisation, cytosolic cytochrome *c* and apoptotic proteins (Mannal et al., 2011, Guillermo-Lagae et al., 2017). HNK treatment have also been found to affect stem cell-like properties of melanoma cells by interrupting various mechanisms including: Notch 1/2, PI3K-AKT-rapamycin (mTOR) and AMP-activated protein kinases signalling pathways (Kaushik et al., 2015, Kaushik et

al., 2014, Kaushik et al., 2012). Moreover, Prasad et al. (2016) have shown that HNK could suppress oxidative activities of nicotinamide adenine dinucleotide phosphate (NADPH) by interrupting interactions between membrane-bound and cytosolic proteins, thereby achieving anti-migration effects. Although recent studies have indicated multiple anti-cancer actions of HNK by its effect on various biological pathways, the exact molecular mechanisms of HNK in melanoma cells have not been fully elucidated.

1.7. Honokiol may target KISS1 / KISS1R signalling pathway to achieve anti-migration effects in human melanoma cells.

An qRT-PCR array carried out by Dr Sharron Vass at Edinburgh Napier University (UK), has indicated that HNK attenuated the mRNA expression of *MMP-2*, *MMP-9*, *NF-κB*, *VEGF-A* and *TIMP-4* in human A375 melanoma cells. Furthermore, expression of *KISS1* and *KISS1R* was upreguated in HNK-treated cells, which was unexpected. Currently, there is only one study published by Cheng et al. (2015), which demonstrated that HNK is able to suppress the process of metastasis in human renal carcinoma cells, by up-regulation of KISS1 / KISS1R signalling at both the transcriptional (mRNA) and translational (protein) level. Cheng et al. (2015) have indicated that HNK upregulates mRNA expression of *TIMP-4*, downregulates mRNA expression of *MMP-7* and *VEGF-C*. Thus, results from Dr Sharron Vass (as yet unpublished) and Cheng et al. (2015) concur that honokiol is able to target KISS1 / KISS1R signalling pathway and this pathway may potentially regulate gene expression of MMPs and other angiogenic factors. Which in turn, may result in anti-metastasic effects in human melanoma cells.

1.8. Introduction of MMP-2, MMP-9, TIMP-4, NF-κB and VEGF-A.

As introduced in **section 1.7**, an qRT-PCR array carried out by Dr Sharron Vass has indicated that HNK attenuated the mRNA expression of *MMP-2*, *MMP-9*, *NF-κB*, *VEGF-A* and *TIMP-4* in human A375 melanoma cells. Therefore, this study has investigated these specific molecules and general introductions regarding these molecules are presented from **section 1.8.1** to **section 1.8.4**.

1.8.1. Matrix metalloproteinase - 2 and - 9

Matrix metalloproteinases, also called matrixins, are a family of structurally related, zinc-dependent endopeptidases, which are able to degrade basement membrane and remodel ECM (Huang, 2018). MMPs can be divided into subgroups based on their structure and substrate specificity, these subgroups include collagenases, stromelysins and stromelysin-like MMPs, matrilysins, gelatinases and other MMPs (Huang, 2018). MMPs generally contain an N-terminal pro-peptide domain, a signal peptide and a catalytic domain (Harlozinska, 2005). The catalytic domain contains a C-terminal haemopexin-like domain region and a highly conserved zinc-binding site (Harlozinska, 2005).

Gelatinases have an additional fibronectin-type II domain that is included between the active site domain and the catalytic domain (Moro et al., 2014). Activation of enzymatic activities of MMPs requires a cysteine residue to bind a Zn^{2+} ion at the active centre, in order to remove a pro-domain region and ensure enzyme latency (Moro et al., 2014). MMP-2 and MMP-9 belong to the gelatinase subgroup of the MMPs family, which play an important role in cancer cellular invasion (Chen et al., 2016). MMP-2 and MMP-9 can degrade many ECM proteins through proteolytic cleavage to regulate ECM remodelling, because basement membrane contains collagens, including Type IV collagen, which is primarily degraded by MMP-2 and MMP-9 (Chen et al., 2016, Fraser et al.,

2019). During tumour metastasis, basement membrane destruction is one of the initial steps to allow tumour invasion and migration (Cheng et al., 2015).

1.8.2. Tissue inhibitors of metalloproteinase - 4

Tissue inhibitors of metalloproteinases (TIMPs) are endogenous inhibitors of the MMP family and play a key role in regulating ECM remodelling during the metastatic process of melanoma tumour cells (Murphy, 2011). TIMPs consist of 184 to 194 amino acids that form a C-sub-domain and an N-domain, TIMPs inhibit the activities of MMPs by forming a tight and noncovalent complex in a 1:1 molar ratio (Murphy, 2011, Sun, 2010, Brew and Nagase, 2010).

TIMPs are a multigene family comprising four members with approximately 40% to 50% sequence identity in human, including *TIMP-1, TIMP-2, TIMP-3*, and *TIMP-4* (Murphy, 2011, Sun, 2010, Brew and Nagase, 2010). Overexpression *TIMP-4* has been shown to reduce the ability of cellular invasion in various tumour cells, such as melanoma (Hofmann et al., 2005). Human TIMP-4 is a non-glycosylated polypeptide consisting of 195 amino acids, which is the largest of the currently recognised human inhibitor of MMPs (Radisky et al., 2017, Melendez-Zajgla et al., 2008). The N-terminal subdomain of TIMP-4 is majorly responsible for inhibiting the activity of MMPs. The C-terminal domain mediates non-inhibitory interactions with some pro-MMP forms, such as pro-MMP-2, by binding to the carboxy-terminal hemopexin domain of the pro-MMP-2, and consequently suppresses activation of pro-MMP-2 in the complex form (Radisky et al., 2017, Melendez-Zajgla et al., 2008).

1.8.3. Vascular endothelial growth factor - A

Vascular endothelial growth factors, also known as vascular permeability factors, are a family of polypeptides with a highly conserved receptor-binding cystine-knot structure (Holmes and Zachary, 2005). The VEGF family consists of five members including: VEGF-A, VEGF-B, VEGF-C, VEGF-D and placental growth factor, which interacts with VEGF receptors including: VEGFR-1, VEGFR-2 and VEGFR-3 (Holmes and Zachary, 2005).

Among these interactions, VEGF-A / VEGFR-2 cascade has been indicated to be a prominent signalling pathway in the development of pathological angiogenesis in various cancer cells, such as human colonic mucosa (Andre et al., 2000), human lung adenocarcinoma cells (Riquelme et al., 2014), human gastric cancer tissues (Lian et al., 2019) and human melanoma cells (Lacal et al., 2005). VEGF-A / VEGFR-2 signalling can promote the formation of neighbouring blood vessel by increasing microvascular permeability, which facilitates the delivery of nutrients, oxygen and growth factors for melanoma invasion and migration (Lian et al., 2019, Wang and Seed, 2003).

1.8.4. Nuclear factor-kappa B

Nuclear factor kappa-light-chain-enhancer of activated B cells, also named as nuclear factor kappa B (NF-κB), is a protein complex that acts as an essential transcriptional factor (Madonna et al., 2012). NF-κB has been reported to play a key role in melanoma metastasis, invasion and proliferation. For example, NF-κB has been shown to regulate the expression of cell cycle–related factors, such as cyclin D1 and cyclin-dependent kinase 2, vascular cell adhesion molecule-1 and metalloproteinases to facilitate the metastasis and invasion of melanoma cells (Gao et al., 2006, Borghaei et al., 2004, Alonso et al., 2004, Langley et al., 2001).

NF-κB is constitutively located in the cytoplasm with either a homo- or heterodimer complex, which comprises five gene-coding subunits including RelA/p65, c-Rel, RelB, p50 and p52 (Madonna et al., 2012, Spandidos et al., 2008). These subunits can induce transcription of specific target genes by binding to the κB enhancer element in DNA sequence, in order to form heterodimers or homodimers (Madonna et al., 2012). In the canonical NF-κB signalling pathway, an inhibitor of nuclear factor kappa B kinase (IKK) complex is activated in response to stimuli (Liu et al., 2017, Spandidos et al., 2010). Upon activation, IKK phosphorylates an inhibitor of nuclear factor kappa B (IκBα) protein and thus activates ubiquitin-dependent degradation of the IκBα in the proteasome. Subsequently, p50/p65 subunits of NF-κB are released and translocate to the nucleus, in order to bind to the κB enhancer element in DNA and promote the progression of transcription (Wang et al., 2017, Liu et al., 2017).

1.9. Hypothesis and aim of the study.

The hypothesis under investigation in this study is that HNK can suppress metastasis of human melanoma cells, through up-regulation of the KISS1 / KISS1R signalling pathway, which has a direct consequence on the regulation of MMPs, some angiogenic factor expression and the expression of TIMPs.

The key aim of this study was to investigate the effects of HNK on cell migration at the cellular and molecular level, utilising the highly malignant human melanoma cell line, A375.

1.10. Objectives of the study.

1. Analyse the physiological and functional effects of HNK in A375 melanoma cells, using a series of experiments including:

a). A cell viability assay to analysis the cytotoxicity of HNK in A375 cells.

b). Fluorescence staining using acridine orange and propidium iodide double staining, and flow cytometry analysis using Annexin V / propidium iodide assays to assess the apoptotic effects of HNK in A375 cells.

c). An alamar blue assay to measure the effect of HNK on metabolic activities in A375 cells.

d). Fluorescence staining using Phalloidin-Atto and 4´,6-diamino-2-phenyl-indole dye to analysis cell morphology changes of A375 cells in response to HNK treatment.

e). A wound healing assay to measure the impacts of HNK in A375 cell migration.

2. In order to investigate the molecular mechanisms of anti-metastatic effects of HNK in A375 cells, a series of experiments were performed including:

a). Quantitative RT-PCR to measure the mRNA expression of *KISS1*, *KISS1R*, *MMP-2*, *MMP-9*, *TIMP-4*, *NF- κB* and *VEGF-A* in A375 cells following HNK treatment.

b). Immunoblotting to measure the protein expression of KISS1, KISS1R, MMP-9, TIMP-4 and NF- κB in A375 cells following HNK treatment.

3. In order to investigate whether Kp-10 alone elicits similar molecular mechanisms as HNK alone, A375 cells were treated with Kp-10. Cells were treated with the combination of Kp-10 and HNK which served as a control. Afterwards, quantitative RT-PCR analyses were conducted in order to measure the mRNA of *KISS1*, *KISS1R*, *MMP-2*, *MMP-9*, *TIMP-4*, *NF-κB* and *VEGF-A*, and immunoblotting analyses were performed in order to measure the protein expression of KISS1R and MMP-9.

Chapter 2. Material and methods

2.1. Honokiol and cell culture

Honokiol powder (> 98% purity) was purchased from Sigma-Aldrich (UK) and dissolved in 100% dimethyl sulfoxide (DMSO) to make an 80mM stock solution and stored at -20°C, as suggested by Kaushik *et al.* (2015) and Cheng *et al.* (2015). The malignant human melanoma cell line A375 (ECACC 88113005) was purchased from European Collection of Authenticated Cell Cultures (UK). A375 cells were cultured in Dulbecco's Modified Eagle Medium (DMEM) (Gibco®, Thermo Fisher Scientific, UK) supplemented with 2mM L-glutamine, 10% fetal bovine serum (FBS) (Gibco®, Thermo Fisher Scientific, UK), 100 unit/mL penicillin (Gibco®, Thermo Fisher Scientific, UK) and 100 µg/mL streptomycin (Gibco®, Thermo Fisher Scientific, UK). A375 cells grown at 37°C in a high humidified atmosphere with 5% CO_2 and passaged once confluent.

2.2. Cell viability assay – cytotoxicity of DMSO

HNK was required to be dissolved in 100% DMSO prior to use, it was therefore important to assess the potential cytotoxicity of DMSO (vehicle control), in order to identify the minimal toxic concentrations of DMSO in human A375 melanoma cell line. A375 cells were seeded at a concentration of 2.0 x 10^5 cells/mL in 6-well plates (Corning® Costar®, Sigma-Aldrich, UK) with 2mL per well, and the cells were grown at 37°C in 5% CO_2 for 24 hours. Cells were left untreated or treated with DMSO (Sigma-Aldrich, UK) for 24 and 48 hours at concentrations of 0.0625%, 0.125%, 0.25%, 0.5% and 1.0%.

At 24- and 48- hours post-treatment, cells were washed with 2mL 0.9% sodium chloride (NaCl; Baxter International Inc. UK) and detached from the surface of the culture vessel by 1% trypsin (Gibco®, Thermo Fisher Scientific, UK).

Afterward, cells were centrifuged (Hettich® Universal 320/320R centrifuge, Sigma-Aldrich, UK) at 626 x *g* for 2 minutes at room temperature and suspended in 1mL 0.9% NaCl. Nigrosin-exclusion staining was performed on 50µL cells combined with 50µL 0.5% nigrosin in phosphate-buffered saline (PBS; Sigma-Aldrich, UK). Cell counting was performed by adding 15µL stained cells to a hemocytometer. The cells were viewed and photographed using a Primovert inverted microscope at a magnification of x 10 (Zeiss, UK).

2.3. Cell viability assay – cytotoxicity of honokiol

To examinate the cytotoxicity of HNK in A375 cells, a cell viability assay was performed as described in **section 2.2**. A375 cells were left untreated or treated with HNK for 24 and 48 hours at concentrations of 10µM, 20µM, 30µM and 40µM. The percentage of DMSO as vehicle control was 0.05%, since this was matched to the maximum percentage of DMSO that cells were exposed to when treating with HNK at a concentration of 40µM.

2.4. Apoptosis assay

A375 cells were seeded at a concentration of 2.0 x 10^5 cells/mL in 6-well plates with 2mL per well and the cells were grown at 37°C in 5% CO_2 for 24 hours. Cells were left untreated or treated with HNK at concentrations of 10µM, 20µM, 30µM and 40µM for 24 hours. The percentage of DMSO as vehicle control was 0.05%, since this was matched to the maximum percentage of DMSO that cells were exposed to when treating with HNK at a concentration of 40µM.

2.4.1. Acridine orange and propidium iodide double staining assay

At 24-hours post-treatment, 10µL acridine orange (stock: 0.3 mg/mL) and 10µL propidium iodide (stock: 1 mg/mL) was added to the cells and incubated for 5 minutes at room temperature. The number of viable cells stained with acridine

orange fluoresce green (excitation/emission: 500nm/526nm) and nonviable cells stained with propidium iodide (PI) fluoresce red (excitation/emission: 535nm/617nm) were counted by using Fluorescence Microscopy (Carl Zeiss AG, German). Approximately 100 - 200 nuclei were counted per image and 5 images per treatment were averaged for statistical analysis. Percentage apoptosis was calculated: dividing the number of cells exhibiting red florescence by the total cell count.

2.4.2. Flow cytometry analysis

Following 24-hours treatment, both adherent (detached by 0.05% trypsin-EDTA) and floating (contained in medium) cells were collected and combined for the apoptotic assays using fluorescein isothiocyanate (FITC) - Annexin V Apoptosis Detection Kit with PI (cat # 640914, BioLegend, San Diego, United States), which was a gift from Dr. Filipa Henderson Sousa (Edinburgh Napier University, UK). According to the manufacturer's instructions, cells were centrifuged at 230 x *g* for 5 minutes and supernatant was discarded, cells were washed by 1mL PBS. Afterward, cell pellets were resuspended in 1mL annexin V binding buffer (cat # 422201, BioLegend, San Diego, United States) and centrifuged at 230 x *g* for 5 minutes. Supernatant was discarded and cell pellets were resuspended in 200µL annexin V binding buffer. The cells were incubated with 5µL FITC fluorochrome-labelled annexin V and 10µL PI solution in the dark for 15 minutes at room temperature. Added 100µL annexin V binding buffer to each test tube and analysed by flow cytometry (BD FACSCelesta™, BD Biosciences, USA).

Reference controls for flow cytometry were i) unstained control, non-treated cells with Annexin V-FITC-negative, PI-negative. ii) Negative control, non-treated cells with Annexin V-FITC-positive, PI-positive. iii) Positive control or compensation controls including: cells treated with 40µM HNK (Annexin V-FITC-

positive) indicating apoptosis, cells were physically scraped (PI-positive) indicating necrosis. Voltages for fluorescence channels was adjusted by using unstained control, voltages of forward scatter and side scatter was 462_volt and 291_volt respectively. Percentage of spectral overlap was calculated (**Table 1**) and compensation setting was adjusted.

Table 1. Fluorescence compensation in flow cytometry.

Fluorochrome	Fluorochrome	Spectral Overlap (%)
Annexin V	Propidium Iodide	0.03
Propidium Iodide	Annexin V	0.96

2.5. Alamar blue assay

A375 cells were seeded at a concentration of 1 x 10^5 cells/mL in 96-well plates (Corning® Costar®, Sigma-Aldrich, UK) with 100µL per well and cultured for 24 hours. Cell culture medium were removed and replaced by 100µL new medium (non-treated control) or medium supplemented with HNK (5µM, 10µM, 20µM, 30µM, 40µM and 50µM). Alamar Blue™ Cell Viability Reagent (Invitrogen, Thermo Fisher Scientific, UK) was added to a final concentration of 10%, incubated for 24 and 48 hours. Metabolic conversion of alamar blue was assessed by measuring the absorbance at 550nm and 600nm (ELISA reader LT-5000MS, Labtech International Ltd, UK) and data analysed using Manta software. Controls included cells treated with vehicle DMSO (0.00625%, 0.0125%, 0.025%, 0.0375%, 0.05% and 0.0625%) and cells treated with 0.1% (v/v) Triton X-100 (Triton™ X-100 Electrophoresis, Fisher BioReagents™, UK) as the positive control for reduction in metabolic activities. Percentage reduction of alamar blue was calculated as suggested by Borzacchiello et al. (2015):

$$\frac{\begin{array}{c}\text{(Absorbance (Ab) of Media Only at 600nm x Ab of Treated Sample at}\\ \text{500nm) – (Ab of Media Only at 550nm x Ab of Treated Sample at 600nm)}\end{array}}{\begin{array}{l}\text{(Ab of the Corresponding Vehicle Control at 550nm x Ab of Media Only at 600nm) –}\\ \text{(Ab of the Corresponding Vehicle Control at 600nm x Ab of Media Only at 550nm)}\end{array}} \text{ x } 100\%$$

2.6. Fluorescence staining

A375 cells were grown on coverslips in 6-well plates at a concentration of 2.0 x 10^5 cells/mL (2mL per well) and cultured at 37°C with 5% CO_2 for 24 hours. Cells were non-treated (NTC) or treated with HNK (10µM, 20µM, 30µM and 40µM) for 24 hours. The percentage of DMSO as vehicle control was 0.05%, since this was matched to the maximum percentage of DMSO that cells were exposed to when treating with HNK at a concentration of 40µM. Cells were fixed with 4% (v/v) freshly diluted formaldehyde solution (Sigma-Aldrich, UK) diluted in Dulbecco's PBS (0.2g KCl, 0.2g KH_2PO_4, 8.0g NaCl, 1.15g Na_2HPO_4, = pH adjusted to 7.4 with HCl) for 3 minutes and permeabilised by Dulbecco's PBS with 0.5% (v/v) Triton X-100 for 3 minutes. Afterwards, cells were stained with 1:500 diluted Phalloidin-Atto 488 (stock: 1 mg/mL; Sigma-Aldrich, UK) and 1:1000 diluted 4´,6-diamino-2-phenyl-indole (DAPI) dye (stock: 1 mg/mL; Thermo Fisher Scientific, UK), which was diluted in Dulbecco's PBS with 0.1% (v/v) Triton X-100 for 30 minutes. Nuclei were stained with DAPI dye and filamentous actin was stained with Phalloidin-Atto 488. The fixed and fluorescently stained cells were imaged (20 x magnification) using a Zeiss Axioskop 2 Plus Microscope (Carl Zeiss AG, Germany).

2.7. Wound healing assay

A375 cells were seeded at a concentration of 4.0 x 10^5 cells/mL in 6-well plates with 2mL per well. The cells were grown to 100% confluence in each well for 24 hours at 37°C with 5% CO_2, and the resulting cell monolayer was scratched with sterile fine pipette tips. Cells were non-treated (NTC) or treated with HNK (10μM, 20μM, 30μM and 40μM) for 24 and 48 hours. The percentage of DMSO as vehicle control was 0.05%, since this was matched to the maximum percentage of DMSO that cells were exposed to when treating with HNK at a concentration of 40μM. The wound space was photographed by a Primovert inverted microscope (Zeiss, UK) at a magnification of x 40. Areas of wound were quantified using Image J Software version 1.8.0_112 (National Institute of Health and the Laboratory for Optical and Computational Instrumentation, United States) in square metric units (μm^2).

2.8. RNA isolation and cDNA synthesis

A375 cells were seeded at a concentration of 1.0 x 10^5 cells/mL in T-25 cell culture flasks (Corning® Costar®, Sigma-Aldrich, UK) with 10mL per flask and the cells were grown at 37°C in 5% CO_2 for 24 hours. Cells were non-treated (NTC) or treated with HNK (10μM and 30μM) for 24 hours. Concentrations of 40μM or above were found to be deleterious. Therefore, cells were treated with 10μM and 30μM HNK in order to compare minimum and maximum inhibitory concentrations. The percentage of DMSO as vehicle control was 0.0375%, since this was matched to the maximum percentage of DMSO that cells were exposed to when treating with HNK at a concentration of 30μM. Total ribonucleic acid (RNA) was isolated using TRIzol reagent (Ambion Life Technologies, Thermo Fisher Scientific, UK), which is a monophasic solution of guanidinium

isothiocyanate and phenol, which can denature proteins and solubilise biological materials (Rio et al., 2010).

According to the manufacturer's protocol, both floating and attaching cells were pelleted by centrifugation at 626 x *g* for 2 minutes at room temperature. Cells were homogenised by adding 1mL TRIzol Reagent. Following this, 200µL chloroform (Thermo Fisher Scientific, UK) was added to the homogenate, left for 10 minutes and centrifuged at 12,000 x *g* for 15 minutes at 4°C. Afterward, the homogenate was separated into a clear upper aqueous layer (containing RNA), an interphase (containing DNA) and a red lower organic layer (containing proteins). The upper aqueous layer was removed into a sterile microfuge tube. RNA was precipitated from the aqueous layer with addition of 2-propanol (Fisher Scientific, UK) and the RNA pellet was washed by 1mL 75% (v/v) ethanol (Fisher Scientific, UK). Finally, the RNA pellet was dissolved in nuclease-free water (Qiagen, Germany).

RNA concentration and integrity were assessed by Bioanalyser 2100 (Agilent Technologies, UK). RNA samples with two clear bands of 28S and 18S ribosomal RNA and samples with an RNA integrity number (RIN) >8.0 were used for quantitative reverse transcription polymerase chain reaction (qRT-PCR) analysis (Fleige and Pfaffl, 2006). Total RNA (1000ng) was reverse transcribed to generate 1000ng cDNA by using High-Capacity RNA-to-cDNA™ Kit (ThermoFisher Scientific, UK). Control included no reverse transcriptase enzyme (no RT).

2.9. End-point PCR and gel electrophoresis

The success of complementary deoxyribonucleic acid (cDNA) synthesis was assessed by end-point PCR using reference glyceraldehyde 3-phosphate dehydrogenase (*GAPDH*) primers as suggested by Cen et al. (2018) (**Table 2**). BioMix™ 2 x reaction mix (cat #BIO-25012, Bioline, UK) was used to perform end-point PCR assays. According to the manufacturer's instructions, each reaction (25µL) included: 12.5µL BioMix™ reaction mix, 50ng cDNA, 100pmol *GAPDH* forward and reverse primers and nuclease-free water (QIAGEN, UK). A reaction with no cDNA served as the no template control. The cycling conditions were: 96°C for 5 minutes (initial denaturation), followed by 25 cycles of; 96°C for 1 minute (denaturation), 55°C for 1 minute (annealing) and 72°C for 30 seconds (extension). Finally, 72°C for 5 minutes (final extension).

Gel electrophoresis was performed on 1% (w/v) agarose in Tris-acetate-EDTA (TAE buffer containing: 40mM Tris, 20mM acetic acid and 1mM EDTA). Agarose gels were supplemented with 0.005% SafeView Nucleic Acid Stain (ThermoFisher Scientific, UK) for DNA visualisation. Prior to loading, 4µL 5 x Sample Loading Buffer (Bioline, Meridian Bioscience, UK) was added to PCR products. The PCR products were loaded on the gels and electrophoresed at 80 volts, until the dye travelled approximately three-quarters of the ways to the bottom of the gels. PCR products (101 base pairs) were quantitated using SYNGENE GeneSys G:BOX Chemi XRQ gel doc camera image acquisition software version 1.7.2.0 (Synoptics Ltd, UK).

2.10. qRT-PCR analysis

Primers were obtained from Eurofins Genomics (UK) and are listed in **Table 2**. Each qRT-PCR (20µL) contained 10µL 2 x PrecisionPLUS qPCR Mastermix with 1:20 SYBR green (Primer Design, UK), 10ng cDNA sample, 100pmol forward and reverse primers and nuclease-free water to achieve the final volume. qRT-PCR amplification (95°C for 15 seconds and 60°C for 1 minute for 40 cycles) was performed in duplicates using a StepOne™ Real-Time PCR system (Applied Biosystems, UK). *GAPDH* (**Table 2**) was used as a stable reference gene under the HNK treatment condition as suggested by Cen et al. (2018).

The relative expression of the target genes was calculated *via* the $2^{(-\Delta\Delta Ct)}$ method (Livak and Schmittgen, 2001). The ΔCt value for each gene was calculated by subtracting the Ct number of housekeeping gene from that of gene of interest, which was used to measure statistical significance as suggested by Livak and Schmittgen (2001). Controls included reactions containing cDNA from a reaction without reverse transcriptase (no RT) and cDNA replaced with nuclease-free water served as the template negative (no cDNA).

Table 2. The forward (F) and reverse (R) primers used in qRT-PCR analysis. Primer sequences for *KISS1*, *MMP-2*, *TIMP-4*, *VEGF-A*, *NF-κB 1* and *GAPDH* were designed using the PrimerBank database and the corresponding PrimerBank IDs are provided (Adapted from: Spandidos et al., 2010, Spandidos et al., 2008, Wang and Seed, 2003). Primer sequences for *KISS1R* and *MMP-9* were based on published literature.

Target Gene	Accession Number	Sequence 5' to 3'	PrimerBank ID / literature citation
Kisspeptin *(KISS1)*	NM_002256	**F:** AGCAGCTAGAATCCCTGGG **R:** AGGCCGAAGGAGTTCCAGT	116829963c1
Kisspeptin receptor *(KISS1R)*	NM_032551	**F:** GCTGGTACGTGACGGTGTTC **R:** AGAGCCTACCCAGATGCTGAG	Francis et al. (2014)
Matrix metallopeptidase 2 (*MMP-2*)	NM_004530	**F:** GATACCCCTTTGACGGTAAGGA **R:** CCTTCTCCCAAGGTCCATAGC	189217851c3
Matrix metallopeptidase 9 (*MMP-9*)	NM_004994	**F:** GCACGACGTCTTCCAGTACC **R:** CAGGATGTCATAGGTCACGTAGC	Fraser et al. (2019)
Tissue inhibitor of metalloprotease 4 (*TIMP-4*)	NM_003256	**F:** ATCTGTGCAACTACATCGAGC **R:** CGAGATGGTACAGGGTACTGTG	319890247c2
Vascular endothelial growth factor A (*VEGF-A*)	NM_003376	**F:** AGGGCAGAATCATCACGAAGT **R:** AGGGTCTCGATTGGATGGCA	284172466c1
Nuclear factor kappa B-1 (*NF-κB 1*)	NM_003998	**F:** GAAGCACGAATGACAGAGGC **R:** GCTTGGCGGATTAGCTCTTTT	259155300c2
Glyceraldehyde 3-phosphate dehydrogenase *(GAPDH)*	NM_001256799	**F:** CTGGGCTACACTGAGCACC **R:** AAGTGGTCGTTGAGGGCAATG	378404907c3

2.11. Protein Extraction

A375 cells were seeded at a concentration of 1.0 x 10^5 cells/mL in T-25 cell culture flasks with 10mL per flask and the cells were grown for 24 hours. Cells were non-treated (NTC) or treated with HNK (10μM and 30μM) for 24 hours. The percentage of DMSO as vehicle control was 0.0375%, since this was matched to the maximum percentage of DMSO that cells were exposed to when treating with HNK at a concentration of 30μM.

2.11.1. Protein Extraction by using SDS and DTT.

A375 floating and attached cells were pelleted by centrifugation at 626 x *g* for 2 minutes at room temperature. The media was removed, cell pellets were resuspended in 1mL 0.9% NaCl and followed by centrifugation at 400 x *g* for 2 minutes, in order to remove any remaining medium. Cell pellets were lysed in PBS (Sigma-Aldrich, UK), Laemmli Sample Buffer (final concentration: 2% (w/v) SDS, 50mM Tris base pH 6.8, 10% (v/v) glycerol, 0.01% (w/v) bromophenol blue in ethanol, 2mM ethylenediaminetetraacetic acid (EDTA)) and 0.1M (w/v) dithiothreitol (DTT) (Sigma-Aldrich, UK), which generated a final cell concentration at 1.0 x 10^4 cells/μL. Protein samples were boiled for 5 minutes at 100°C and stored at -20°C.

2.11.2. Protein extraction by using RIPA lysis buffer.

Media was removed and cells were washed by ice-cold PBS twice. Cells were detached by 0.05% trypsin-EDTA and cell pellets were collected by centrifugation at 626 x *g* for 2 minutes. Cell pellets were lysed in ice cold radioimmunoprecipitation assay (RIPA) lysis buffer (150mM sodium chloride, 1.0% (v/v) NP-40, 1.0% (w/v) sodium deoxycholate, 0.1% (w/v) sodium dodecyl sulfate, 25mM Tris-HCl, pH 7.6; cat #89900, ThermoFisher Scientific, UK) supplemented with protease inhibitors (cOmplete™, Mini, EDTA-free protease

inhibitor cocktail; cat #11836170001, Sigma-Aldrich, UK) on ice for 20-30 minutes and clarified by centrifugation at 16,000 x *g* for 15 minutes at 4°C. Protein concentrations were measured using Detergent Compatible (*DC*) Protein Assay Kit I (cat #5000111, Bio-Rad Laboratories, Inc, UK) according to the manufacturer's protocol. The lysis buffer, protease inhibitor and *DC* Protein Assay Kit I were gifted from David Hughes (Edinburgh Napier University, UK). Protein samples were prepared in Laemmli Sample Buffer and boiled at 100°C for 5 minutes prior to use.

2.12. Immunoblotting

Protein samples (20µg - 40µg) were resolved on an 8% to 15% sodium dodecyl sulfate–polyacrylamide gel (SDS-PAGE) electrophoresis according to molecular weight of protein of interest. Subsequently, protein was transferred to Amersham™ Protran® Premium nitrocellulose membranes (Merck Group, UK) or polyvinylidene fluoride membranes (Thermo Fisher Scientific, UK) following the method by Towbin et al. (1992). Final concentration in transfer buffer: 25mM Tri-base (VWR International, UK), 192mM glycine (VWR International, UK), 10% (v/v) methanol (Sigma-Aldrich, UK) and 0.1% (w/v) SDS (VWR International, UK) (Towbin et al., 1992). Ponceau S staining (0.1% (w/v) Ponceau S in 5.0% (v/v) acetic acid; Sigma-Aldrich, UK) was used to assess transfer success and quality. Membranes were blocked with 5% or 3% (w/v) non-fat skimmed dried milk powder (Marvel) in 0.1% (v/v) PBS-Tween® 20 (PBST; Sigma-Aldrich, UK) for 1 hour at room temperature to prevent non-specific antibody binding.

Membranes were incubated for 24 hours at 4°C with constant shaking in primary antibodies (**Table 3**) at a dilution of 1 in 500 to 1 in 1,000 in 5% or 3% (w/v) non-fat skimmed milk / 0.1% (v/v) PBST. Membranes were washed in 0.1% (v/v) PBST for 5 minutes (x 3), in order to minimise background and remove unbound

antibodies. Membranes were incubated with secondary antibodies (**Table 3**) at a dilution of 1 in 20,000 in 0.1% (v/v) PBST for 1 hour at room temperature with constant shaking, followed by washing membranes in 0.1% (v/v) PBST for 5 minutes (x 3). Membranes were visualised by LI-COR Biosciences Odessy imaging system (United States) with ImageStudio 2.0 Software (LI-COR Biosciences, United States). Intensity of bands was quantified by densitometry using Image J software version 1.8.0_112 (National Institute of Health and the Laboratory for Optical and Computational Instrumentation, United States) and was normalised to loading controls.

Table 3. Details of antibodies.

Antibody Type	Antibody Name	Concentration	Reference Number	Manufacturer
Primary	Anti-Kisspeptin	1:500	ab19028	AbCam, UK
Primary	Anti-Kisspeptin	1:500	SAB1410731	Sigma-Aldrich, UK
Primary	Anti-GPR54	1:500	ab137483	AbCam, UK
Primary	Anti-GPR54	1:500	SAB2700212	Sigma-Aldrich, UK
Primary	Anti-MMP-9	1:1,000	HPA001238	Sigma-Aldrich, UK
Primary	Anti-TIMP-4	1:1,000	SAB4502974	Sigma-Aldrich, UK
Primary	Anti-NF-kB p65	1:500	sc-109	Santa Cruz Biotechnology, Inc. US.
Primary	Monoclonal Anti-α-Tubulin	1:1,000	T6074	Sigma-Aldrich, UK
Secondary	IRDye® 680LT Goat anti-Rabbit IgG	1:20,000	926-68021	LI-COR Biosciences, US
Secondary	IRDye® 800CW Goat anti-Mouse IgG	1:20,000	926-32210	LI-COR Biosciences, US

2.13. Overexpression of *KISS1* and *KISS1R* gene in A375 cells.

2.13.1. Plasmid DNA quality

Human tagged open reading frame clone of *KISS1* (RC206859) and *KISS1R* (RC218403) were purchased from OriGene Technologies company (USA). Propagation and isolation of the plasmid DNA was previously performed by Dr. Sharron Vass (Edinburgh Napier University, UK). Restriction digestion was performed by using XhoI restriction endonucleases (Promega, UK) according to the manufacturer's instructions. Briefly, a restriction enzyme digestion reaction (20µL) included: 2µL 10 x restriction enzyme buffer, 0.2µL acetylated bovine serum albumin (10 µg/µL), 0.5µL XhoI restriction enzyme (10 µg/µL), 500ng plasmid DNA and deionised water to achieve the final volume. Restriction digestion was incubated for 1 hour at 37°C. The size of plasmid DNA was identified by 1% (w/v) agarose gel electrophoresis (**section 2.9**). Uncut plasmids served as the negative control.

2.13.2. Transfection of *KISS1* and *KISS1R* plasmid DNA into A375 cells.

This study has initially assessed different amounts of vehicle control plasmid pmaxGFP (500ng, 1µg and 2µg) (Lonza Group Ltd, Switzerland), in order to determine the most effective transfection amounts of plasmid DNA. The vehicle control pmaxGFP plasmids were introduced into A375 cells *via* electroporation-based transfection, by using Cell Line Nucleofector™ Kit V (Lonza Group Ltd, Switzerland).

According to the Amaxa® optimised instructions (Amaxa® Nucleofector® Technology, Lonza Group Ltd, Switzerland), cells were dissociated in 0.5% trypsin-EDTA (Fisher Scientific, UK) and numbered to achieve a concentration

of 1 x 10^6 cells/mL. One millilitre 1 x 10^6 cells were centrifugated at 90 x *g* for 10 minutes at room temperature. For each nucleofection assay, cells were resuspended in 100µL Nucleofector® Solution and combined with different amounts of plasmid pmaxGFP. Electroporation was performed by using Nucleofector™ 2b Device (Nucleofector® Program X-001). Following nucleofection completion, 500µL full medium was immediately added to the cells, which were plated into 6-well plates and incubated for 24 hours.

Following 24 hours post-transfection with pmaxGFP, cells were fixed by 4% (v/v) freshly diluted formaldehyde solution (Sigma-Aldrich, UK) diluted in Dulbecco's PBS. Cells were stained with 1:1000 diluted DAPI dye (indicating nuclei), which was diluted in Dulbecco's PBS with 0.1% (v/v) Triton X-100 for 20 minutes. The fixed and fluorescently stained cells were imaged (10 x magnification) using a Zeiss Axioskop 2 Plus Microscope (Carl Zeiss AG, Germany). Percent transfection efficiency was calculated as following:

$$\text{Transfection Efficiency \%} = \frac{\text{Number of fluorescent cells in the field}}{\text{Total number of cells in the field}} \times 100\%$$

Based on the results, *KISS1* and *KISS1R* plasmid DNA at an amount of 2µg was chosen for the subsequent transfection experiments, the protocol performed was similar to the transfection of pmaxGFP plasmids as described above (**section 2.13.2**). Following 24 hours post-transfection, protein was extracted (**section 2.11.1**) and immunoblotting (**section 2.12**) was performed. Cells were transfected with 2µg pmaxGFP vector, which served as the vehicle control. Cells that were not transfected served as the negative control.

2.14. siRNA transfection

2.14.1. Identifying the best reagent for siRNA transfection.

Small interfering RNA of *KISS1R* (siRNA ID: SASI_Hs01_00119337) was purchased from Sigma-Aldrich (UK). Gibco™ Opti-MEM™ I Reduced Serum Medium (ThermoFisher Scientific, UK) was a gift from Dr. Fern Findlay-Greene (Edinburgh Napier University, UK). Transfections were performed using either Invitrogen™ Lipofectamine 2000 Transfection Reagent (cat #11668027, ThermoFisher Scientific, UK) or Invitrogen™ Oligofectamine™ Transfection Reagent (cat #12252011, ThermoFisher Scientific, UK) following the manufacturers' protocols.

Twenty-four hours before transfection, A375 cells were seeded at a concentration of 1.5 x 10^5 cells/mL in 6-well plates with 2mL per well and the cells were grown at 37°C in 5% CO_2 for 24 hours. Medium was removed and the cells were washed twice with PBS. One millilitre medium without FBS and antibiotics was added to the cells and incubated for 1 hour prior to transfection. *KISS1R* siRNA oligomer (6µL; stock concentration: 20µM) was diluted with 250µL Gibco™ Opti-MEM™ I Reduced Serum Medium. Either 6µL Lipofectamine 2000 or 6µL Oligofectamine was diluted with 250µL Gibco™ Opti-MEM™ I Reduced Serum Medium and incubated for 5 minutes at room temperature.

Diluted oligomer and diluted transfection reagent were combined and incubated for 20 minutes at room temperature, afterward, the complexes were added to the cells (final diluted concentration of *KISS1R* siRNA oligomer was 0.06µM). After incubation at 37°C for 4 hours, 1mL medium with 20% FBS without antibiotics was added to the corresponding transfected cells. Un-transfected

cells served as the negative control. Following 24-hours post-transfection, protein was extracted (**section 2.11.1**) and immunoblotting (**section 2.12**) was performed.

2.14.2. Identifying the most effective volume of Lipofectamine 2000 transfection reagent.

The protocol performed was similar to **section 2.14.1**. In order to identify the most effective working volumes of Lipofectamine 2000 transfection reagent and the working concentration of *KISS1R* siRNA oligomer, two groups were assessed as show below (i and ii). Corresponding vehicle controls were either 4µL or 2µL Lipofectamine 2000 only. Un-transfected cells served as the negative control.

i). Combined 4µL *KISS1R* siRNA oligomer (stock: 20µM) with 4µL Lipofectamine 2000 (final diluted concentration of *KISS1R* siRNA oligomer was 0.04µM).

ii). Combined 2µL *KISS1R* siRNA oligomer (stock: 20µM) with 2µL Lipofectamine 2000 (final diluted concentration of *KISS1R* siRNA oligomer was 0.02µM).

2.14.3. Transfection of *KISS1R* siRNA with or without honokiol treatment.

The protocol performed was similar to **section 2.14.1**. Transfection of *KISS1R* siRNA with or without HNK treatment groups are shown in **Table 4** and a summarised process is shown **Figure 2.1**. Due to the disruption of project determining optimal timings for maximum silencing of protein and transfection efficiency were not performed.

Table 4. Transfection of *KISS1R* siRNA with or without honokiol.

	Honokiol Treated (30µM) Groups	**Honokiol Untreated Groups**
Group 1	Treatment only	A375 cells only (non-treated control)
Group 2	A375 cells were also transfected with *KISS1R* siRNA oligomer.	A375 cells were transfected with *KISS1R* siRNA oligomer
Group 3	A375 cells were also treated with Lipofectamine 2000 reagent only (without transfection).	A375 cells were treated with Lipofectamine 2000 reagent only (without transfection).
Vehicle Control	A375 cells treated with 0.0375% DMSO, since this was matched to the maximum percentage of DMSO that cells were exposed to when treating with HNK at a concentration of 30µM.	

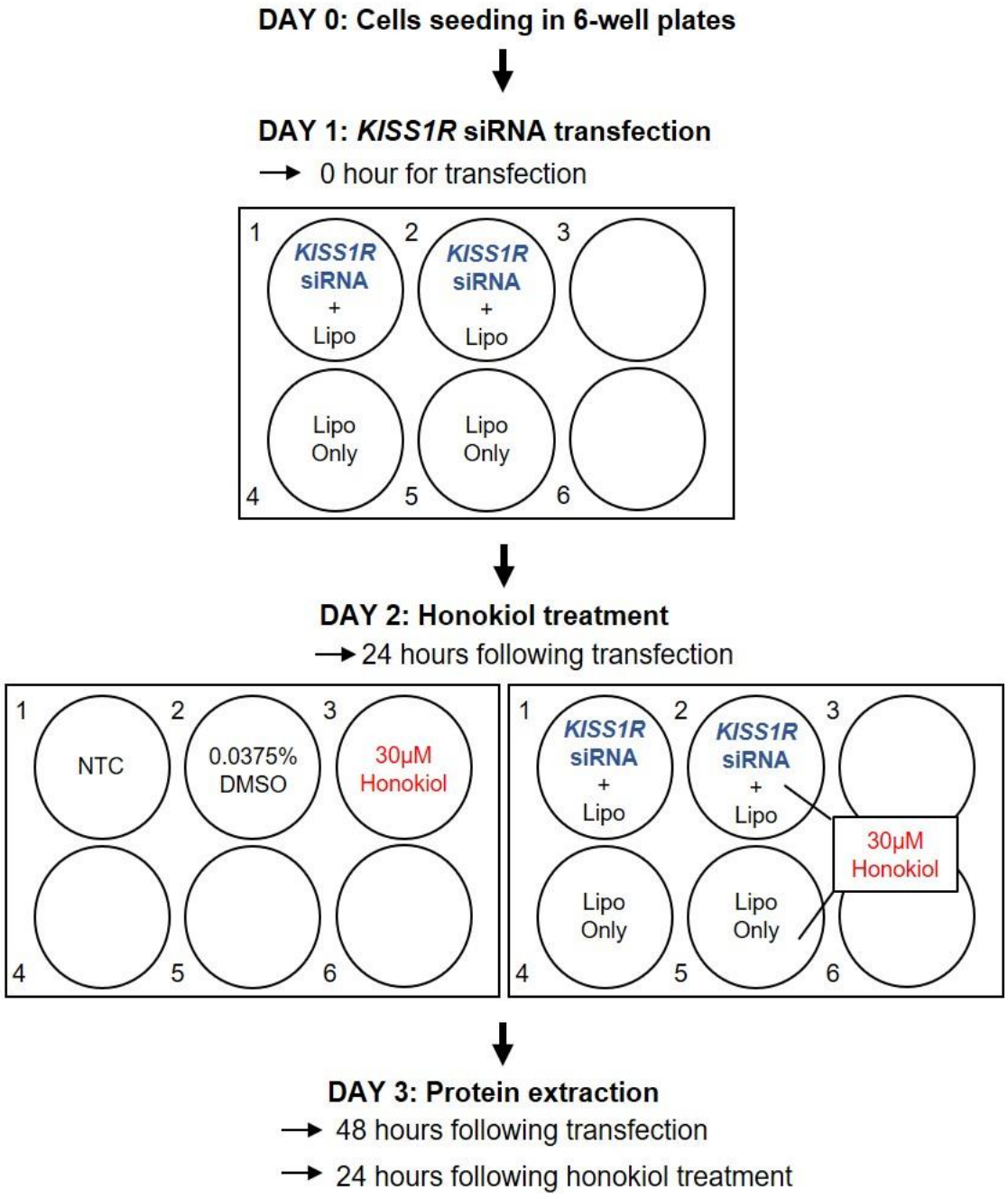

Figure 2.1. A summarised protocol of *KISS1R* siRNA transfection with or without honokiol treatment. Cells were seeded in 6-well plates for 24 hours before transfection. Cells were treated with 30μM honokiol following the 24 hours post-transfection. Protein was extracted on the subsequent day. **KISS1R**: kisspeptin receptor. **Lipo**: Lipofectamine™ 2000 transfection reagent. **NTC**: non-treated control. **DMSO**: dimethyl sulfoxide.

2.15. Kisspeptin-10 treatment with or without honokiol.

Human kisspeptin-10 (H-YNWNSFGLRF-NH2) was purchased from Isca Biochemicals company (UK). Kp-10 was dissolved in 100% DMSO and stored at -20°C. A375 cells were seeded at a concentration of 1.5 x 10^5 cells/mL in 6-well plates with 2mL per well and the cells were grown at 37°C in 5% CO_2 for 24 hours. Cells were treated with 100nM Kp-10, with or without 30μM HNK. Non-treated cells served as the negative control. The percentage of DMSO as vehicle control was 0.1%, since this was matched to the maximum percentage of DMSO that cells were exposed to when treating with both 30μM HNK and 100nM Kp-10. RNA was isolated (**section 2.8**) and qRT-PCR analysis (**section 2.10**) was performed. Protein was extracted (**section 2.11.1**) and then immunoblotting (**section 2.12**) was performed.

2.16. Statistical analysis

All statistical analyses were conducted by GraphPad Prism 8.0 (GraphPad Software, San Diego, California, USA) and the results are expressed as mean ± SEM. Statistically significant differences were evaluated by one-way ANOVA followed by a Tukey's post-hoc test for comparisons between vehicle control and HNK-treated groups, as well as comparisons between non-treated group and vehicle control. A p value ≤ 0.05 was regarded as statistically significant.

Chapter 3. Results

3.1. Effects of dimethyl sulfoxide on cell viability of human A375 cells after 24h and 48h treatment.

HNK is supplied as a crystalline solid and has poor aqueous solubility, thus, HNK was dissolved in an organic solvent prior to use (Cen et al., 2018). Dimethyl sulfoxide (DMSO) is used to dissolve both polar and non-polar compounds and DMSO is also highly miscible with water and other organic liquids (Hebling et al., 2015). However, DMSO has been indicated to be toxic to most human cell lines at concentrations exceeding 1% (Galvao et al., 2014, Yuan et al., 2014). Therefore, the first step was to assess the cytotoxicty of DMSO (which is the solvent for HNK and used as the vehicle control in this study) by a cell viability assay. This permits determination of the minimal cytotoxic concentration of DMSO in human A375 cells.

As shown in **Figure 3.1** and **Figure 3.2**, the number of A375 cells and the viability of cells reduced in a concentration-dependent manner after 24- and 48-hours exposure. Treatment with 0.5% and 1% DMSO reduced approximately 50% cell number after 24- and 48-hours exposure (24 hours, 0.5% vs NTC, 44% reduction, 1.0% vs NTC, 70% reduction; 48 hours, 0.5% vs NTC, 43% reduction, 1.0% vs NTC, 64% reduction). It is important to note that treatment with DMSO at 0.125%, the percentage viability of cells was 98% and 95% at 24 and 48 hours, respectively. These data suggested that DMSO treatment did not cause cytotoxicity up to a 0.125% concentration in human A375 melanoma cell line. Thus, in subsequent experiments in this study, the percentage of DMSO as vehicle control matched to the concentration of DMSO in the highest treatment. This may be 0.0375%, 0.05% and 0.1% depending on the experimental conditions.

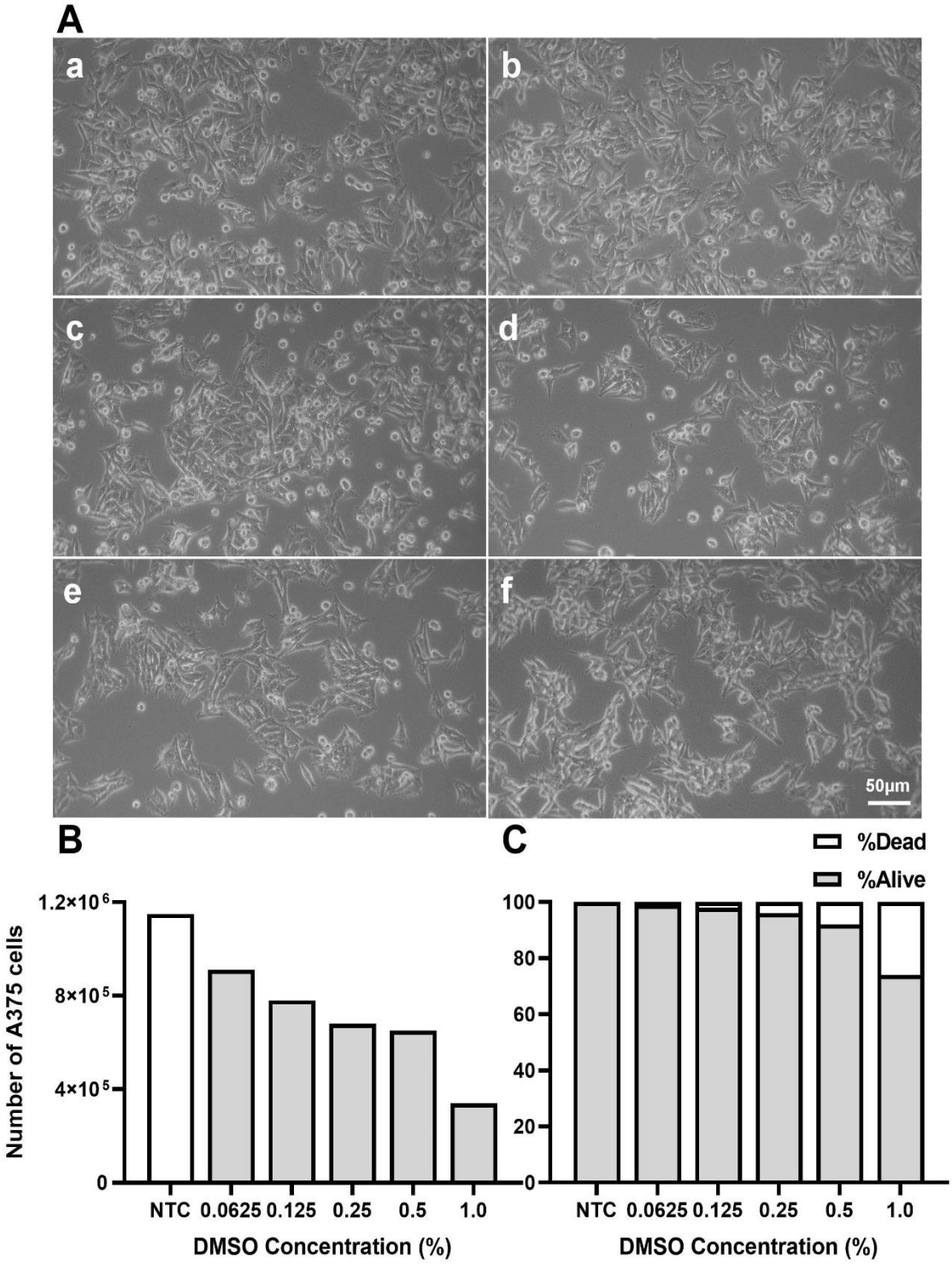

Figure 3.1. Effects of dimethyl sulfoxide on cell viability of human A375 cells after 24 hours treatment. A375 cells were seeded in 6-well plates and incubated for 24 hours. Cells were non-treated control (**NTC**) (**a**) or treated with dimethyl sulfoxide (**DMSO**) at increasing concentrations of 0.0625% (**b**), 0.125% (**c**), 0.25% (**d**), 0.5% (**e**) and 1.0% (**f**) for 24 hours. Viable cells (**B** and **C**) were counted by using Nigrosin-staining method. Data represents the mean of two cell counts from one sample, n=1.

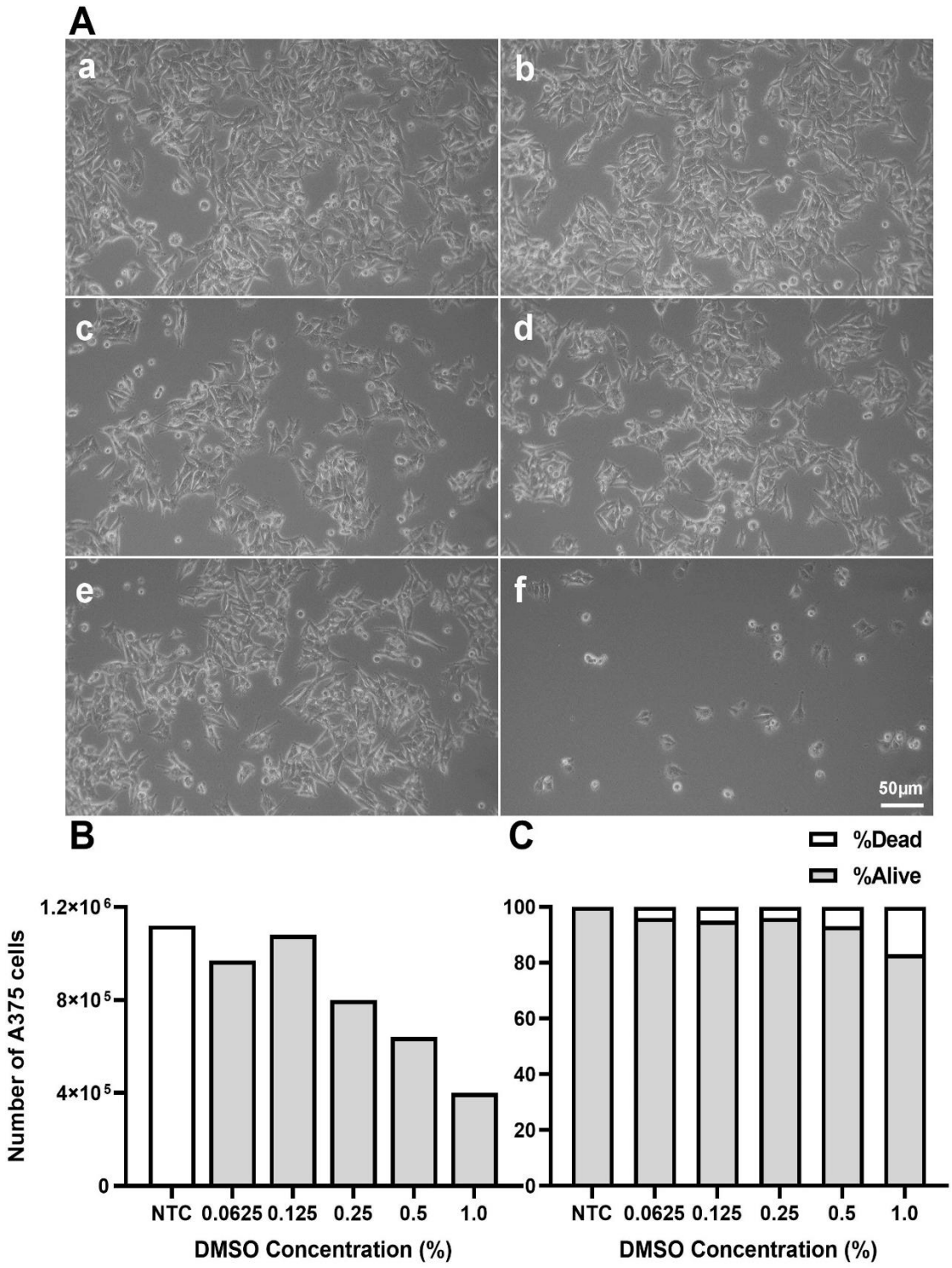

Figure 3.2. Effects of dimethyl sulfoxide on cell viability of human A375 cells after 48 hours treatment. A375 cells were seeded in 6-well plates and incubated for 24 hours. Cells were non-treated control (**NTC**) (**a**) or treated with dimethyl sulfoxide (**DMSO**) at increasing concentrations of 0.0625% (**b**), 0.125% (**c**), 0.25% (**d**), 0.5% (**e**) and 1.0% (**f**) for 48 hours. Viable cells (**B** and **C**) were counted by using Nigrosin-staining method. Data represents the mean of two cell counts from one sample, n=1.

3.2. Investigating the physiological and functional effects of honokiol in human A375 melanoma cells.

3.2.1. Effects of honokiol on cell viability of human A375 cells after 24h and 48h treatment.

Previous studies have indicated that HNK is able to exhibit anti-metastatic effects in various types of cancer, such as colon (Lai et al., 2015), blood (Gao et al., 2016), breast (Nagalingam et al., 2012) and lung (Zhu et al., 2019). The concentration of HNK used in these *in vitro* experiments are between 0μM and 100μM, in which different concentration ranges have been found to significantly reduce cell viability in varying cancer cell lines (Ong et al., 2019). Therefore, in order to examinate the cytotoxicity of HNK in human A375 melanoma cells, a cell viability assay was conducted.

It was shown that the number of A375 cells and the percentage of alive cells reduced in a concentration-dependent manner after 24- and 48-hours treatment (**Figure 3.3** and **Figure 3.4**). Treatment with 30μM and 40μM HNK effectively decreased cell numbers and maximum effects were observed at 48 hours of 40μM HNK treatment with respect to non-treated control (**Figure 3.4**). Cells treated with 30μM and 40μM HNK showed alterations in morphology as compared to non-treated control (**Figure 3.3** and **Figure 3.4**). These findings indicate that HNK dose-dependently decreased viability of human A375 melanoma cells, suggesting that HNK has inhibitory effects on cellular proliferation of A375 cells. HNK has also been demonstrated to exhibit cytotoxic effects against A375 cells at a concentration higher than 30μM.

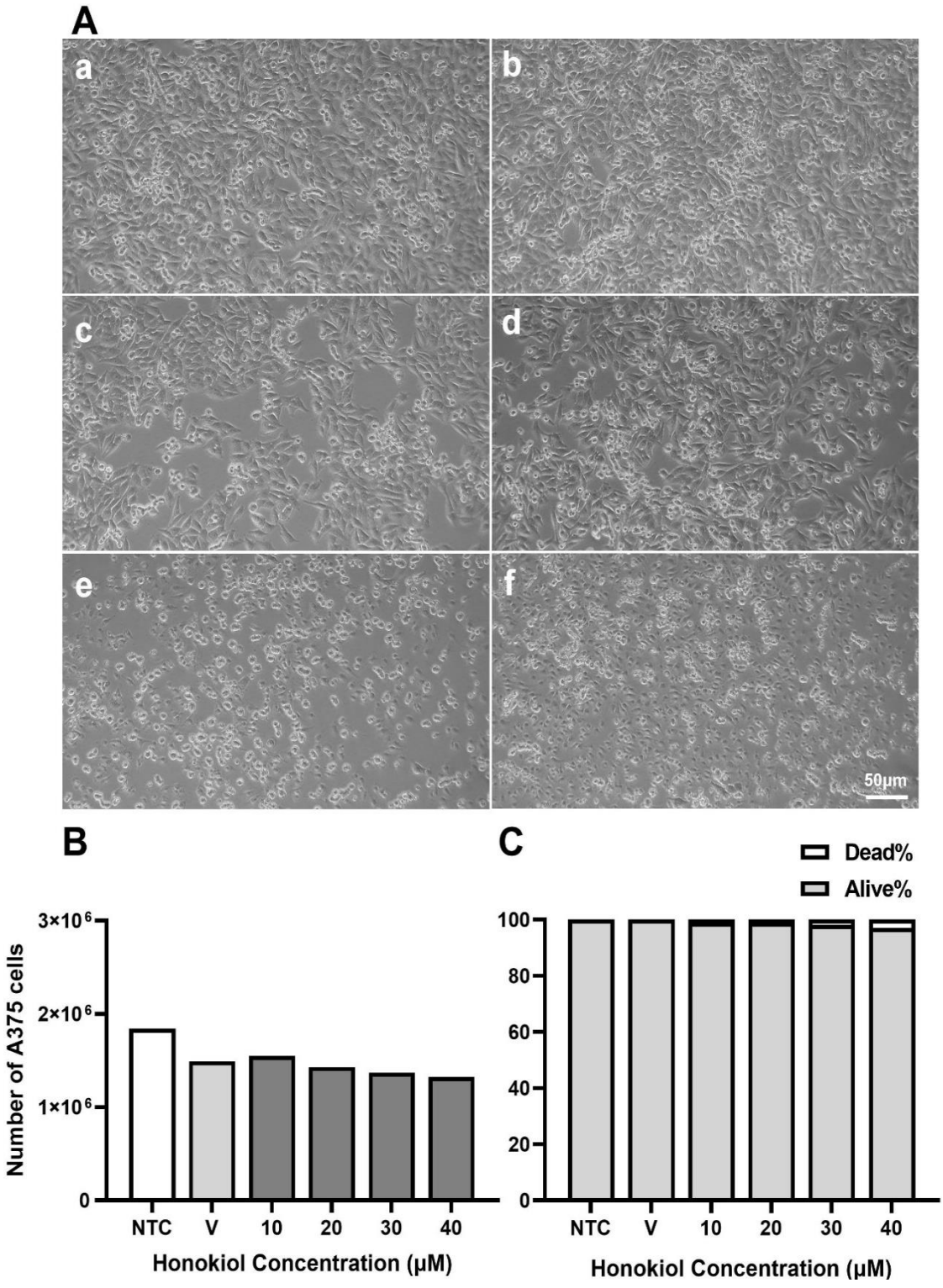

Figure 3.3. Effects of honokiol on cell viability of human A375 cells after 24 hours treatment. A375 cells were seeded in 6-well plates and incubated for 24 hours. Cells were non-treated control (**NTC**) (**a**) or treated with honokiol at concentrations of 10µM (**c**), 20µM (**d**), 30µM (**e**) and 40µM (**f**) for 24 hours. The percentage of DMSO as vehicle control (**V**) (**b**) was 0.05%, since this reflected the maximum percentage of DMSO that cells were exposed to when treating

with HNK at a concentration of 40μM. Viable cells (**B** and **C**) were counted by using Nigrosin-staining method. Data represents the mean of two cell counts from one sample, n=1.

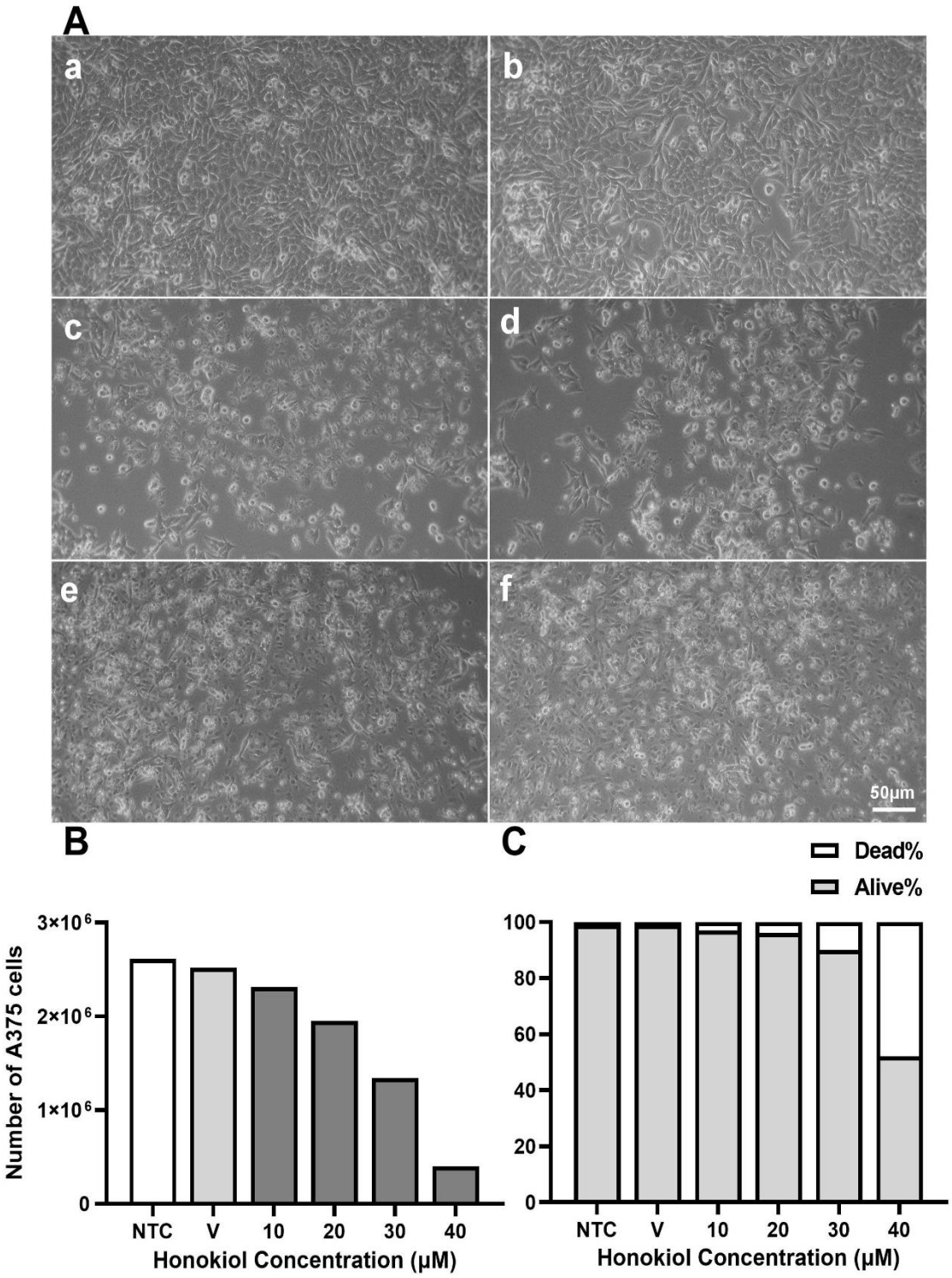

Figure 3.4. Effects of honokiol on cell viability of human A375 cells after 48 hours treatment. A375 cells were seeded in 6-well plates and incubated for

24 hours. Cells were non-treated (**NTC**) (**a**) or treated with honokiol at concentrations of 10μM (**c**), 20μM (**d**), 30μM (**e**) and 40μM (**f**) for 48 hours. The percentage of DMSO as vehicle control (**V**) (**b**) was 0.05%, since this reflected the maximum percentage of DMSO that cells were exposed to when treating with HNK at a concentration of 40μM. Viable cells (**B** and **C**) were counted by using Nigrosin-staining method. Data represents the mean of two cell counts from one sample, n=1.

3.2.2. Honokiol induces apoptosis in human A375 melanoma cells in a concentration-dependent manner.

In the cell viability assay, it was found that HNK has inhibitory effects on cellular survival of human A375 melanoma cells. Suppression of tumour cellular proliferation can be caused by the induction of apoptosis (Gupta et al., 2010). Therefore, in order to investigate whether the induction of apoptosis contributed to HNK-mediated inhibition of cellular proliferation in A375 cell line, fluorescence microscopy analysis by using an acridine orange (AO) and propidium iodide (PI) double staining assay was performed. AO is a cell-permeant nuclear staining dye that emits green fluorescence, which can penetrate alive and dead cells and thus stains all nucleated cells (Li and Yan, 2018). PI is a chromosome counterstain that emits red fluorescence when it binds to denatured DNA. PI is only able to detect dead cells since it is not permeant to live cells (Li and Yan, 2018).

As shown in **Figure 3.5A**, green fluorescence-stained nucleus of the cells indicates normal appearance of healthy alive cells, however, those stained red signified apoptosis. The abundance of apoptotic cells increased in line with the concentration of HNK, which was quantified by the number of red fluorescent cells divided by the total cell number. Thus, the proportion of cells undergoing apoptosis was increasing in a concentration-dependent manner (**Figure 3.5B**). These findings demonstrate that HNK dose-dependently induces apoptotic effects in human A375 melanoma cells, suggesting that the induction of apoptosis may contribute to HNK-mediated inhibition of cellular proliferation in human A375 cells.

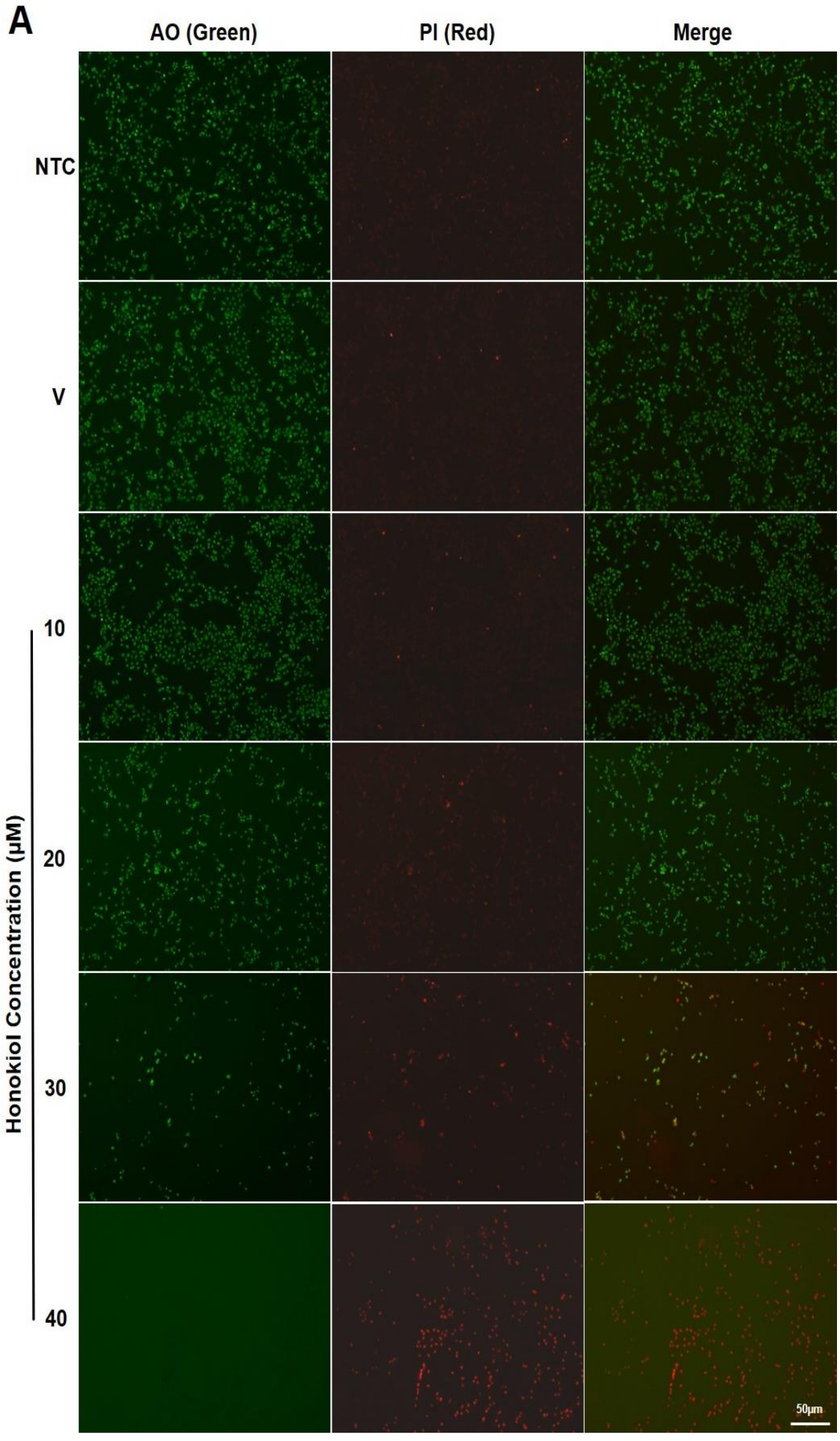
A
AO (Green)
PI (Red)
Merge
NTC
V
10
20
30
40
Honokiol Concentration (μM)
50μm

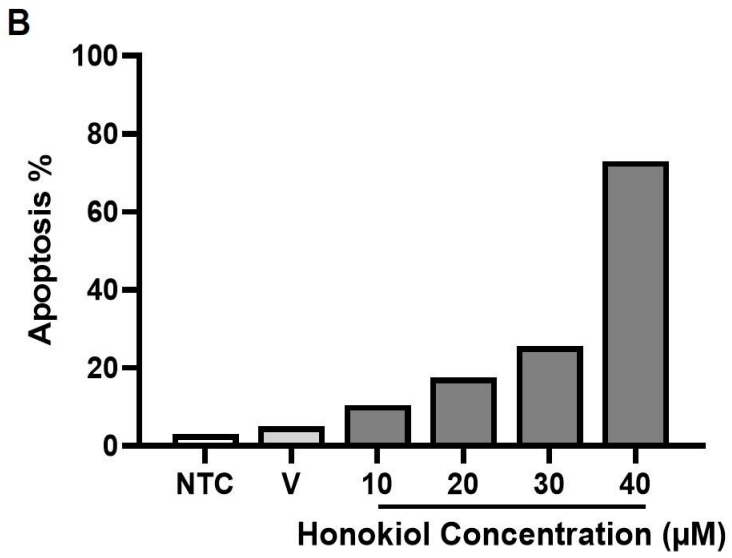

Figure 3.5. Honokiol induces apoptosis in human A375 melanoma cells in a concentration-dependent manner. A375 cells were seeded in 6-well plates and incubated for 24 hours. Cells were non-treated (**NTC**) or treated with increasing concentrations of honokiol (10μM, 20μM, 30μM, 40μM). The percentage of DMSO as vehicle control (**V**) was 0.05%, since this reflected the maximum percentage of DMSO that cells were exposed to when treating with HNK at a concentration of 40μM. (**A**) Acridine orange (**AO**, emit green fluorescence) and propidium iodide (**PI**, emit red fluorescence) solutions were directly added to the cells and representative images were shown. (**B**) Approximately 100 - 200 nuclei were counted per image and 5 images per treatment were captured. Data represent the mean percentage apoptosis (n=1).

3.2.3. Large numbers of A375 cells are detected in the later stage of apoptosis in response to honokiol at concentrations of 30μM and 40μM.

To clarify the stage of apoptotic cell death in A375 cell population following HNK treatment, flow cytometry analysis by using Annexin V and propidium iodide (PI) apoptosis assay was conducted. Annexin V / PI apoptosis assay is based on the principle that healthy cells are hydrophobic and phosphatidyl serine is expressed in the inner membrane, which is facing the cytosolic side (Abbady et al., 2017, Lakshmanan and Batra, 2013, Rieger et al., 2011). In the early stages of apoptosis, the phosphatidyl serine is translocated from the inner to outer plasma membrane, and thus the exposed phosphatidyl serine is detected by Annexin V. The necrotic and late apoptotic cells lose the integrity of plasma membrane, which allow PI to pass through the plasma membrane, bind to nucleic acids and thus display red florescence (Abbady et al., 2017, Lakshmanan and Batra, 2013, Rieger et al., 2011).

As shown in the dot plots (**Figure 3.6A**), the cells in left-lower quadrant (Annexin V-/PI-) represent healthy population, whereas the cells in the right-lower quadrant (Annexin V+/PI-) appeared to be undergoing early apoptosis. Late apoptosis was demonstrated in right-upper quadrant (Annexin V+/PI+) and necrosis was observed in the left-upper quadrant (Annexin V-/PI+). **Figure 3.6B** reveals that a large number of cells were detected in the later stage of apoptosis in response to HNK at concentrations of 30μM and 40μM. The percentage of necrotic cells appeared to be higher at 30μM of HNK than that of necrotic cells at a concentration of 40μM, suggesting that more independent replicates are required to evaluate differences and variations in the experiments. These data indicate that larger numbers of apoptotic A375 cells are detected in the later

stage in response to 30µM and 40µM HNK. Together with the cell viability data, these findings demonstrate that HNK has cytotoxic properties against human melanoma cancer cells.

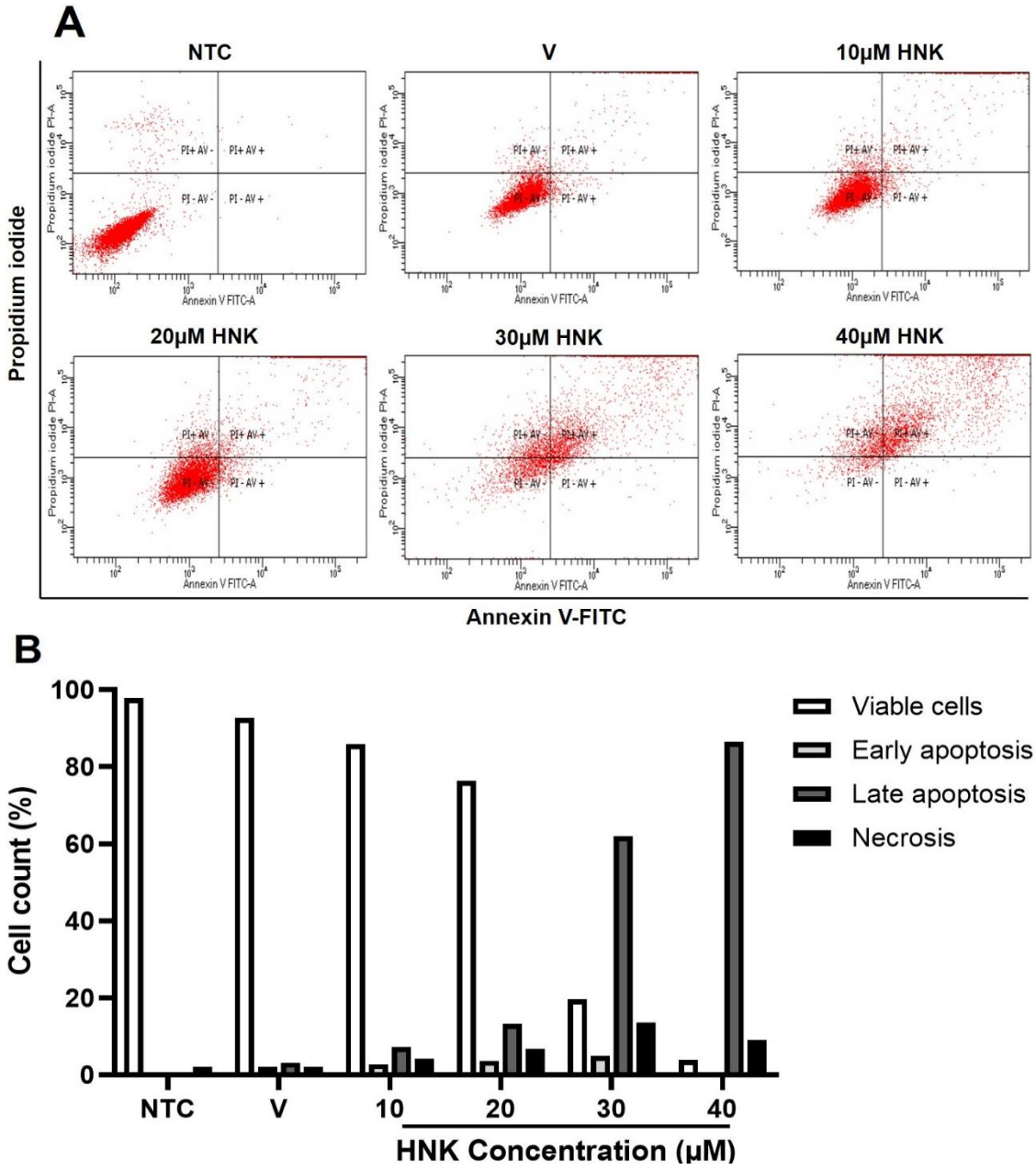

Figure 3.6. Large numbers of A375 cells are detected in the later stage of apoptosis in response to honokiol at concentrations of 30µM and 40µM. A375 cells were seeded in 6-well plates and incubated for 24 hours. Cells were non-treated (**NTC**) or treated with increasing concentrations of honokiol (10µM, 20µM, 30µM, 40µM). The percentage of DMSO as vehicle control (**V**) was 0.05%, since this reflected the maximum percentage of DMSO that cells were exposed to when treating with HNK at a concentration of 40µM. Annexin V (**AV**)

- fluorescein isothiocyanate (**FITC**) and propidium iodide (**PI**) apoptosis assay was performed and analysed by flow cytometry. (**A**) Cells population in lower left quadrant are viable. Cells in lower right quadrant represent early apoptosis. The upper right quadrant represents late apoptosis, and in upper left corner are cells at the necrosis. (**B**) Distribution of cells at death in different stages were quantified by flow cytometry. Values are presented in means of percentage of cell count (n=1).

3.2.4. Honokiol does not affect metabolic activity of human A375 melanoma cells until a concentration of 50μM is applied.

Mitochondrial respiration is another important physiological activity in tumour cells to maintain cellular proliferation (Antico Arciuch et al., 2012). Thus, the subsequent experiment was to examine effects of HNK on metabolic activities of A375 cells by an alamar blue assay. As shown in **Figure 3.7**, the percentage reduction of alamar blue in the HNK treatment groups (5μM, 10μM, 20μM, 30μM and 40μM) had no major difference from that in the non-treated control. However, treatment with 50μM HNK showed a significant decrease in percentage reduction of alamar blue compared to non-treated control (24 hours, 100.0 ± 0.0% NTC vs 68.85 ± 2.33% 50μM, $p<0.001$; 48 hours, 100.0 ± 0.0% NTC vs 69.12 ± 4.89% 50μM, $p=0.009$). These results demonstrate that HNK may not induce any significant effects to metabolic activities of A375 cells until a concentration of HNK ≥ 50μM is applied. However, this result was in contrast with the results from cell viability assays (**section 3.2.1**) and apoptosis assays (**sections 3.2.2** and **3.2.3**). The calculation of percentage reduction alamar blue is based on the absorbance of honokiol-treated groups and the absorbance of the corresponding concentrations of vehicle control (DMSO), and therefore it is not possible to present vehicle control data individually.

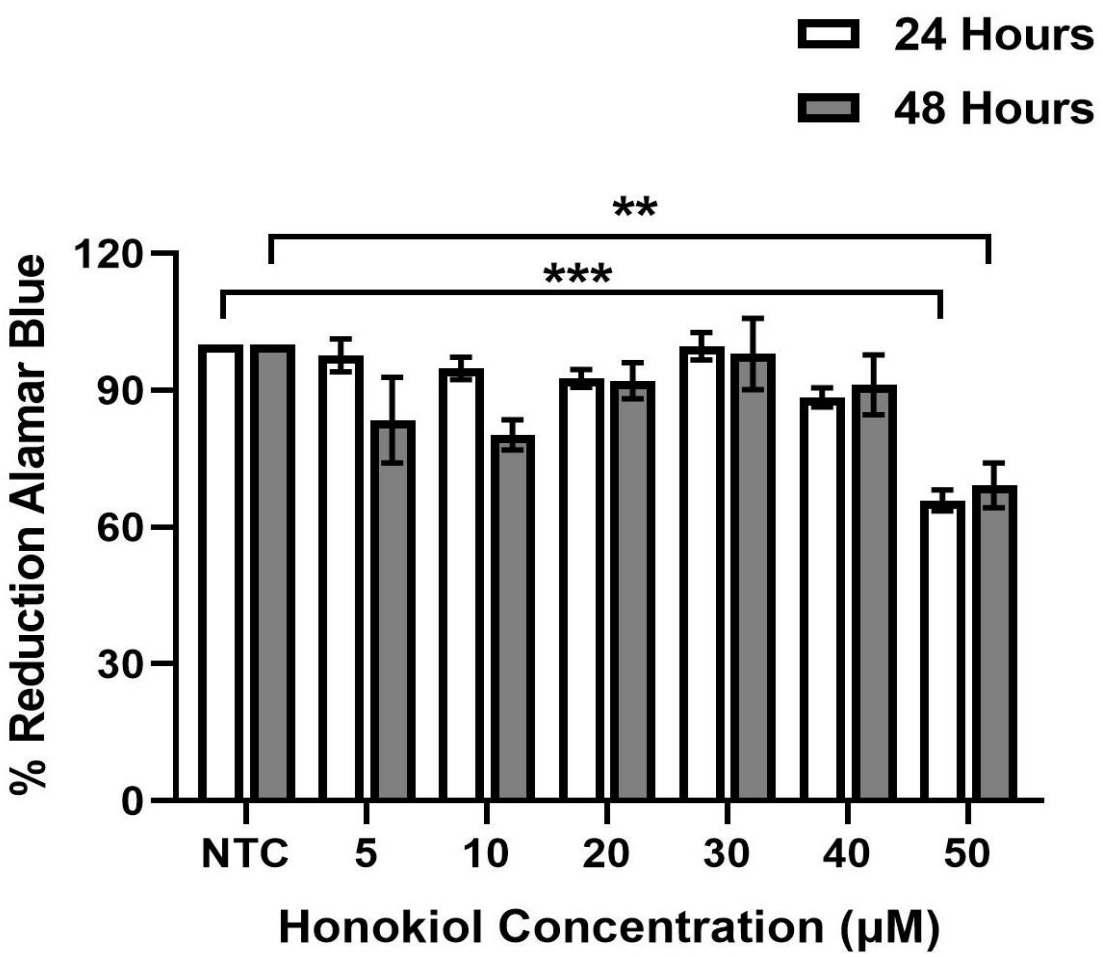

Figure 3.7. Honokiol does not affect metabolic activities of human A375 melanoma cells until a concentration of 50µM is applied. Human melanoma A375 cells were non-treated (**NTC**) or treated with increasing concentrations of honokiol (5µM, 10µM, 20µM, 30µM, 40µM, 50µM) for 24 and 48 hours. Cell metabolic activity, indicated by percentage reduction of alamar blue, was assessed spectrophotometrically at 600nm and 550nm. Data represent the mean percentage reduction alamar blue ± SEM (n=3). One-way ANOVAs with Tukey multiple comparisons test were performed to evaluate significance comparing the honokiol treatment to the NTC (**$p \leq 0.01$, ***$p \leq 0.001$).

3.2.5. Examination of altered cell morphology in response to honokiol treatment.

In cell viability assays, it was observed that treatment with 30μM and 40μM HNK induced morphological alterations. Filamentous actin (F-actin) cytoskeleton networks play a key role in regulating cellular shape and are responsive to change in mechanical forces during cell migration and division (Stricker et al., 2010, Wang et al., 2018). In order to determine whether HNK had any effect on cellular morphology, cells were stained with DAPI to detect DNA, and phalloidin 488 to detect F-actin. It was found that A375 cells developed a more elongated shape in HNK treatment (30μM and 40μM) group (**Figure 3.8E and 3.8F – arrowhead**) compared with non-treated control and vehicle control (**Figure 3.8A and 3.8B**). These data indicate that HNK may disrupt F-actin networks in A375 cells at concentrations of 30μM and 40μM.

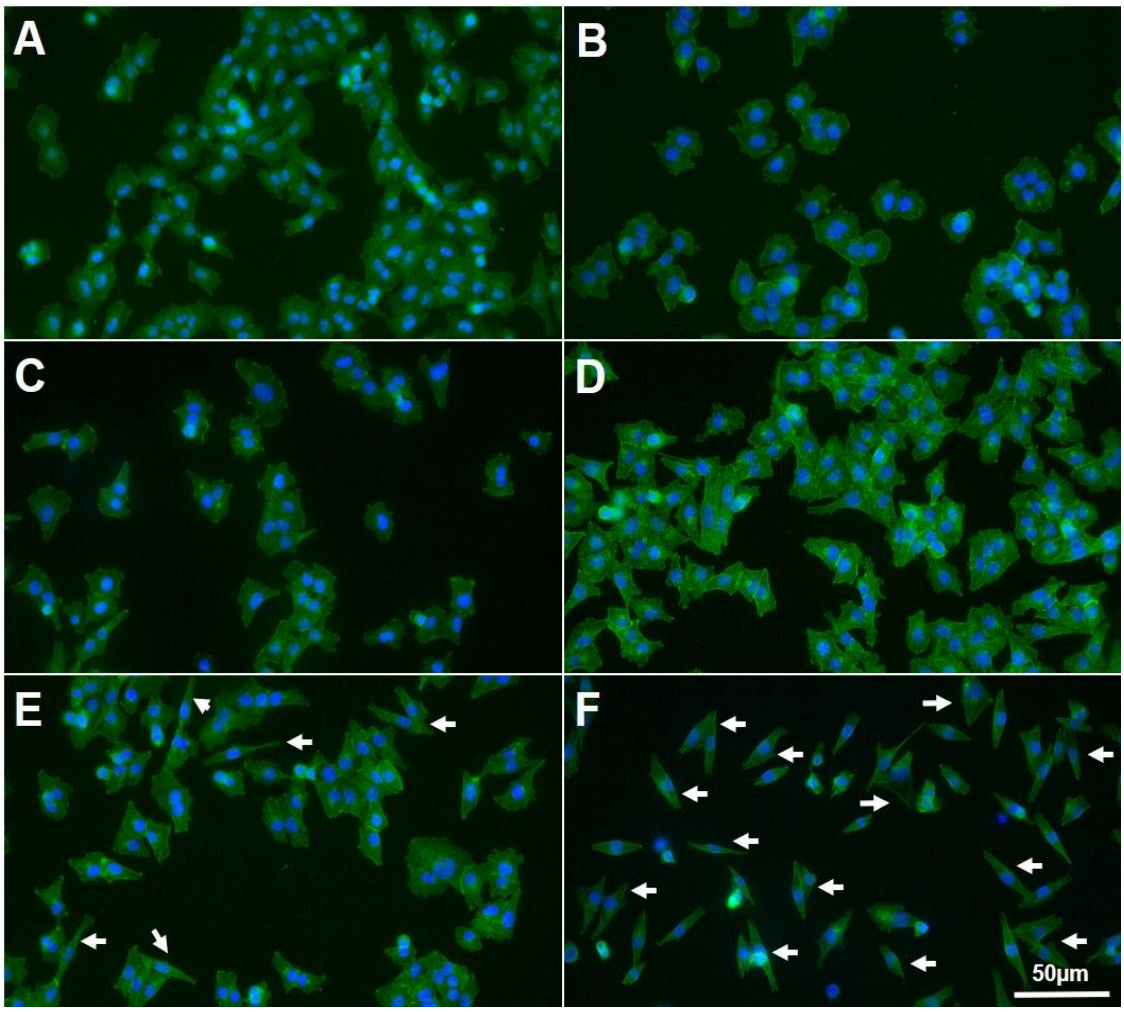

Figure 3.8. Human A375 melanoma cells have an elongated shape after honokiol treatment at concentrations of 30µM and 40µM. A375 cells were untreated (**A**) or treated with honokiol at concentrations of 10µM (**C**), 20µM (**D**), 30µM (**E**) and 40µM (**F**) for 24 hours and subjected to fluorescence analysis of filamentous actin. The percentage of DMSO as vehicle control (**B**) was 0.05%, since this reflected the maximum percentage of DMSO that cells were exposed to when treating with HNK at a concentration of 40µM. Nuclei were stained with DAPI (blue) and filamentous actin was stained with phalloidin (green) (n=1). **Arrowhead**: elongated cells.

3.2.6. Honokiol inhibits migration potential in human A375 melanoma cells in a concentration-dependent manner.

In order to determine if HNK would inhibit cell migration of human A375 melanoma cells, a wound healing assay was performed. In this assay, cells were permitted to grow to 100% confluence, and then a small scratch wound was administered using a pipette tip. Cells were then left untreated, treated with vehicle or increasing concentrations of HNK, and recovery of growth across the wound was analysed.

As shown in **Figure 3.9A**, following 24- and 48-hours incubation, in non-treated control, vehicle control (0.05% DMSO) and treatment with 10μM and 20μM HNK, the major wound area was covered by migrating melanoma cells. However, the major area of wound was less covered by the migrating melanoma cells treated with HNK at concentrations of 30μM and 40μM. The area of wound was quantified by Image J software, which uses an algorithm that permits an area to square pixel conversion (Ferreira and Rasband, 2012). The square pixel unit was calibrated to square micrometres according to Image J User Guide (Ferreira and Rasband, 2012). As shown in **Figure 3.9B** and **3.9C,** it was found that the area of wounds was significantly higher in HNK-treated groups as compared to non-treated control and vehicle control and this effect was in a concentration-dependent manner (24 hours, 20μM, p=0.03; 30μM, p<0.001; 40μM, p<0.001 respectively; 48 hours, 10μM, p=0.08; 20μM, p<0.001; 30μM, p<0.001; 40μM, p<0.001 respectively).

These results demonstrate that HNK dose-dependently inhibits the migration of highly metastatic A375 cells. Based on the combined results from cell viability, flow cytometry and wound healing assay, the changes in the indicators at 24h were obvious, thus, to investigate the molecular mechanism of anti-migration

effects in response to HNK, subsequent experiments were analysed at 24h time point. Furthermore, in order to compare two different concentrations of HNK, subsequent experiments were performed using 10μM and 30μM, since 10μM HNK did not elicit inhibitory effects in A375 cells, whilst a concentration of 30μM could generate significant inhibitory effects of A375 cells.

Altogether, these findings demonstrate that HNK has inhibitory effects on cellular proliferation, metabolic activities and migration capacities of A375 cells. It has also been indicated that HNK induces apoptotic effects and disrupts F-actin networks in A375 cells. Following the characterisation of HNK-mediated physiological and functional effects in A375 cells, the next method of analysis investigated the mRNA and protein expression of selected molecules that are known to be associated with tumour metastasis in HNK-treated A375 cells, in order to identify the exact molecular mechanisms of anti-metastatic effects of HNK in human melanoma cells.

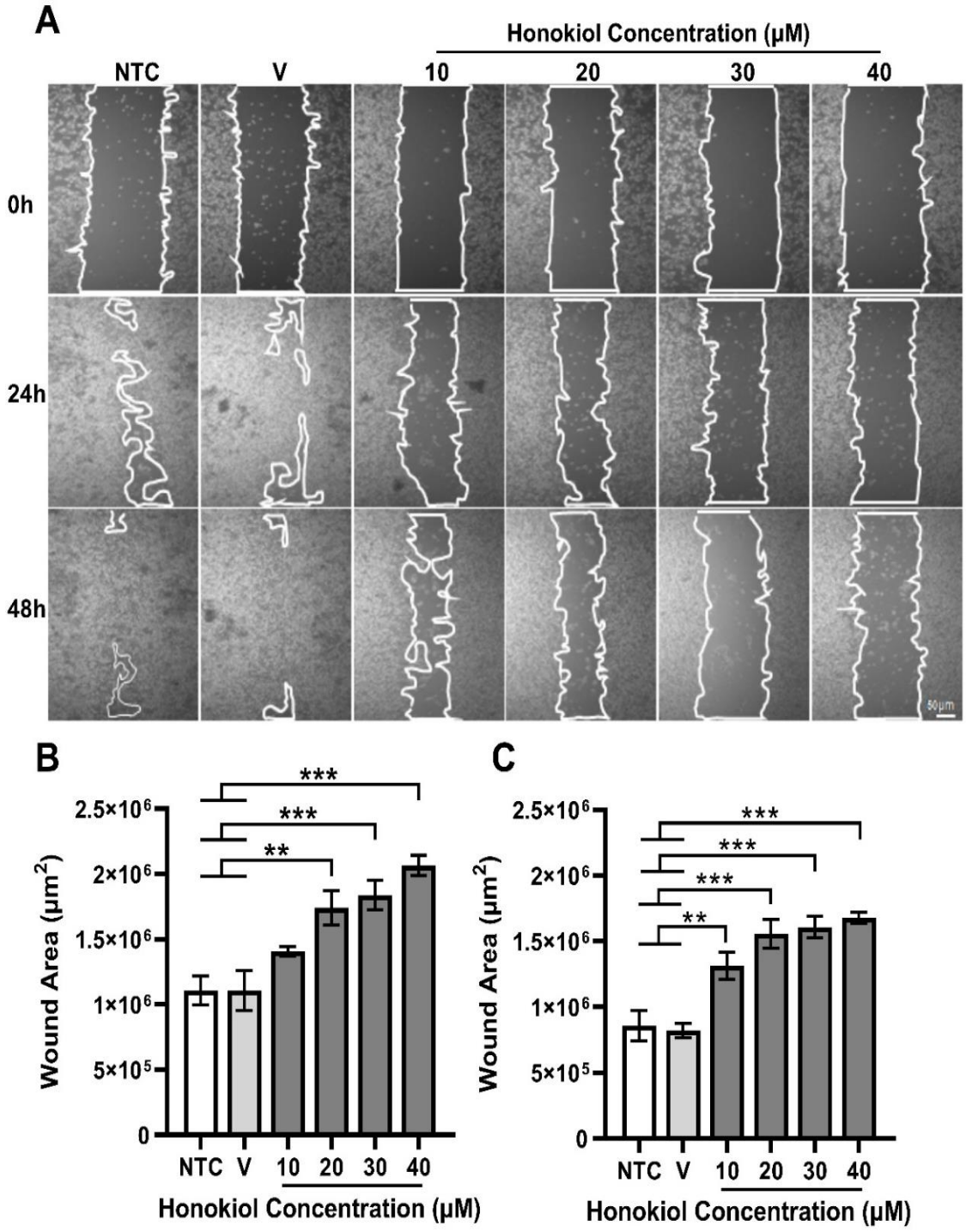

Figure 3.9. Honokiol inhibits migration potential in human A375 melanoma cells. A375 cells were cultured for 24 hours until a monolayer was formed and scratched with sterile pipette tips. Cells were non-treated (**NTC**) or treated with increasing concentrations of honokiol (10μM, 20μM, 30μM, 40μM). The percentage of DMSO as vehicle control (**V**) was 0.05%, since this reflected the maximum percentage of DMSO that cells were exposed to when treating with HNK at a concentration of 40μM. (**A**) Control (0 h) panel indicates the original

area of wound after making a scratch. The space between the solid white lines shows the area of wounds. The wound area at 24 hours (**B**) and 48 hours (**C**) post-treatment was measured by Image J software. Data represent the mean wound area (μm^2) ± SEM (n=3). One-way ANOVAs with Tukey multiple comparisons test were performed to evaluate significance comparing the honokiol treatment to the non-treated control and vehicle control (**$p \leq 0.01$, ***$p \leq 0.001$).

3.3. Investigating the molecular mechanisms of anti-metastatic effects of honokiol in human A375 melanoma cells.

HNK-mediated intracellular signalling has been demonstrated to generate different roles in physiological and pathological conditions, however, the molecular mechanisms underlying the involvement of HNK-mediated intracellular signalling in the regulation of tumour metastasis have yet to be fully elucidated (Ong et al., 2019). Therefore, to investigate the mRNA and protein expression of selected molecules that are known to be associated with tumour metastasis (KISS1, KISS1R, MMP-2, MMP-9, TIMP-4, NF-κB and VEGF-A) in HNK-treated A375 melanoma cells, qRT-PCR and immunoblotting analyses were conducted.

3.3.1. Assessment of RNA integrity and cDNA quality for the success of qRT-PCR.

Prior to performing qRT-PCR, it is important to assess the integrity of RNA, since the high integrity of RNA is one of the most critical elements for the overall success of qRT-PCR (Taylor et al., 2010, Desjardins and Conklin, 2010). In addition, using totally and partially degraded RNA samples can generate false negative results (Kuang et al., 2018, Fleige and Pfaffl, 2006). Therefore, Agilent

Bioanalyzer 2100 analysis was performed to assess the integrity of RNA samples.

As shown in **Figure 3.10A**, based on the gel-like image obtained from Agilent 2100 Bioanalyzer, two clear bands of 28S and 18S ribosomal RNA (rRNA) were observed in all samples. The size of rRNA bands were further confirmed by agarose gel electrophoresis (**Figure 3.10B**), it was observed that the molecular weight of 28S rRNA bands were approximately twice the molecular weight of the 18S rRNA bands (2000bp 28S rRNA vs 1000bp 18S rRNA). The entire electrophoretic trace of eukaryotic total RNA can also be quantified by Agilent 2100 Bioanalyzer according to the proprietary algorithms, based on a numbering system from 1.0 to 10.0, in which an RNA integrity number (RIN) of 1.0 corresponds to the most degraded and 10.0 corresponds to the most intact (Schroeder et al., 2006, Taylor et al., 2010). According to the minimum information for publication of quantitative real-time PCR experiments (MIQE) guidelines, RNA samples presenting RIN values above 8.0 is recommend to produce reliable quantification of messenger RNA (mRNA) expression by qRT-PCR (Bustin et al., 2009). It was shown that RIN values in all RNA samples were ranged from 8.5 to 10.0, and all RNA samples had relatively strong and clear 18S and 28S peaks (**Appendix A**). Thus, RIN values together with the 2:1 ratio rRNA bands (28S 2000bp vs 18S 1000bp) that can be seen in the gel indicate all groups had intact and high-quality RNA samples to produce the most reliable and efficient quantification of mRNA expression in qRT-PCR analyses.

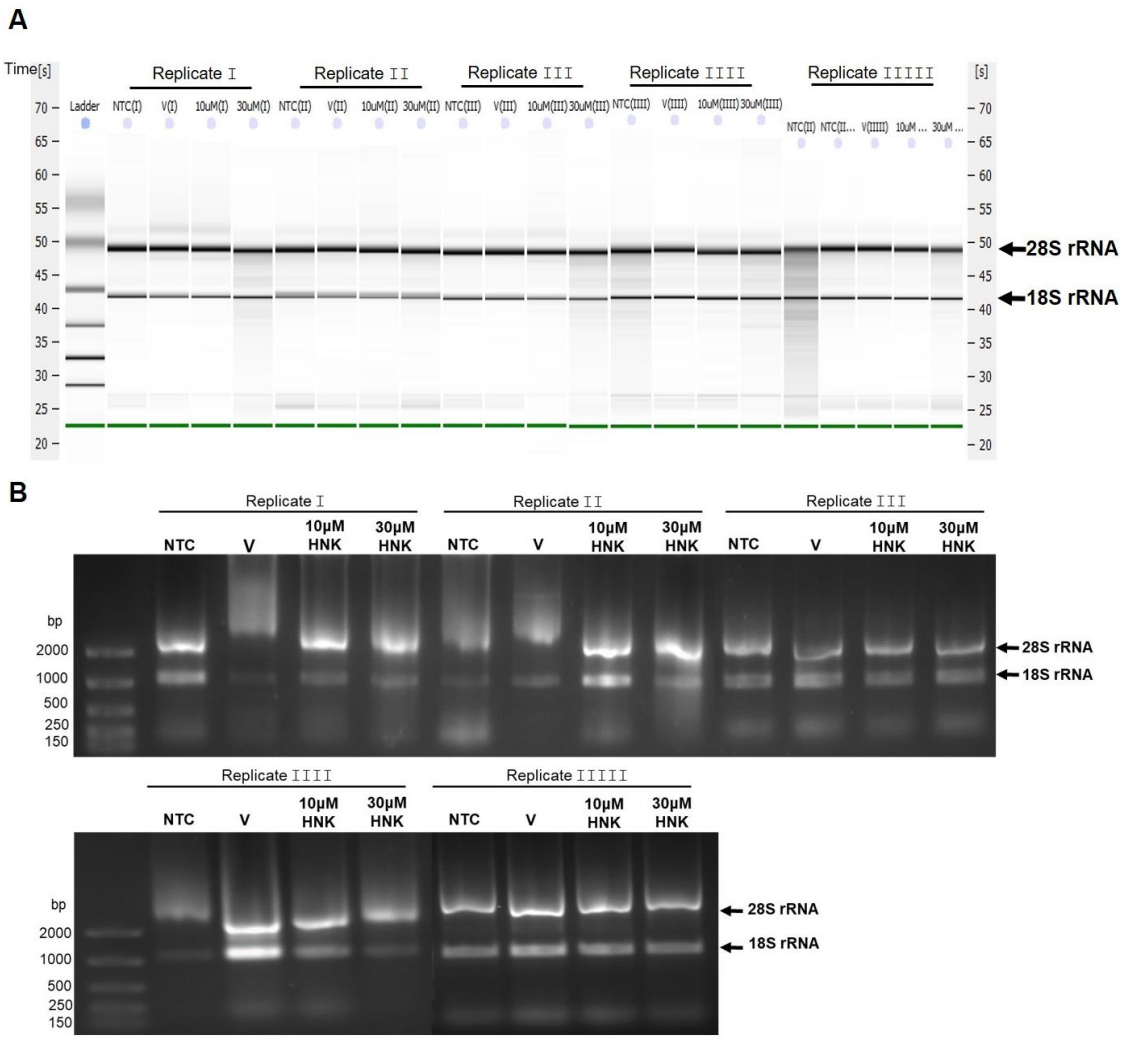

Figure 3.10. The gel illustration of RNA integrity from five biologically independent replicates. Human melanoma A375 cells were non-treated (**NTC**) or treated with honokiol (**HNK**) (**10μM** and **30μM**) for 24 hours. The percentage of DMSO as vehicle control (**V**) was 0.0375%, since this reflected the maximum percentage of DMSO that cells were exposed to when treating with HNK at a concentration of 30μM. Total RNA was isolated by TRIzol reagent, RNA integrity was assessed by the digital gel obtained with the Agilent 2100 Bioanalyzer (**A**) and the size of ribosomal RNA (**rRNA**) bands were further confirmed by 1% (w/v) agarose electrophoresis (28S 2000bp vs 18S 1000bp) (**B**). [**s**]: seconds. **bp**: base pairs.

Following the identification of RNA integrity, total RNA was reverse transcribed to cDNA and the successful cDNA synthesis was confirmed by end-point PCR using reference *GAPDH* primers (**Table 2**) as suggested by Cen et al. (2018). Using 1% (w/v) agarose gel electrophoresis (**Figure 3.11**), a clear amplicon at 101bp was detected in all samples (non-treated control, vehicle control, 10μM and 30μM HNK treatment in five biological replicates), which indicated that the cDNA synthesis was successful. Faint bands were observed in control groups (no reverse transcriptase and no cDNA template) and the size of these bands was smaller than 100bp, indicating primer dimers. Altogether, these findings indicate that all samples had intact and good quality RNA samples to ensure reliable and efficient quantification of mRNA expression in the following qRT-PCR analyses.

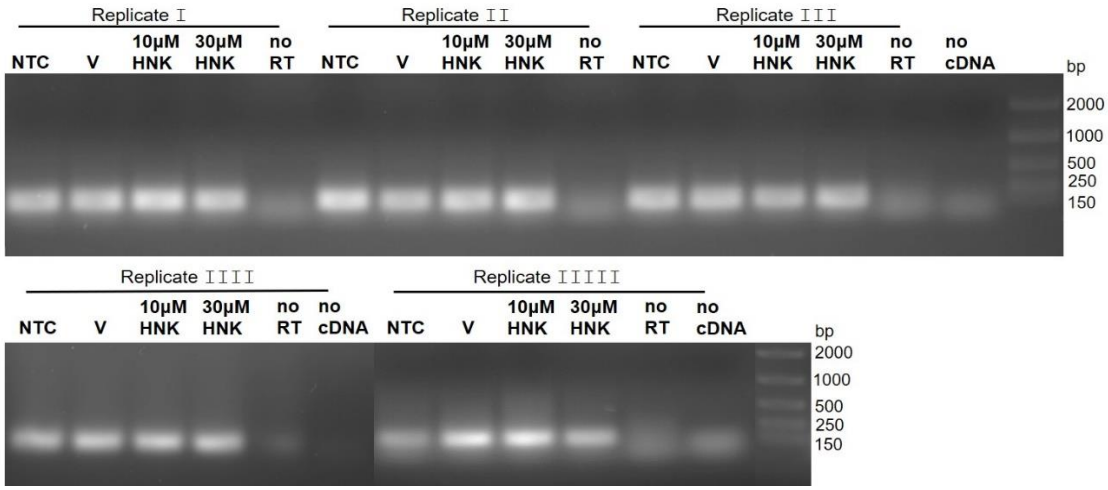

Figure 3.11. Quality of cDNA synthesis in 1% (w/v) agarose gel. Human melanoma A375 cells were non-treated (**NTC**) or treated with honokiol (**HNK**) (10μM and 30μM) for 24 hours. The percentage of DMSO as vehicle control (**V**) was 0.0375%, since this reflected the maximum percentage of DMSO that cells were exposed to when treating with HNK at a concentration of 30μM. Total RNA was isolated and converted RNA to complementary DNA (**cDNA**) using a reverse transcriptase (**RT**) enzyme. The success of cDNA synthesis was assessed by end-point PCR using glyceraldehyde 3-phosphate dehydrogenase

(*GAPDH*) primers. The expected size of the PCR product (*GAPDH*) was 101bp. **bp**: base pairs.

3.3.2. Effects of honokiol on the mRNA expression of selected metastasis-associated molecules in human A375 melanoma cells.

In order to investigate whether HNK regulated the expression of selected metastasis-associated genes, qRT-PCR analyses were carried out on untreated and HNK-treated (with 10μM and 30μM for 24h) A375 cells and the expression level of the mRNA for each transcript was compared. As shown in **Figure 3.12**, **Figure 3.13** and **Figure 3.14**, upon treatment with 30μM HNK for 24 hours, *KISS1* mRNA expression was significantly upregulated by 2.96±0.36-fold compared to the vehicle-treated control group (p=0.031). In addition, HNK significantly downregulated mRNA expression of *MMP-2* by 0.55±0.09-fold compared to the vehicle-treated control group (p=0.43). There were no significant differences in the mRNA expression of *KISS1R* (1.80±0.62), *VEGF-A* (2.49±0.44), *NF-κB* (1.31±0.12), *MMP-9* (5.28±2.45) and *TIMP-4* (4.70±0.54) upon HNK treatment. These findings demonstrate that HNK alters the expression of selected molecules that are known to be involved in either remodelling the extracellular matrix (*MMP-2*, *MMP-9* and *TIMP-4*), regulating transcription (*NF-κB*) or angiogenesis (*VEGF-A*). HNK also markedly upregulated metastasis-suppressor gene *KISS1* and its receptor, *KISS1R* in A375 cells, implying that KISS1 / KISS1R signalling pathway may be involved in the HNK-mediated molecular mechanisms.

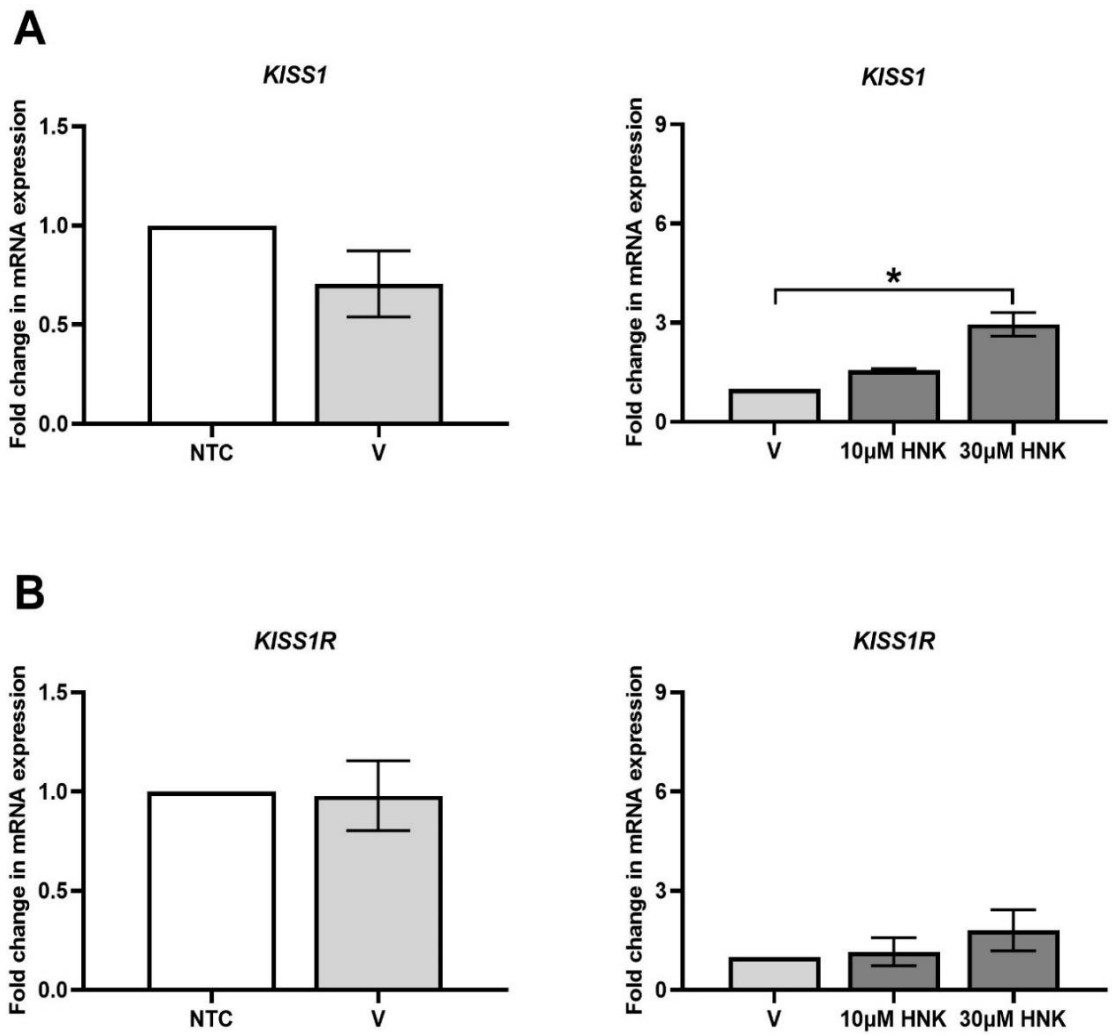

Figure 3.12. Effects of honokiol on *KISS1* and *KISS1R* mRNA expression in human A375 melanoma cells. A375 cells were non-treated (**NTC**) or treated with honokiol (**HNK**) (10μM and 30μM) for 24 hours. The percentage of DMSO as vehicle control (**V**) was 0.0375%, since this reflected the maximum percentage of DMSO that cells were exposed to when treating with HNK at a concentration of 30μM. Relative mRNA expression of kisspeptin (***KISS1***) (**A**) and kisspeptin receptor (***KISS1R***) (**B**) was analysed by qRT-PCR following total RNA extraction and reverse transcription. Samples for each experimental group were performed in duplicate and normalised to glyceraldehyde 3-phosphate dehydrogenase (*GAPDH*) mRNA levels as a housekeeping gene. For **NTC vs Vehicle**: results are represented as fold-changes in vehicle-treated control over non-treated cells. For **Vehicle vs HNK**: results are expressed as fold-changes in HNK-treated group over vehicle-treated control. Statistical analysis was performed on ΔC_T values *via* one-way ANOVA with Tukey multiple comparisons test (*$p \leq 0.05$). Data represent mean values ± SEM (n = 3).

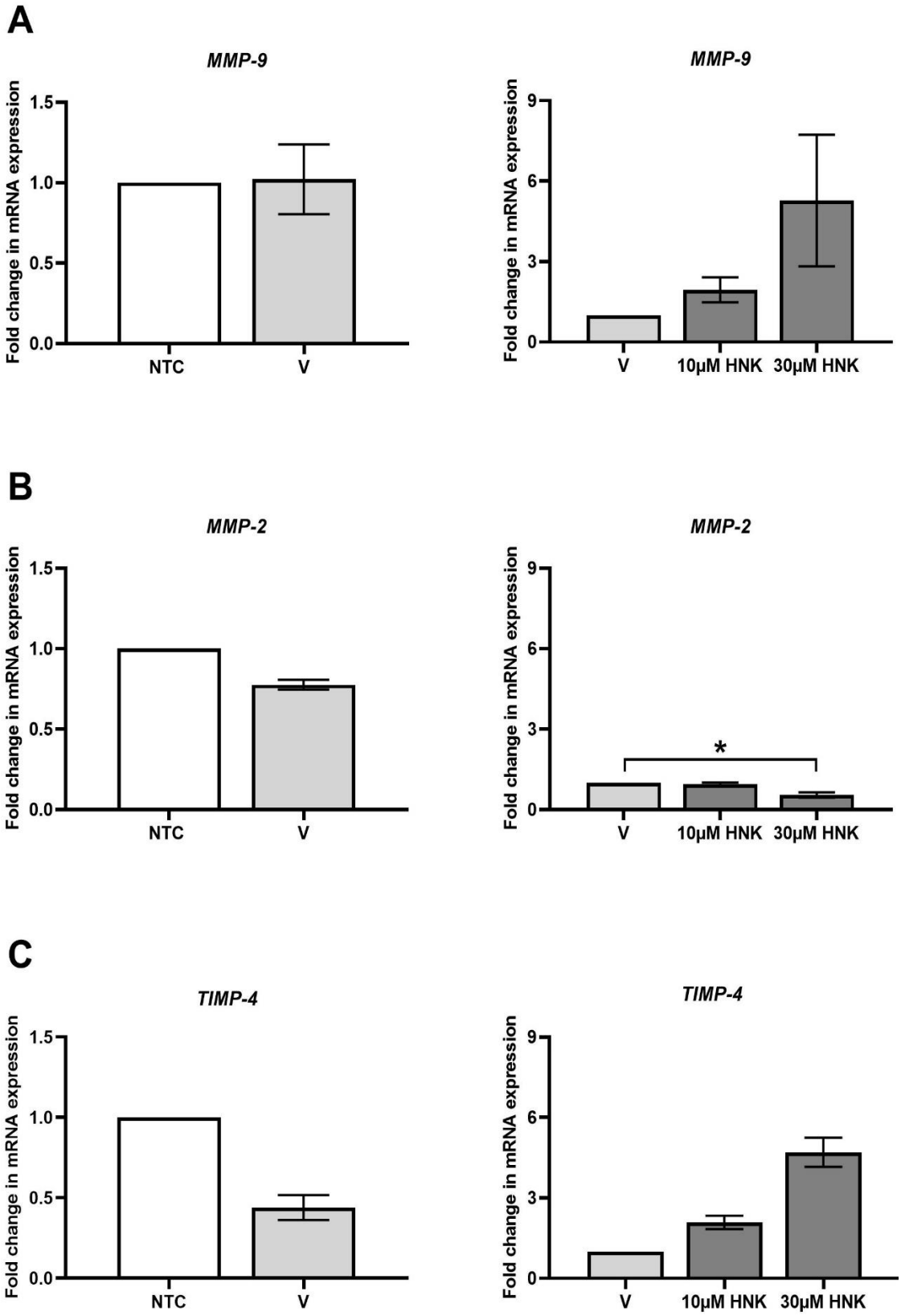

Figure 3.13. Effects of honokiol on *MMP-9*, *MMP-2* and *TIMP-4* mRNA expression in human A375 melanoma cells. A375 cells were non-treated (**NTC**) or treated with honokiol (**HNK**) (10μM and 30μM) for 24 hours. The percentage of DMSO as vehicle control (**V**) was 0.0375%, since this reflected

the maximum percentage of DMSO that cells were exposed to when treating with HNK at a concentration of 30µM. Relative mRNA expression of matrix metalloproteinase-9 (***MMP-9***) (**A**), matrix metalloproteinase-2 (***MMP-2***) (**B**) and tissue inhibitor of metalloprotease-4 (***TIMP-4***) (**C**) was analysed by qRT-PCR following total RNA extraction and reverse transcription. Samples for each experimental group were performed in duplicate and normalised to glyceraldehyde 3-phosphate dehydrogenase (*GAPDH*) mRNA levels as a housekeeping gene. For **NTC vs Vehicle**: results are represented as fold-changes in vehicle-treated control over non-treated cells. For **Vehicle vs HNK**: results are expressed as fold-changes in HNK-treated group over vehicle control. Statistical analysis was performed on ΔC_T values *via* one-way ANOVA with Tukey multiple comparisons test (*$p \leq 0.05$). Data represent mean values ± SEM (n = 3).

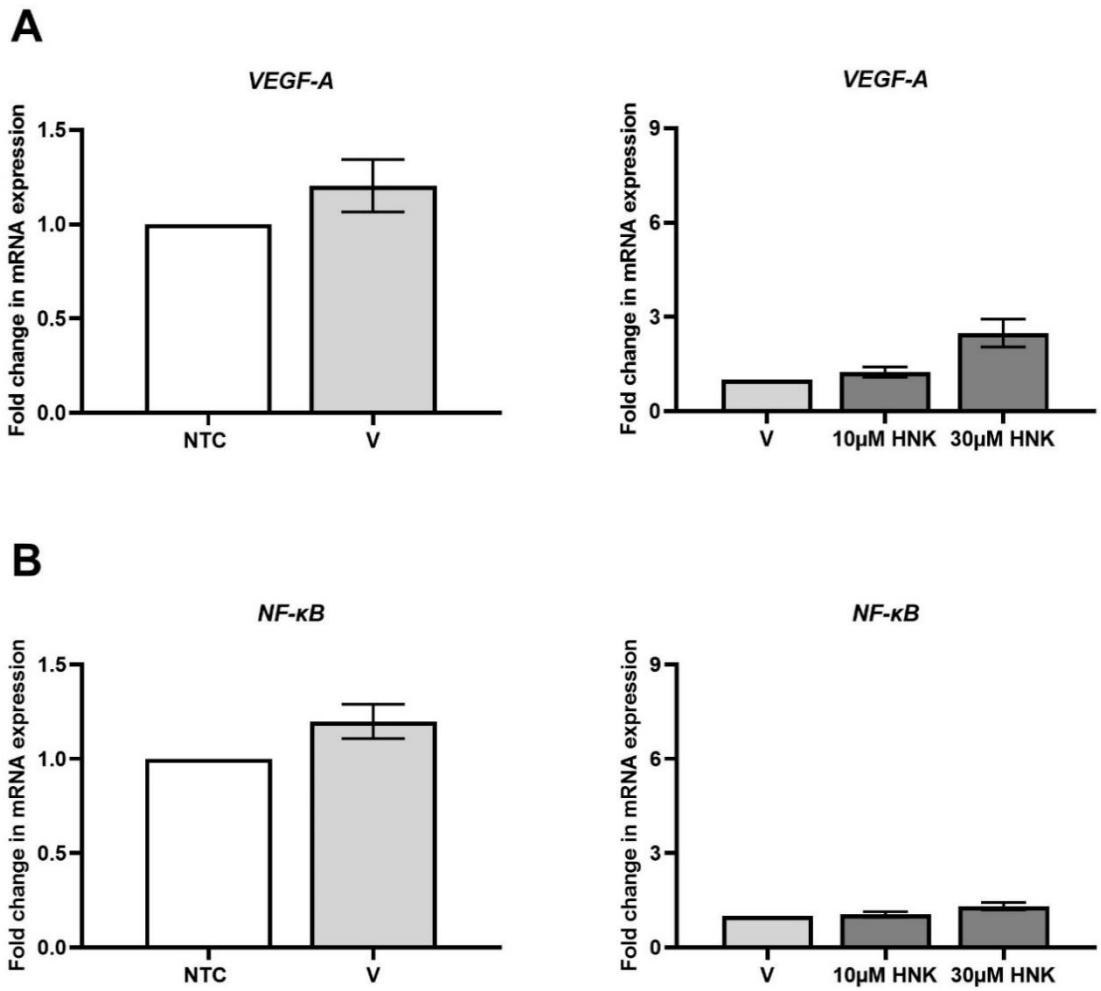

Figure 3.14. Effects of honokiol on *VEGF-A* and *NF-kB* mRNA expression in human A375 melanoma cells. A375 cells were non-treated (**NTC**) or treated with honokiol (**HNK**) (10μM and 30μM) for 24 hours. The percentage of DMSO as vehicle control (**V**) was 0.0375%, since this reflected the maximum percentage of DMSO that cells were exposed to when treating with HNK at a concentration of 30μM. Relative mRNA expression of vascular endothelial growth factor A (***VEGF-A***) (**A**) and nuclear factor kappa B (***NF-κB***) (**B**) was analysed by qRT-PCR following total RNA extraction and reverse transcription. Samples for each experimental group were performed in duplicate and normalised to glyceraldehyde 3-phosphate dehydrogenase (*GAPDH*) mRNA levels as a housekeeping gene. For **NTC vs Vehicle**: results are represented as fold-changes in vehicle-treated control over non-treated cells. For **Vehicle vs HNK**: results are expressed as fold-changes in HNK-treated group over vehicle-treated control. Statistical analysis was performed on ΔC_T values *via* one-way ANOVA with Tukey multiple comparisons test, there was no statistically significant difference. Data represent mean values ± SEM (n = 3).

3.3.3. Optimisation of Western blotting

Initially, this study has attempted a series of experimental parameters, in order to optimise conditions for immunoblotting to examine protein of interest including: blotting membranes (nitrocellulose membranes vs polyvinylidene difluoride membrane; pore sizes of 0.2µm vs 0.45µm), transfer buffers (Towbin transfer buffer vs Bis-Tris transfer buffer), primary antibodies (Abcam vs Sigma) and secondary antibodies (goat anti-mouse IgG or goat anti-rabbit IgG at 800nm channel vs at 680nm channel). Despite these different approaches, no detectable bands were observed for KISS1 and KISS1R protein, therefore, an alternative approach was taken.

3.3.3.1. Troubleshooting: no protein bands following KISS1 and KISS1R primary antibody incubation.

In order to troubleshoot the issue of no bands following KISS1 and KISS1R primary antibody incubation, *KISS1* and *KISS1R* genes were overexpressed in A375 cells to upregulate the protein levels. The first step was to analyse two commercially available OriGene plasmids containing *KISS1* and *KISS1R* cDNA. The *KISS1* and *KISS1R* plasmids were cleaved by XhoI restriction enzyme and the digested plasmids were examined by agarose gel electrophoresis. As shown in **Figure 3.15**, it was observed that the size of cleaved *KISS1* and *KISS1R* plasmids were around 5000 base pair (bp) and 6000 bp respectively, which was the correct fragment size according to the manufacture's datasheet (*KISS1* plasmid: 5300bp; *KISS1R* plasmid: 6100bp). Undigested plasmids run at higher molecular weight due to maintained circular conformation, supercoiled or superhelical formation, and this was as expected (Lee et al., 2012b, Levy et al., 2000). These findings indicate that *KISS1* and *KISS1R* plasmids are good quality to use in the subsequent transfection experiments.

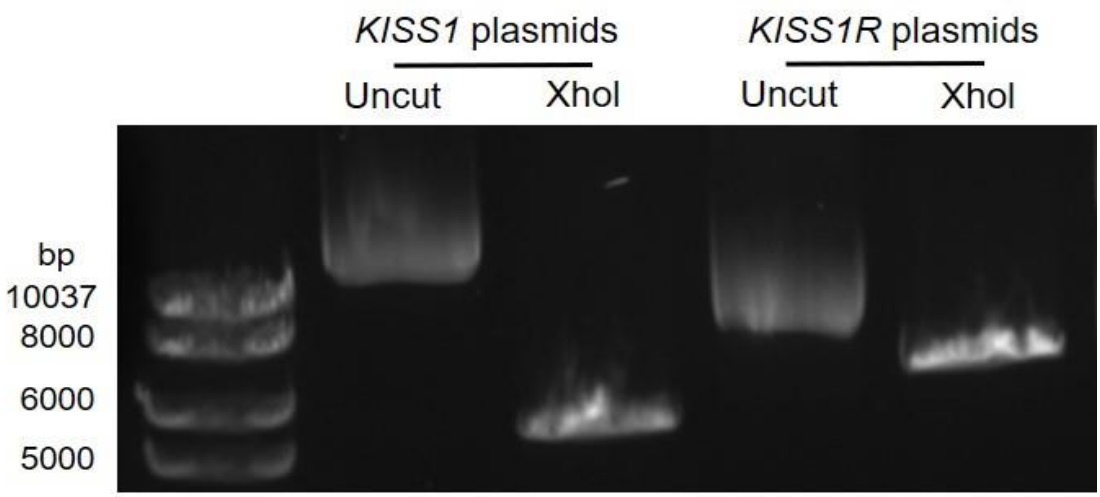

Figure 3.15. Agarose gel electrophoresis of cleaved and uncut *KISS1* and *KISS1R* plasmids. *KISS1* and *KISS1R* plasmids were cleaved by XhoI restriction enzyme. 1% (w/v) agarose gel electrophoresis was performed to indicate the quality of DNA plasmids. **bp**: base pair.

Following the assessment of plasmid quality, and prior to transfecting *KISS1* and *KISS1R* DNA plasmids, it was important to identify the most effective transfection amounts of plasmid DNA in A375 cells. Therefore, various amounts of vehicle control plasmid pmaxGFP (500ng, 1µg and 2µg) were introduced into A375 cells. Following post-transfection, cells were fixed to a glass slide and stained with DAPI. The number of fluorescent cells was counted in a random area (three areas were counted in each group), which is summarised in **Appendix B**. The achieved transfection rate was 30.94% ± 2.57, 59.71% ± 3.14 and 91.02% ± 1.51 at an amount of 500ng, 1µg and 2µg, respectively (**Figure 3.16**). This suggested that an amount of 2µg plasmid generated the highest transfection rate in A375 cells. Based on these results, *KISS1* or *KISS1R* plasmid DNA amount at 2µg was chosen for the subsequent overexpression experiments.

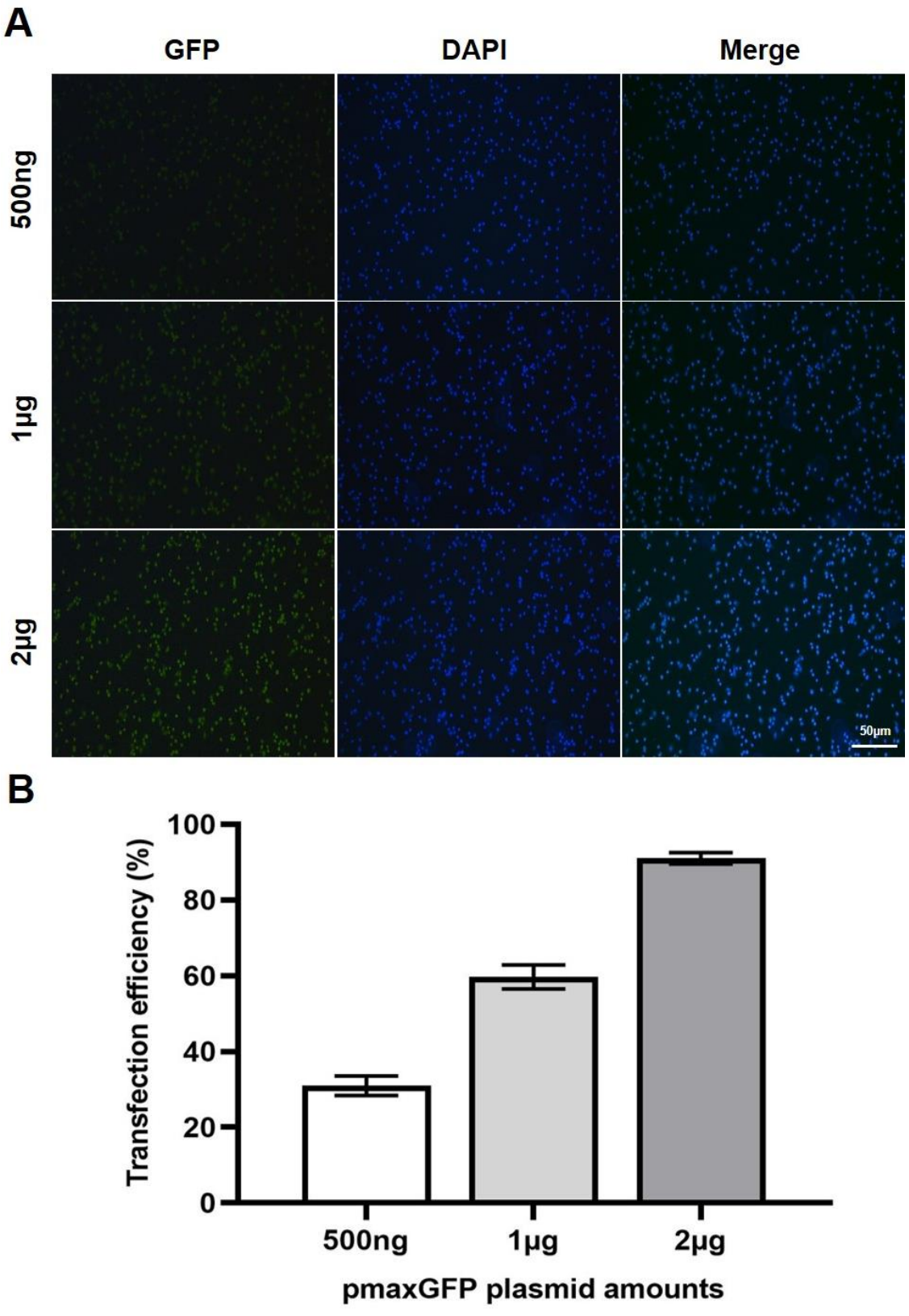

Figure 3.16. Transfection efficiency of pmaxGFP plasmids in A375 melanoma cells. A375 cells were transfected by nucleofection with increasing amounts of pmaxGFP plasmids (500ng, 1µg and 2µg) and incubation for 24 hours. Cells were mounted with DAPI (blue) to stain nuclear. (**A**) Three random

fields were imaged in each group and representative images were shown. (**B**) Percentage of transfected cells normalised to total DAPI cells (in a random field) was quantified. Data represents mean value ± SD (three area were count in each condition, n=1).

A375 cells were transfected with the pmaxGFP vector (2µg) served as a vehicle control to indicate the success of transfection, since green fluorescent proteins (GFP) exhibited green fluorescence when exposed to light (at a wavelength of 488nm) under fluorescence microscopy (**Figure 3.17**). Following the successful transfection of *KISS1* and *KISS1R* plasmids (2µg), immunoblotting was performed in order to test the effectiveness of KISS1 and KISS1R primary antibody. Coomassie blue staining could not be performed due to insufficient quantity of protein samples. Ponceau S staining did not work as polyvinylidene difluoride membrane will not stain with ponceau. However, it was observed that KISS1R primary antibody could specifically detect the correct size of protein bands of 43 kilodalton (**Figure 3.18**). Unfortunately, no bands were observed following KISS1 primary antibody incubation, indicating antibody may have lost activity due to storage (**Figure 3.18**). These findings demonstrate that KISS1R primary antibody can specifically detect the correct size of protein band, whereas the KISS1 primary antibody fails to detect any protein bands. Therefore, this study is only able to show the protein expression of KISS1R in the subsequent immunoblotting analyses.

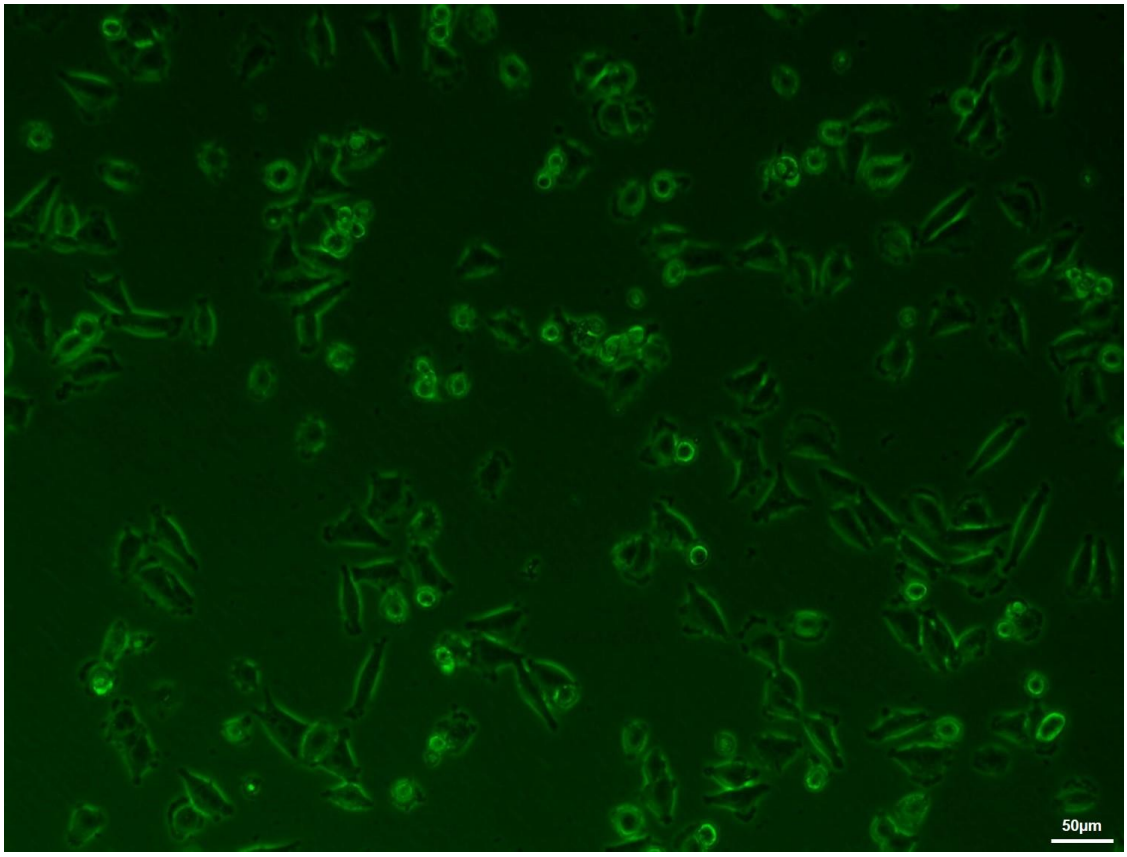

Figure 3.17. The success of transfection is indicated by pmaxGFP vector. A375 cells were imaged directly on culture plates after 24 hours transfection, cells were successfully transfected exhibiting green light under fluorescence microscopy at a wavelength of 488nm. GFP: green fluorescent protein.

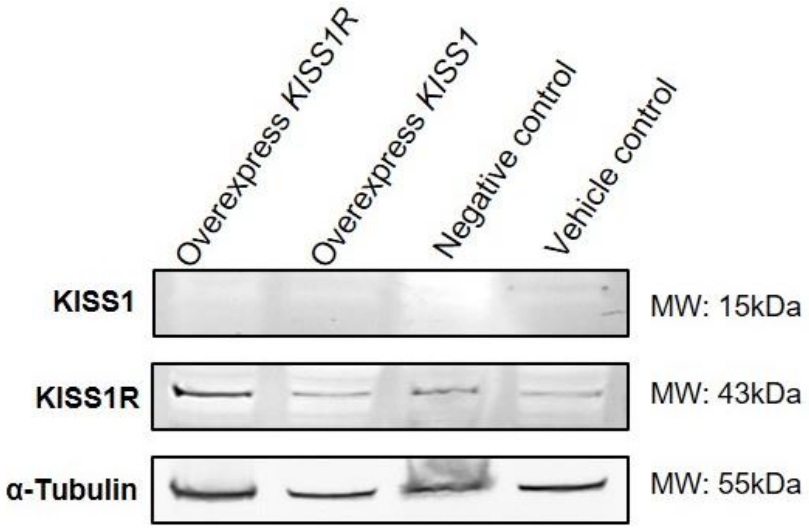

Figure 3.18. **Western blots following overexpression of *KISS1* and *KISS1R* in A375 melanoma cells.** Protein was extracted in 24 hours post-transfection

with 2µg kisspeptin (***KISS1***) and 2µg kisspeptin receptor (***KISS1R***) plasmids, then immunoblotting was performed. Cells that were transfected with 2µg pmaxGFP vector served as the vehicle control. Cells that were not transfected served as the negative control (n=1). **α-Tubulin**: alpha tubulin. **MW**: molecular weight. **kDa**: kilodalton.

3.3.3.2. Identifying the effective protein extraction method for human A375 melanoma cell line.

Following establishment of immunoblotting conditions, this study then compared two experimental groups (**Group A** and **Group B**) to identify the most effective lysis buffer to extract protein in A375 cells and the best method to generate equal amount of protein concentration in loading controls.

Group A. A375 cells were extracted by radioimmunoprecipitation assay (RIPA) buffer and protein concentrations were quantified by the Lowry protein assay.

Group B. A375 cells were extracted by SDS and DTT and protein concentrations were dependent on the same amount of cell number.

As shown in **Figure 3.19**, an immunoblot of group A has higher background than that of group B. Proteins extracted from A375 cells were more soluble in group B, and the protein bands were better resolved compared to group A, suggesting group B was the better protein extraction method than group A. These data indicate that SDS and DTT is the most appropriate lysis buffer to extract protein in A375 cells.

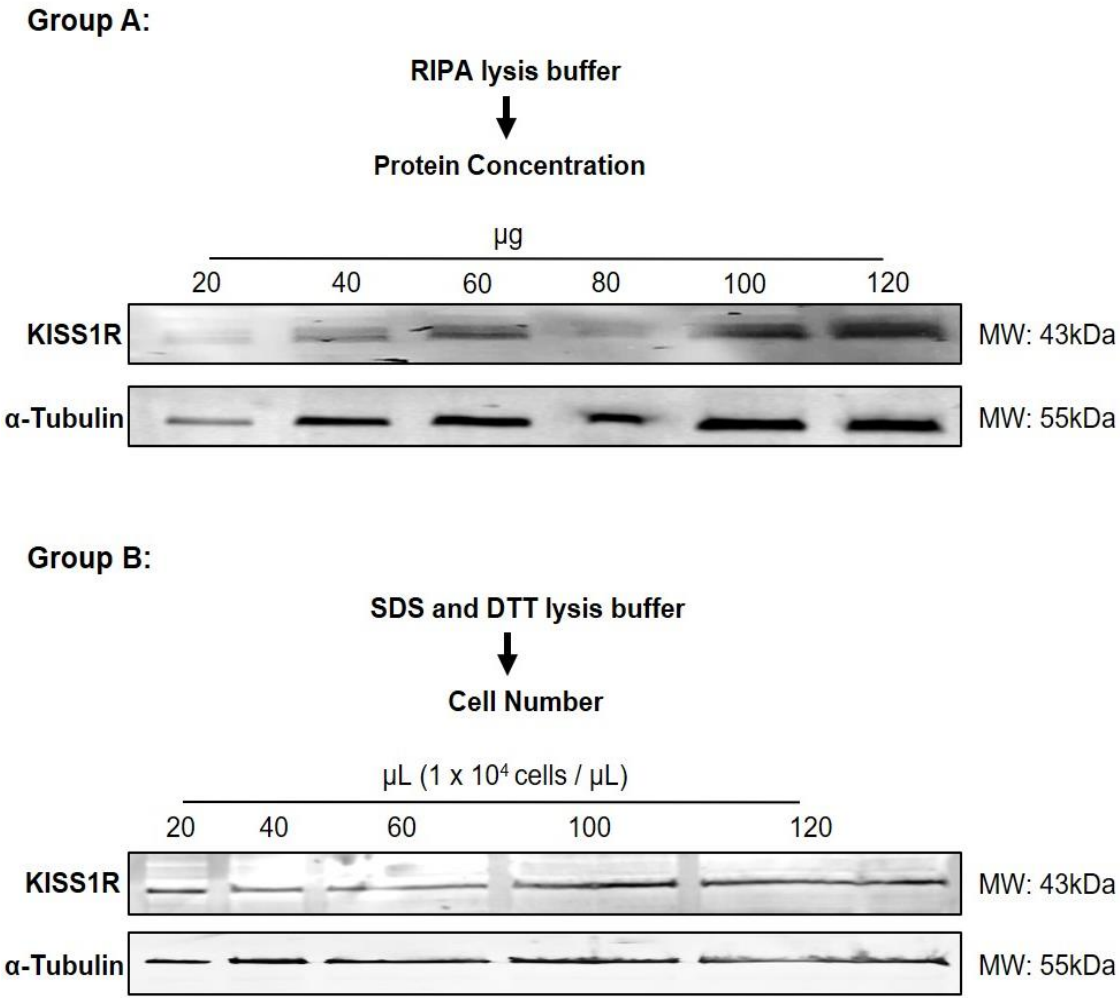

Figure 3.19. Identifying the most effective lysis buffer to extract protein in human A375 melanoma cells. (**Group A**) Proteins were extracted by radioimmunoprecipitation assay (**RIPA**) lysis buffer and quantified by the Lowry protein assay. (**Group B**) Proteins were extracted by sodium dodecyl sulfate (**SDS**) and dithiothreitol (**DTT**) lysis buffer and quantification was dependent on the number of cells (1 x 10^4 cells / µL). An increase protein concentration or cell number was loaded and analysed by immunoblotting. **KISS1R**: kisspeptin receptor. **α-Tubulin**: alpha tubulin. **MW**: molecular weight. **kDa**: kilodalton. **µg**: microgram. **µL**: microliter.

3.3.4. Effects of honokiol on the KISS1R, MMP-9, NF-κB and TIMP-4 protein expression in A375 melanoma cells.

In order to identify whether HNK also affected the expression of selected tumour-associated molecules (KISS1R, MMP-9, NF-κB and TIMP-4) at the translational levels, immunoblotting analyses were performed. In agreement with the qRT-PCR validation data, it was found that treatment with 30μM HNK significantly increased protein expression of KISS1R (p=0.015) and MMP-9 (p=0.047) (**Figure 3.20** and **Figure 3.21**). Whilst the detectable level of TIMP-4 (p=0.048) protein was significantly decreased by HNK, which was in conflict with the qRT-PCR data (**Figure 3.22**). However, among the three replicates, the intensity of TIMP-4 protein bands was not consistent upon 30μM HNK treatment, indicating that the result was not able to be conclusive and further replicates are required to be conducted. Protein expression of NF-κB appeared unchanged with HNK treatment and there was no significant difference compared with vehicle control (p>0.999) (**Figure 3.23**). These findings demonstrate that HNK affects the expression of selected proteins that are known to be involved in the regulation of tumour metastasis.

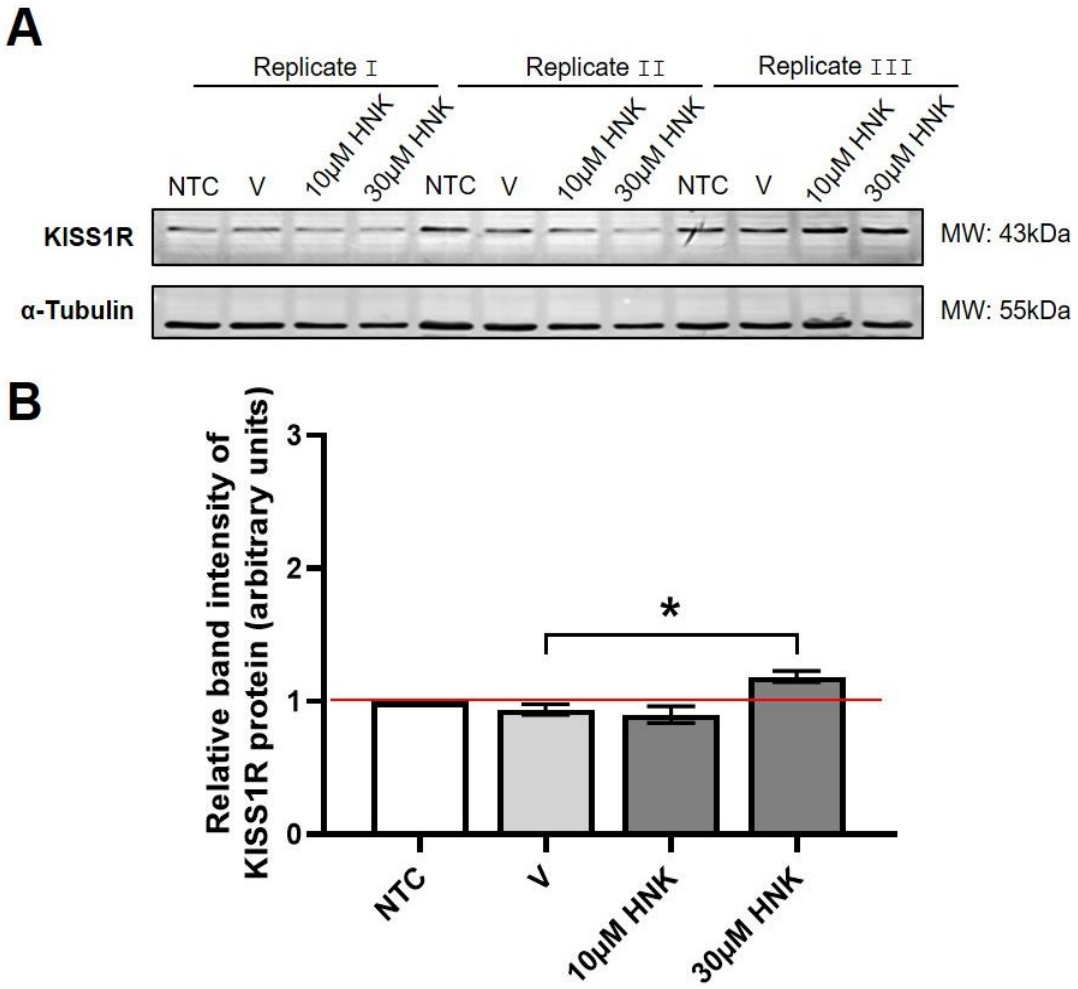

Figure 3.20. Honokiol increases protein expression of kisspeptin receptor. A375 cells were non-treated (**NTC**) or treated with honokiol (**HNK**) (10μM and 30μM) for 24 hours. The percentage of DMSO as vehicle control (**V**) was 0.0375%, since this reflected the maximum percentage of DMSO that cells were exposed to when treating with HNK at a concentration of 30μM. (**A**) Protein lysates separated on 12.5% SDS-page gel were immunoblotted for kisspeptin receptor (**KISS1R**) and alpha tubulin (**α-tubulin**). (**B**) Image J software was used to analyse densitometry. KISS1R density normalised to alpha tubulin was quantified. Relative band intensity in treatment groups was calculated by multiplying the corresponding ratio of NTC respectively. Data is expressed as the mean ± SEM (n = 3) and was analysed by one-way ANOVA with Tukey multiple comparisons test (*$p \leq 0.05$). **MW**: molecular weight. **kDa**: kilodalton.

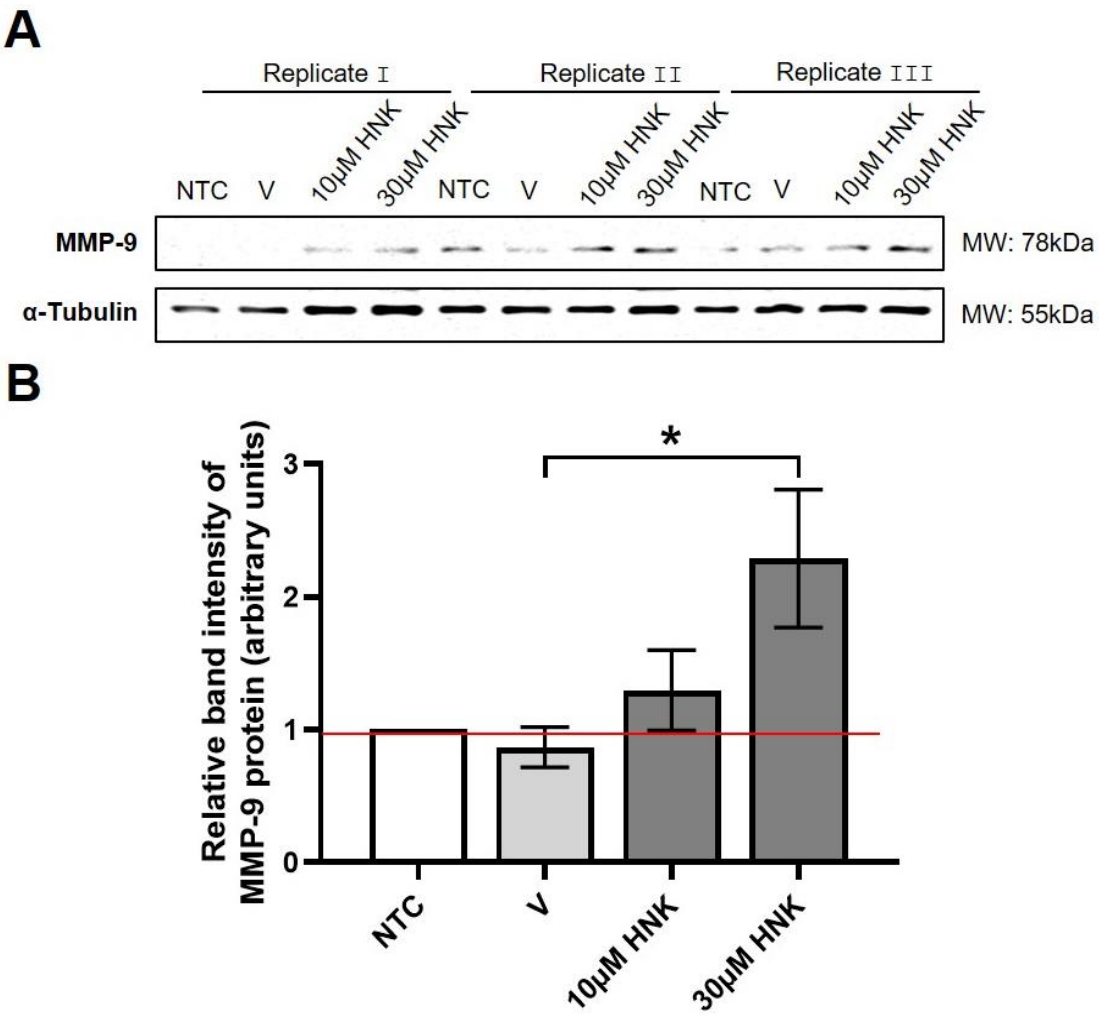

Figure 3.21. Honokiol increases protein expression of matrix metallopeptidase 9. A375 cells were non-treated (**NTC**) or treated with honokiol (**HNK**) (10μM and 30μM) for 24 hours. The percentage of DMSO as vehicle control (**V**) was 0.0375%, since this reflected the maximum percentage of DMSO that cells were exposed to when treating with HNK at a concentration of 30μM. (**A**) Protein lysates separated on 8.0% SDS-page gel were immunoblotted for matrix metallopeptidase 9 (**MMP-9**) and alpha tubulin (**α-tubulin**). (**B**) Image J software was used to analyse densitometry. MMP-9 density normalised to alpha tubulin was quantified. Relative band intensity in treatment groups was calculated by multiplying the corresponding ratio of NTC respectively. Data is expressed as the mean ± SEM (n = 3) and was analysed by one-way ANOVA with Tukey multiple comparisons test (*$p \leq 0.05$). **MW**: molecular weight. **kDa**: kilodalton.

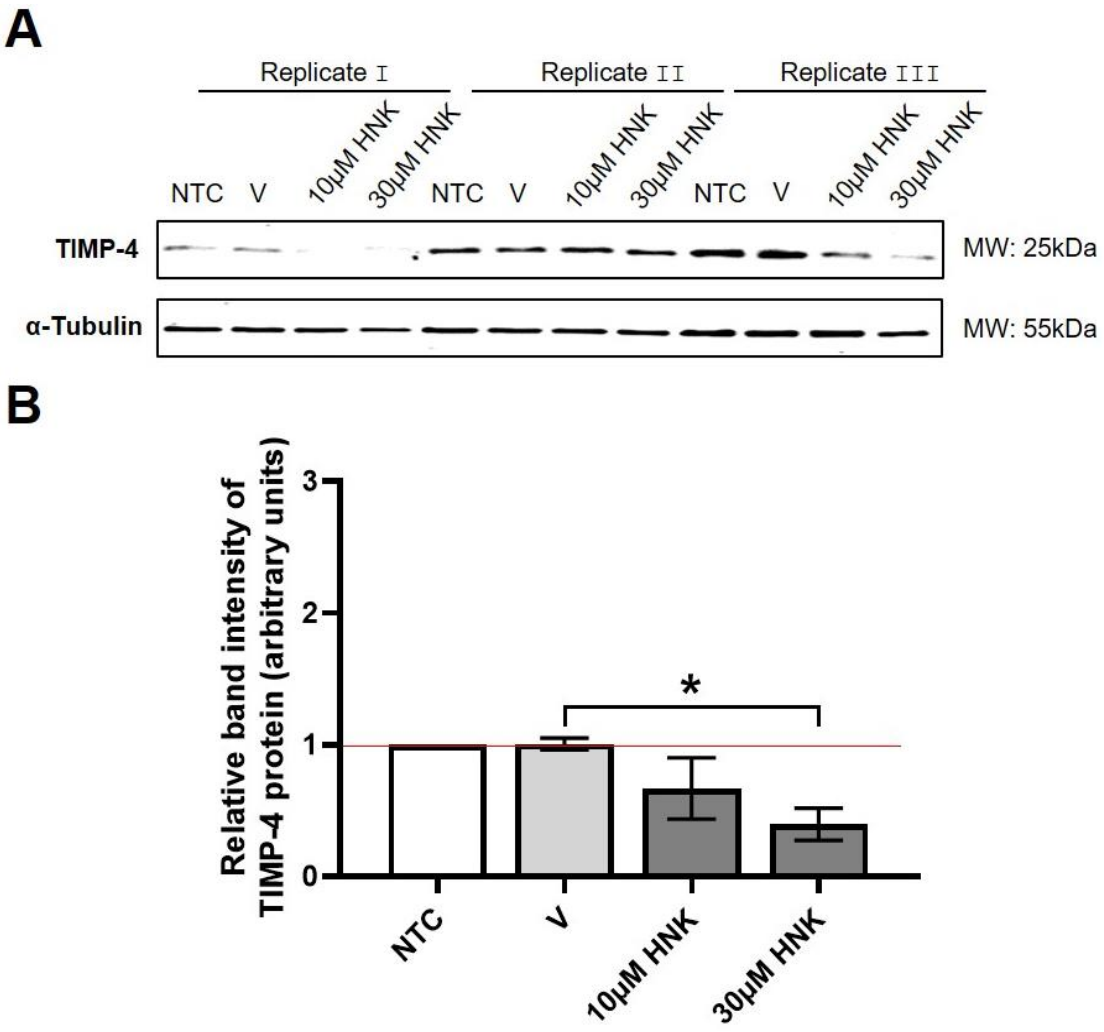

Figure 3.22. Honokiol may decrease protein expression of tissue inhibitors of metalloproteinase 4. A375 cells were non-treated (**NTC**) or treated with honokiol (**HNK**) (10μM and 30μM) for 24 hours. The percentage of DMSO as vehicle control (**V**) was 0.0375%, since this reflected the maximum percentage of DMSO that cells were exposed to when treating with HNK at a concentration of 30μM. (**A**) Protein lysates separated on 12.5% SDS-page gel were immunoblotted for tissue inhibitors of metalloproteinase 4 (**TIMP-4**) and alpha tubulin (**α-tubulin**). (**B**) Image J software was used to analyse densitometry. TIMP-4 density normalised to alpha tubulin was quantified. Relative band intensity in treatment groups was calculated by multiplying the corresponding ratio of NTC respectively. Data is expressed as the mean ± SEM (n = 3) and was analysed by one-way ANOVA with Tukey multiple comparisons test (*$p \leq 0.05$). **MW**: molecular weight. **kDa**: kilodalton.

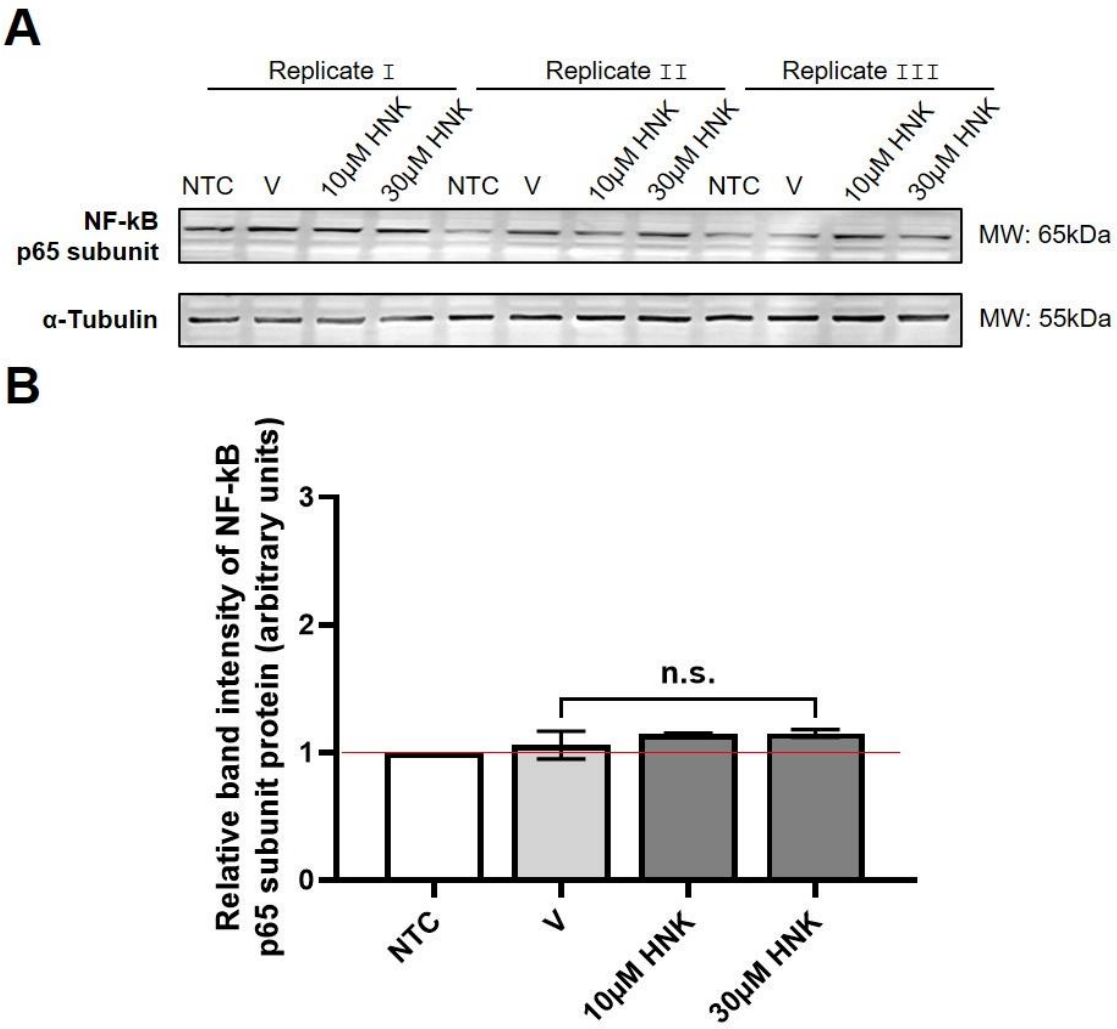

Figure 3.23. Honokiol may has no effects on nuclear factor kappa B p65 subunit protein expression. A375 cells were non-treated (**NTC**) or treated with honokiol (**HNK**) (10μM and 30μM) for 24 hours. The percentage of DMSO as vehicle control (**V**) was 0.0375%, since this reflected the maximum percentage of DMSO that cells were exposed to when treating with HNK at a concentration of 30μM. (**A**) Protein lysates separated on 12.5% SDS-page gel were immunoblotted for nuclear factor kappa B (**NF-κB**) p65 subunit and alpha tubulin (**α-tubulin**). (**B**) Image J software was used to analyse densitometry. NF-kB p65 subunit density normalised to alpha tubulin was quantified. Relative band intensity in treatment groups was calculated by multiplying the corresponding ratio of NTC respectively. Data is expressed as the mean ± SEM (n = 3) and was analysed by one-way ANOVA with Tukey multiple comparisons test (n.s., no significance). **MW**: molecular weight. **kDa**: kilodalton.

3.3.5. Kisspeptin-10 treatment with or without honokiol in A375 melanoma cells.

Kp-10 has been demonstrated to be a physiological activator of KISS1 / KISS1R signalling pathway (Francis et al., 2014), therefore, modulation of kisspeptin signal transduction pathways by artificial Kp-10 in A375 melanoma cells was performed in this study. In addition to the Kp-10 treatment, A375 cells were also treated with Kp-10 and 30μM HNK together, in order to gain further insights into the molecular mechanism of KISS1 / KISS1R signalling upon HNK treatment. Following these treatments, qRT-PCR and immunoblotting analyses were conducted to measure mRNA and protein expression of selected molecules that are known to be associated with tumour metastasis (KISS1, KISS1R, MMP-2, MMP-9, TIMP-4, VEGF-A and NF-κB) in A375 cells.

It was found that combined treatment of Kp-10 and HNK in A375 cells induced alterations in morphology as compared to Kp-10 treatment alone (**Figure 3.24**). Prior to performing qRT-PCR, RNA integrity was assessed by Agilent Bioanalyzer 2100. It was shown that two clear bands of 28S and 18S ribosomal RNA (rRNA) were observed in a gel-like image, as well as RNA integrity numbers in all RNA samples were higher than 8.0 (**Appendix C**), implying that all samples had intact and high-quality RNA samples to ensure reliable and efficient quantification of mRNA expression in the following qRT-PCR analyses.

As shown in **Figure 3.25** and **Figure 3.26**, Kp-10 alone decreased mRNA expression of *MMP-2*, increased mRNA expression of *KISS1*, *TIMP-4*, *VEGF-A* and *NF-κB* compared to the vehicle control, and the expression of MMP-9 was increased at both the transcript and protein level. Notably, Kp-10 slightly reduced mRNA expression of *KISS1R*, however, immunoblots showed that protein expression of KISS1R was increased following Kp-10 treatment (**Figure**

3.25 and **Figure 3.26**). It is important to note that qRT-PCR data was analysed by only one biological replicate, whereas the alteration in protein expression was assessed by two replicates. Therefore, it is most likely that KISS1R expression increased after exposure to Kp-10, however, further biological replicates are still required in order to minimise for any inferential analysis and variation in the experiments.

Compared with Kp-10 treatment alone, combined treatment of Kp-10 and HNK decreased mRNA expression of *KISS1* and *MMP-2*, weakly increased mRNA expression of *TIMP*-4 and *VEGF-A*, and increased KISS1R and MMP-9 expression at both the transcript and protein level. *NF-κB* mRNA expression remained unchanged. Unfortunately, protein expression of TIMP-4 and NF-kB was not analysed due to insufficient quantity of protein samples.

Taken together, these findings demonstrate that Kp-10 markedly upregulated mRNA expression of *KISS1* and increased mRNA and protein expression of KISS1R, suggesting that Kp-10 treatment may activate KISS1 / KISS1R signalling pathway in human A375 melanoma cells. Following Kp-10 treatment, the alterations of mRNA expression in selected metastasis-associated molecules indicate that KISS1 / KISS1R signalling may be involved in the regulation of tumour metastasis. The alteration of gene expression is noticeably increased by the combined treatment of Kp-10 and HNK, which further supports the indication that KISS1 / KISS1R signalling could be one of the key targets of HNK in regulating selected metastasis-associated molecules in human A375 melanoma cells. However, further experiments should also include HNK treatment alone as part of the groups for comparisons.

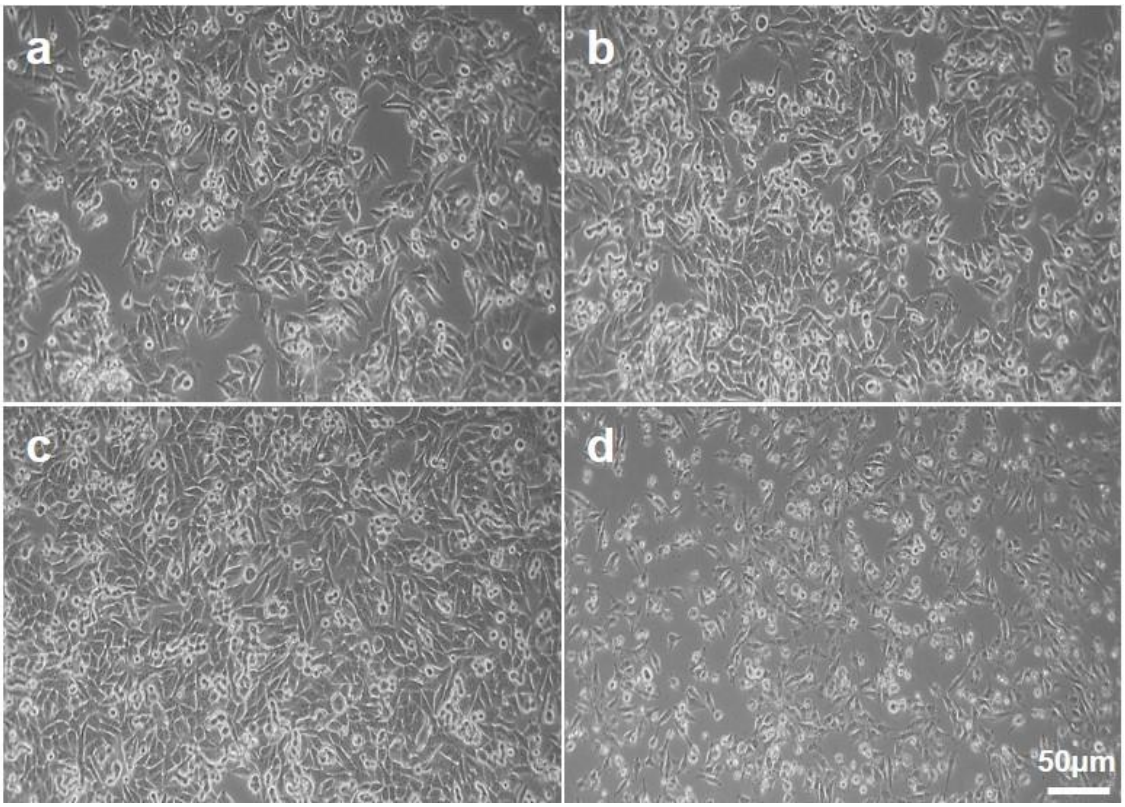

Figure 3.24. Representative images of human A375 melanoma cells followed by treatment with kisspeptin-10 and combination of kisspeptin-10 and honokiol. A375 cells were non-treated (**a**) or treated with 100nM kisspeptin-10 alone (**c**) or combined treatment with 100nM kisspeptin-10 and 30µM honokiol (**d**) for 24 hours (n=1). The percentage of DMSO as vehicle control (**b**) was 0.1%, since this reflected the maximum percentage of DMSO that cells were exposed to when treating with combination of 30µM honokiol and 100nM kisspeptin-10. Representative photographs were taken at a magnification of x 10. Scale bar represents 50µm.

A

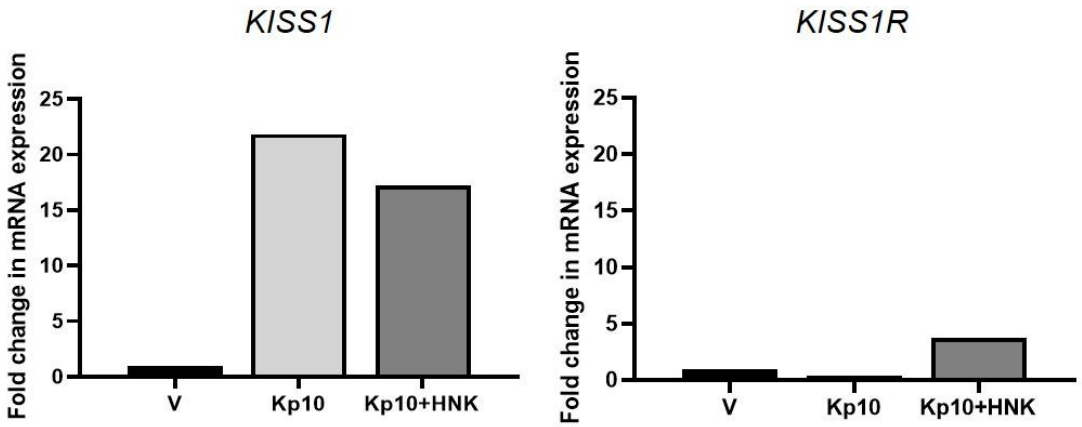
KISS1
KISS1R
Fold change in mRNA expression
0
5
10
15
20
25
V
Kp10
Kp10+HNK

B

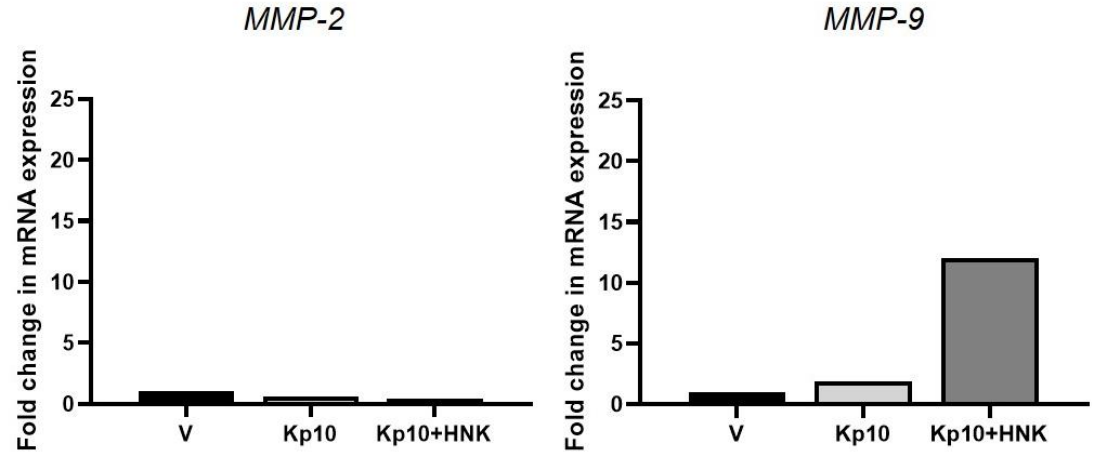
MMP-2
MMP-9
Fold change in mRNA expression
0
5
10
15
20
25
V
Kp10
Kp10+HNK

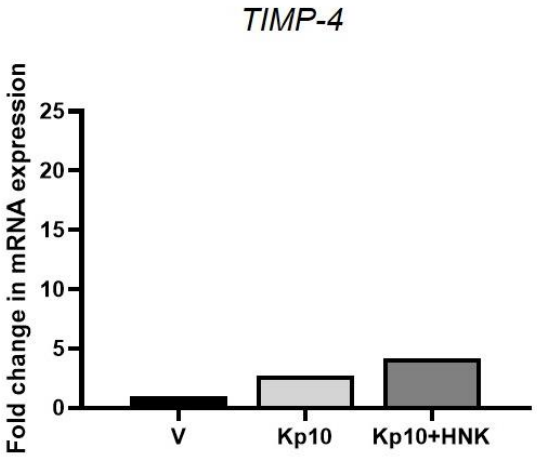
TIMP-4
Fold change in mRNA expression
0
5
10
15
20
25
V
Kp10
Kp10+HNK

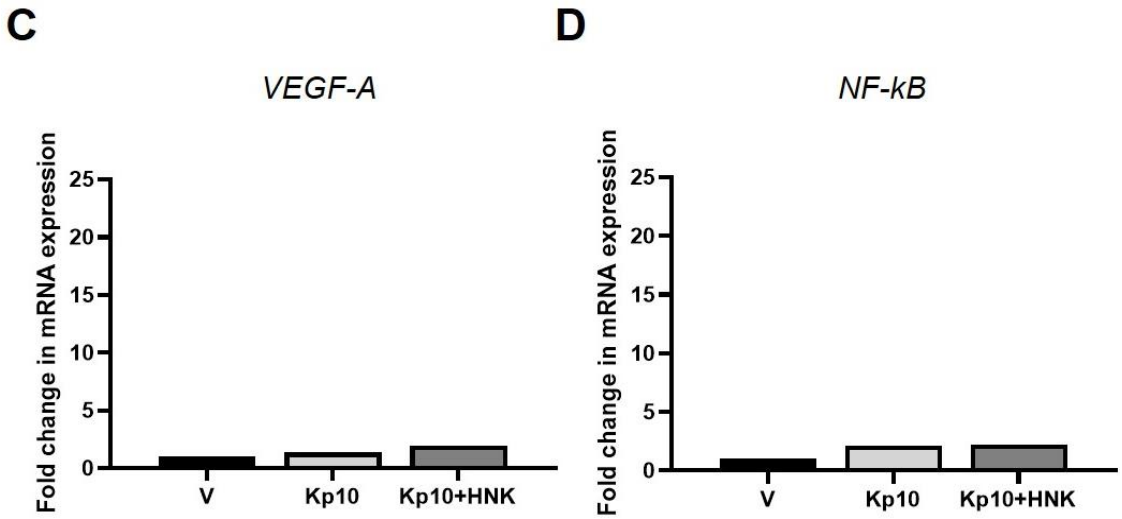

Figure 3.25. Effects of kisspeptin-10 treatment with or without honokiol on mRNA expression of selected tumour-associated molecules in human A375 melanoma cells. A375 cells were treated with 100nM kisspeptin-10 (**Kp-10**) with or without 30μM honokiol (**HNK**) for 24 hours. The percentage of DMSO as vehicle control (**V**) was 0.1%, since this reflected the maximum percentage of DMSO that cells were exposed to when treating with combination of 30μM honokiol and 100nM kisspeptin-10. Following total RNA extraction and reverse transcription, relative mRNA expression was analysed by qRT-PCR including: kisspeptin (***KISS1***) and kisspeptin receptor (***KISS1R***) (**A**); matrix metalloproteinase-9 (***MMP-9***), matrix metalloproteinase-2 (***MMP-2***) and tissue inhibitor of metalloprotease-4 (***TIMP-4***) (**B**); vascular endothelial growth factor A (***VEGF-A***) (**C**) and nuclear factor kappa B (***NF-κB***) (**D**). Samples for each experimental group were performed in duplicate and normalised to glyceraldehyde 3-phosphate dehydrogenase (*GAPDH*) mRNA levels as a housekeeping gene. For **Vehicle vs Kp-10 or Kp-10+HNK**: results are expressed as fold-changes in Kp-10 treated with or without HNK group over vehicle-treated control (n = 1).

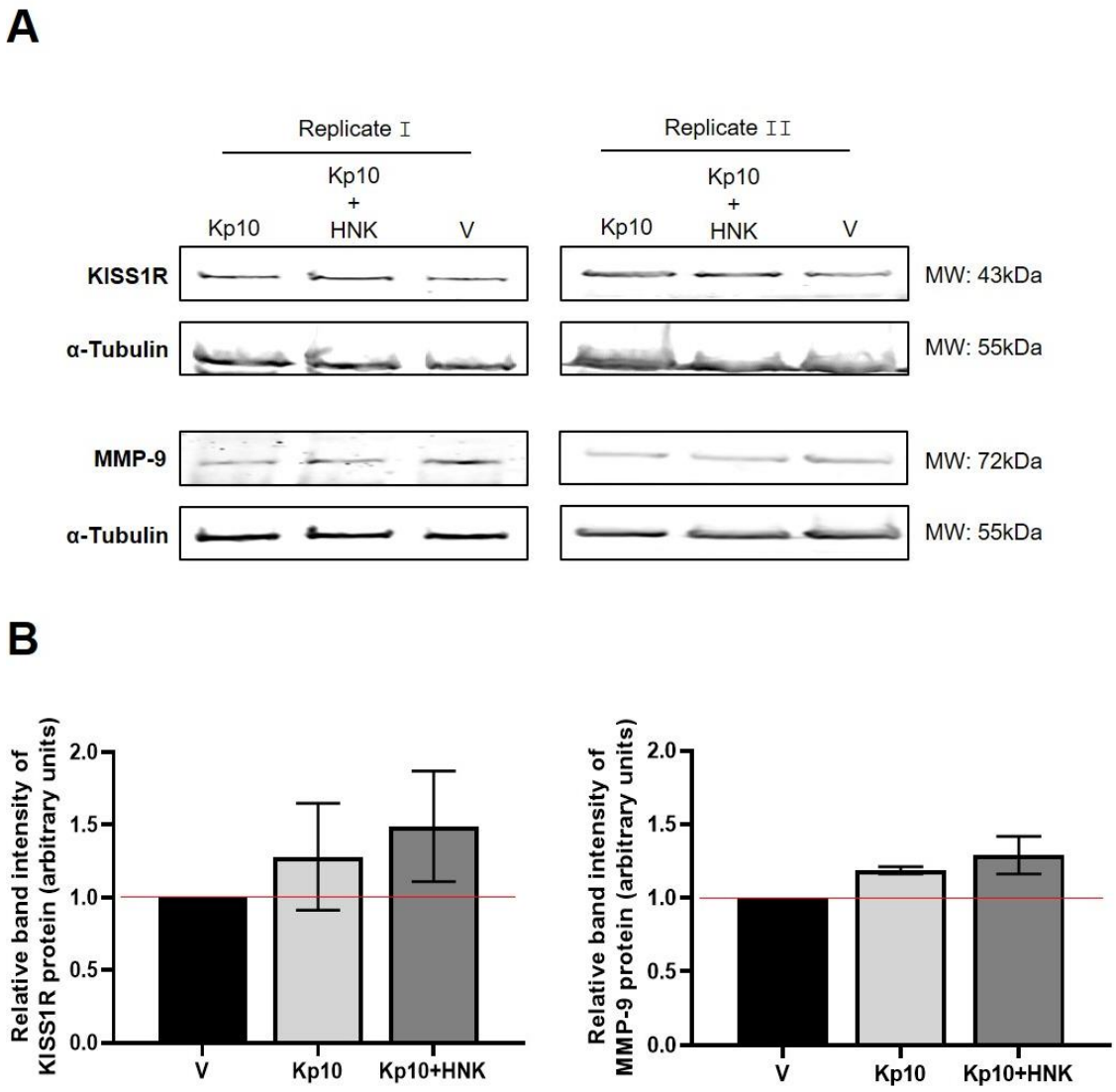

Figure 3.26. Effects of kisspeptin-10 treatment with or without honokiol on protein expression of KISS1R and MMP-9 in human A375 melanoma cells. A375 cells were treated with 100nM kisspeptin-10 (**Kp-10**) with or without 30μM honokiol (**HNK**) for 24 hours. The percentage of DMSO as vehicle control (**V**) was 0.1%, since this reflected the maximum percentage of DMSO that cells were exposed to when treating with combination of 30μM honokiol and 100nM kisspeptin-10. (**A**) Protein lysates separated on 8.0% and 12.5% SDS-page gel were immunoblotted for matrix metallopeptidase 9 (**MMP-9**) and kisspeptin receptor (**KISS1R**) respectively. Alpha tubulin (**α-tubulin**) served as a loading control. (**B**) Image J software was used to analyse densitometry. MMP-9 or KISS1R density normalised to alpha tubulin was quantified. Relative band intensity in treatment groups was calculated by multiplying the corresponding ratio of NTC respectively. Data is expressed as the mean ± SD (n = 2). **MW**: molecular weight. **kDa**: kilodalton.

3.4. Summary of results

In this study, it was identified that HNK effectively exhibited anti-proliferative, anti-migration and apoptotic effects in human A375 melanoma cancer cells. HNK was found to significantly reduce metabolic activities of A375 cells at a concentration of 50μM. HNK was also shown to change cellular morphology in A375 cells, by induction of an elongated shape. Incubation with HNK has been demonstrated to markedly upregulate mRNA expression of *KISS1* and its receptor, *KISS1R* at both the transcription and translation levels, suggesting that KISS1 / KISS1R signalling pathway might be a key molecular mechanism underlying the HNK-mediated ability to suppress the metastatic capabilities of A375 cells.

To investigate further, at a molecular level, a number of relevant genes, encoding proteins that are known to be involved in tumour metastasis were analysed following HNK treatment. It was shown that HNK upregulated *MMP-9*, *VEGF-A* and *TIMP-4* expression and downregulated *MMP-2* expression, however, *NF-κB* expression remained unchanged, suggesting that HNK-modulated KISS1 / KISS1R signalling pathway could alter the expression of selected tumour-associated molecules, which in turn, might be associated with HNK-mediated anti-migration effects that observed in A375 cells.

Furthermore, treating A375 cells with Kp-10 dramatically upregulated *KISS1* and *KISS1R* expression, suggesting that KISS1 / KISS1R signalling pathway might be activated by Kp-10 treatment. It was shown that Kp-10 upregulated *MMP-9*, *TIMP-4*, *NF-κB* and *VEGF-A* expression, but downregulated *MMP-2* expression. The alterations of mRNA expression in the selected metastasis-associated molecules indicate that KISS1 / KISS1R signalling may be involved in the regulation of tumour metastasis. It was further shown that the alteration of gene

expression was noticeably increased or decreased by the combined treatment of Kp-10 and HNK, which strengthens the indication that KISS1 / KISS1R signalling pathway could be one of the important targets of HNK in regulating selected metastasis-associated molecules in human A375 melanoma cancer cells.

Chapter 4. Discussion

Malignant melanoma is the leading cause of skin cancer-induced death in the world (Bray et al., 2018). Long-term efficiency of current therapies for treating melanoma patients are limited by adverse effects and rapid resistance to treatments, and therefore alternative therapies with minimal toxicity and high efficiency are urgently needed (Mannal et al., 2011). Honokiol is one such potential therapeutic agent, which has been demonstrated to exhibit anti-metastatic effects in various cancer cells and generate minimal toxicity in male Sprague-Dawley rats (Ong et al., 2019, Wang et al., 2011). qRT-PCR array results from Dr Sharron Vass (as yet unpublished) and Cheng et al. (2015) have concurred that KISS1 / KISS1R signalling pathway could be one of the targets of HNK. Therefore, the major aim of this study was to identify the molecular interactions of KISS1 / KISS1R signalling pathway and their role in regulating selected metastasis-associated molecules in response to HNK treatment, utilising the highly malignant human melanoma cells, A375.

4.1. Dimethyl sulfoxide reduces cell viability of human A375 melanoma cells in a concentration-dependent manner.

This study initially examined the toxicity of vehicle control (DMSO) in human A375 melanoma cells by a cell viability assay, in order to identify the lowest usable concentration eliciting the minimum cellular toxicity in the subsequent experiments. It was found that the number of A375 cells and the cell viability were reduced in a concentration-dependent manner. In addition, DMSO treatment has also been shown not to cause cytotoxicity up to 0.125% in A375 cells after 24h and 48h treatment.

Previous studies have suggested that the exact toxic concentration of DMSO is dependent on cell types. For example, in human retinal ganglion cells, an MTT

assay has shown that cell viability was significantly decreased when DMSO concentrations ≥ 2.0% (2% DMSO vs 0% DMSO, 35% reduction in cell growth; at 24h of treatment), and a half-maximal inhibitory concentration (IC_{50}) was calculated to be 2.14% after 24h treatment (Galvao et al., 2014). In human lung adenocarcinoma CL1–5 cells, *in vitro* cell cytotoxicity assay has measured the cell viability following 48 hours treatment with DMSO, it was found that DMSO treatment did not cause cytotoxicity up to a 2% concentration (approximately 50% reduction in cell growth was observed at concentrations of ≥ 5.0%; IC_{50}=5.0%) (Wang et al., 2012a). By comparison, in this study, a 5% reduction in cell viability was observed at a concentration of 0.125% DMSO (48h treatment), suggesting that A375 melanoma cells may be more sensitive to DMSO compared to other tumour cells.

As the A375 melanoma cell line was sensitive to DMSO at concentrations above 0.125%, this concentration was not exceeded. The percentage of DMSO used as vehicle control was matched to the concentration of DMSO present in the highest treatment, and this was either 0.0375%, 0.05% or 0.1% depending on the experimental conditions. One of the limitations of this experiment is that only one independently biological replicate was performed. Ideally, three biological replicates would be required to assess the minimum toxicity of DMSO used in human A375 melanoma cells.

4.2. Honokiol reduces cell viability of human A375 melanoma cells in a concentration-dependent manner.

In this study, the cytotoxicity of HNK against human A375 melanoma cell line was assessed by a cell viability assay, it was revealed that cell viability was reduced in a concentration-dependent manner and treatment with 30μM HNK for 48h reduced cell viability by 10%. These data suggest that HNK has inhibitory effects on cellular proliferation of A375 cells and HNK exhibits cytotoxic effects against A375 melanoma cells at concentrations of > 30μM. In agreement, it has been previously reported that HNK treatment had significant cytotoxic effects in A375 cell line in a dose range of 0–60μM with a IC_{50} value below 40μM (Kaushik et al., 2014). However, HNK treatment has been shown to have no obvious cytotoxicity in human UACC-62 and SKMEL-2 melanoma cell lines when the concentration was lower than 50μM, which suggests that different cell lines may have different drug sensitivities (Guillermo-Lagae et al., 2017).

Interestingly, some studies have also compared cytotoxic effects of HNK in the same cancer cell types but with different malignance grade. For instance, Huang et al. (2018) have compared the drug sensitivity between OC2 and OCSL cell lines (both are human oral squamous cell carcinoma), in which the OCSL cells with malignant phenotype were more sensitive to HNK than OC2 cells. Similar results have been found in human bladder cancer cell lines, for example, Hsiao et al. (2019) have compared cytotoxic effects of HNK in human transitional cell carcinoma, human urinary bladder carcinoma and human bladder papillary transitional cell carcinoma grade-III. It was shown that human bladder papillary transitional cell carcinoma with grade-III malignancy exhibited the highest sensitivity to HNK treatment. These studies have suggested that cytotoxicity of

HNK in various cancer cell lines might be associated with levels of malignant grade (Hsiao et al., 2019, Huang et al., 2018b).

Furthermore, HNK has been demonstrated to exert minimal cytotoxicity in normal and healthy cell lines compared to cancer cells. For example, it was found that HNK significantly reduced cell viability of human ovarian cancer cells at a concentration of 25μM after 24h treatment, while the significant decrease was not observed in human non-cancer fibroblast cells even at a concentration of 100μM (Lee et al., 2019). In agreement, it has been shown that the IC_{50} of HNK in treated normal human fibroblast cells was higher than oral squamous cell carcinoma (Hs68 cell line, IC_{50}=70μM vs OCSL cell line, IC_{50}=33μM; at 24h of treatment) (Huang et al., 2018b). It is important to note that the minor to no toxicity of HNK against healthy cells should be emphasised as the key advantage in cancer treatment, since current chemotherapeutic drugs have been reported to cause various sides effects that harm cancer patients (Ong et al., 2019). One of the limitations of this study is that lack of cell viability assay to examine the cytotoxicity of HNK treatment in healthy melanocytes cells as a safety evaluation, which could be one of the important experiments to be carried out in further studies.

In addition to the low toxicity in human healthy cell lines, HNK has been indicated to exhibit chemotherapeutic effects in animal models. For example, in the SKH-1 hairless mouse with ultraviolet radiation-induced skin tumorigenesis, it was shown that treatment with HNK (30μg / 200μL of acetone per mouse applied topically; 5 days / week for 30 weeks) resulted in a significant 78% reduction in tumour size as compared to untreated groups (200μL of acetone) (Chilampalli et al., 2010). Similarly, intraperitoneal injection of HNK (1mg HNK / 100μL PBS; everyday) into ovarian tumour-bearing animals (xenograft model of 1×10^7

SKOV3 cells in BALB/C mice) was found to significantly suppress tumour growth (about 70%) and reduce microvessel density (about 60%) as compared to the untreated control (100μL PBS) (Li et al., 2008). However, it is unknown that the exact tumour concentration can be targeted by HNK treatment in the *in vivo* microenvironment. Apart from that, a safe and effective dosage of HNK to be used in treating human cancer clinically remain unidentified, therefore, further studies are required to be conducted in order to investigate the effective therapeutic concentrations of HNK to be used in chemotherapy.

As to the stability of HNK, a recent study has shown that HNK was degraded in a pH-dependent manner, for example, at pH 7.4, the concentration of HNK was decreased to 84% at room temperature, and reduced to 29% at 37 °C (Usach et al., 2021). The pH levels in human body are different from one area to another and a tightly controlled range in the blood is between 7.35 and 7.45 (Schwalfenberg, 2012). This suggested that an alkaline pH level in the blood (at 37 °C) may contribute to the degradation of HNK prior to accessing melanoma cells through the bloodstream, and thereby limiting pharmacological effectiveness of HNK. Thus, further studies are needed to be carried out in order to develop efficient drug carriers to deliver HNK to the targeted melanoma cells.

4.3. Honokiol induces apoptosis in human A375 melanoma cells in a concentration-dependent manner.

In the cell viability assay, it was found that HNK has inhibitory effects on cellular proliferation of human A375 melanoma cells. Suppression of tumour cell proliferation can be caused by the induction of apoptosis (Gupta et al., 2010). Therefore, this study investigated whether the induction of apoptosis contributed to HNK-mediated inhibition of cellular proliferation in A375 cells. Fluorescence microscopy analysis using an acridine orange and propidium iodide double

staining assay and flow cytometry analysis by using Annexin V and propidium iodide apoptosis assay were performed.

In agreement with the cell viability results, it was shown that HNK dose-dependently induced apoptotic effects in human A375 melanoma cells and a large number of cells were detected in the latter stage of apoptosis in response to HNK at concentrations of 30μM and 40μM. This suggested that honokiol may be able to potentiate the apoptotic machinery to mediate apoptotic effects, and thereby inhibit cellular proliferation in human A375 melanoma cells. Consistent results have been demonstrated in human melanoma cells (Mannal et al., 2011), chondrosarcoma cells (Chen et al., 2010), glioblastoma cells (Liang et al., 2014), lung squamous cell carcinoma cells and lung squamous cell carcinoma xenograft mice models (Pan et al., 2014). In which HNK was shown to generate apoptotic effects by triggering the activation of caspase-9 which involves caspase-3-mediated apoptotic cell death, *via* the release of cytochrome *c* from the mitochondrial intermembrane space into the cytosol (intrinsic apoptosis pathways) (Chen et al., 2010).

Although this study did not measure relevant apoptotic proteins following HNK treatment in A375 melanoma cells, it has been demonstrated in many cancer cell types, that exposure to HNK dose-dependently increased Bax and Bak protein levels, while reducing the expression of B-cell lymphoma / leukemia-2 (Bcl-2) and Bcl-xL, in turn, contributing to an increase in the pro-apoptotic : anti-apoptotic Bcl-2 ratio (Chen et al., 2010, Arora et al., 2011, Yan and Peng, 2015, Fan et al., 2018, Lu et al., 2017). Bcl-2 family proteins play an important role in regulating intrinsic apoptosis pathways through the balance of anti- and pro-apoptotic members, suggesting that HNK-induced apoptosis against human cancer cells, such as A375 melanoma cells, may be associated with modulating

expression of the Bcl-2 family proteins (Huang et al., 2018a, Shamas-Din et al., 2013). Further studies are needed to examine this hypothesis in order to elucidate the exact mechanisms underlying HNK-mediated apoptosis in human A375 melanoma cells.

4.4. Honokiol does not affect metabolic activity of human A375 melanoma cells ≤ 50μM.

Mitochondrial respiration is another important physiological activity in tumour cells to maintain cellular proliferation (Antico Arciuch et al., 2012). Thus, the subsequent experiment was to examine effects of HNK on metabolic activities of A375 cells by an alamar blue assay. It was found that percentage reduction of alamar blue in the HNK treatments (5μM, 10μM, 20μM, 30μM and 40μM) did not show any statistically significant difference from the untreated control. However, a statistically significant reduction has been observed when A375 cells treated with 50μM HNK, suggesting that HNK treatment may not result in any significant change to mitochondrial metabolic potential of A375 cells until a concentration of HNK ≥ 50μM is applied. In contrast, some studies have demonstrated that HNK is able to suppress mitochondrial function at a concentration lower than 50μM. For example, treatment with 40μM HNK in human neuroblastoma has been found to disrupt the mitochondrial permeability transition pore and thereby affect mitochondrial function (Lin et al., 2012). Similarly, an extracellular flux assay has shown that HNK induced mitochondrial dysfunction in human lung cancer cells at levels as low as 6.25μM (Pan et al., 2014).

In this study, the alamar blue data are robust as three independent biological replicates were conducted in the assay. However, the results are in contrast with the results from cell viability assays (**section 4.2**) and apoptosis assays

(**section 4.3**), in which HNK should be able to elicit its inhibitory effects of metabolic activities in A375 cells at a concentration of 30μM. Due to the presence of positive control, the reagent does appear to work, however, this assay may not be as sensitive as other methods of detection. Further experiments are still required to examine the impacts of HNK on metabolic activities in A375 cells, for instance, by measuring oxygen consumption rate using an extracellular oxygen consumption assay.

4.5. Examination of altered cell morphology in response to honokiol treatment.

In the cell viability assays, it was observed that treatment with 30μM and 40μM HNK induced morphological alterations. Therefore, this study investigated whether HNK had any effect on cellular morphology, by examining cells that were stained with DAPI to detect DNA, and phalloidin to detect F-actin. It was observed that A375 cells treated with increasing concentrations of HNK developed an elongated morphology. When A375 cells were stained with phalloidin, which binds to F-actin, this staining extended to full length of the cell. This suggests a potential link between HNK and polymerisation of F-actin. Similar findings have been reported in human renal epithelial cells, which found that treatment with 10μM HNK for 24 hours increased the polymerisation of actin cytoskeleton by 1.6-fold (Wang et al., 2018). Previous studies have indicated that HNK may affect actin cytoskeleton associated gene / protein by targeting various molecular pathways. For example, it was found that HNK could stimulate the activity of a Rho-family GTPase member, RhoA, in order to trigger downstream effector Rho-associated protein kinases in human renal cell carcinoma cells (Cheng et al., 2016). These kinases then phosphorylate myosin light chain and induce excessive formation of actin stress fibres, which

contribute to the suppression of cellular mobility in human cancer cells (Cheng et al., 2016, Shoji et al., 2009).

In agreement, HNK has been found to increase gene and protein expression of master kinase liver kinases B1 (LKB1) in human breast cancer cells (Sengupta et al., 2017). The HNK-mediated LKB1 overexpression can phosphorylate AMPK-related kinases, which results in the decrease of p70 ribosomal protein S6 kinase 1 (p70S6K1) phosphorylation in human breast cancer cells (Nagalingam et al., 2012). It was reported that p70S6K1 plays an important role to regulate actin cytoskeleton in the acquisition of migratory properties in human ovarian cancer cells, by acting as an actin filament cross-linking protein and as a Rho family GTPase-activating protein, such as Rac1 and Cdc42 (Ip et al., 2011). Inhibition of p70S6K1 has also been shown to significantly suppress actin cytoskeleton reorganisation, which impedes cellular mobility and migratory behaviour in human prostate cancer cells (Amaral et al., 2016). These studies suggest HNK treatment may disrupt cellular cytoskeleton network, and therefore may contribute to the suppression of cellular mobility and migratory behaviour in human A375 melanoma cells.

4.6. Honokiol inhibits migration capacities of human A375 melanoma cells in a concentration-dependent manner.

This study has examined whether HNK was able to suppress migratory behaviour of metastatic melanoma cells by a wound healing assay, it was found that wound area was significantly higher in HNK-treated groups compared to control groups and this effect was observed at concentrations ≥ 20μM. These data suggests that HNK significantly inhibited the migration of highly metastatic A375 cells in a concentration-dependent manner. Similar findings have been reported in human lung adenocarcinoma cells (Zhu et al., 2019, Dai et al., 2018),

neuroblastoma cells (Yeh et al., 2016), bladder cancer cells (Shen et al., 2017), lung squamous cells carcinoma (Cen et al., 2018), renal cancer cells (Li et al., 2014) and glioblastoma stem cell-like cells (Fan et al., 2018), implying that HNK can exhibit anti-migration effects in a variety of human cancer cells.

The underlying molecular mechanisms of anti-migration effects of HNK in human cancer cells are beginning to be explored. For example, in human non-small-cell lung cancer cells, it was reported that HNK suppresses epithelial mesenchymal transition (EMT) – mediated migration and invasion by targeting c-FLIP signalling pathway (cellular fas-associated death domain-like interleukin-1-β-converting enzyme-inhibitory protein), and thus leads to the downregulation of mesenchymal protein expression, such as Snail and N-cadherin (Lv et al., 2016). In agreement, HNK has been shown to suppress the phosphorylation of signal transducer and activator of transcription 3 (STAT3) and reduce recruitment of STAT3 to the promoter of zinc finger E-box-binding homeobox transcription factor 1 (Zeb1), thereby inhibiting transcriptional activities of *Zeb1* (Avtanski et al., 2014). The HNK-mediated STAT3 inactivation can mitigate the repressive effects of *Zeb1* from E-cadherin promoter, which increases gene and protein expression of E-cadherin, and thus results in the suppression of EMT and reduction of invasive phenotype in human breast cancer cells (Avtanski et al., 2014). In addition to the regulation of mesenchymal and epithelial makers, HNK has also been demonstrated to target tuberous sclerosis 1 and 2 complex/AMPK/mTOR signalling pathway to reduce MMP-9 production in human ovarian carcinoma cells (Lee et al., 2019). Taken altogether, these studies have suggested that HNK is able to modulate multiple signal transductions to achieve anti-migration effects in human cancer cells.

Although recent studies have indicated multiple anti-cancer actions of HNK by its effect on various biological pathways, the exact molecular mechanisms of HNK in human melanoma cancer cells have not been fully elucidated. In order to further characterise the molecular mechanisms of anti-metastatic effects of HNK in human A375 melanoma cells, the subsequent experiments were designed to investigate the impacts of HNK on mRNA and protein expression of selected tumour metastasis-associated molecules.

4.7. Effects of honokiol on the mRNA and protein expression of selected metastasis-associated molecules in human A375 melanoma cells.

In order to gain further mechanistic insights into the molecular events underlying migration suppression of A375 melanoma cells treated with HNK, this study has evaluated the mRNA and protein expression of selected molecules that are known to be associated with tumour metastasis by qRT-PCR and immunoblotting analyses. It has been suggested that *KISS1* and its only G-protein coupled receptor, *KISS1R*, may be associated with anti-metastatic activities in various tumour cells (Guzman et al., 2018). An qRT-PCR array carried out by Dr Sharron Vass at the Edinburgh Napier University (UK), has indicated that HNK can upregulate mRNA expression of *KISS1* and *KISS1R* in A375 melanoma cells. Therefore, this study initially measured the expression of KISS1 and KISS1R in HNK-treated A375 cells.

It was shown that treatment with 30μM HNK (24h) markedly upregulated mRNA expression of metastasis-suppressor gene *KISS1* and its receptor, *KISS1R* at both transcription and translation levels. Consistent with a study by Cheng et al. (2015), it has demonstrated that treatment with 40μM HNK (24h) in human renal cell carcinoma cells can significantly increase expression of KISS1 and KISS1R at both the transcription and translation levels. It has also indicated that

knockdown of *KISS1* can partially reverse the anti-invasion effects of HNK in renal cell carcinoma cells. Results from this study and Cheng et al. (2015) have concurred that KISS1 / KISS1R signalling pathway appears to be one of the targets of HNK, which in turn, may be associated with the observed HNK-mediated anti-migration effects in human A375 melanoma cancer cells.

Based on the original qRT-PCR array data (obtained by Dr Sharron Vass), the analysis was extended to measure the mRNA and protein expression of selected molecules that are known to be involved in either remodelling the extracellular matrix (MMP-2, MMP-9 and TIMP-4), regulating transcription (NF-kB) or angiogenesis (VEGF-A), in response to HNK treatment. It was shown that HNK significantly downregulated the mRNA expression of *MMP-2*, whereas the mRNA and protein expression of MMP-9 was increased by HNK treatment. The mRNA expression of *TIMP-4* was increased, however, the level of detectable protein expression of TIMP-4 appeared to be decreased by HNK. In addition, following HNK treatment in A375 cells, NF-kB expression remained unchanged at both transcription and translation levels, however, the mRNA expression of *VEGF-A* was increased.

4.7.1. Honokiol simultaneously downregulates *MMP-2* mRNA expression and upregulates the mRNA and protein expression of MMP-9 in human A375 cells.

MMP-2 and MMP-9 proteins play an important role in regulating the migration process of melanoma tumour cells, because MMP-2 and MMP-9 are capable of degrading many ECM proteins through proteolytic cleavage to regulate ECM remodelling, and thereby allow melanoma cells to invade the surrounding tissues (Chen et al., 2016). MMP-2 and MMP-9 both belong to the gelatinase subgroup of the MMPs family, therefore, ideally, MMP-2 and MMP-9 should be

regulated in series through a direct signal cascade. However, this study has demonstrated an unexpected result is that HNK dramatically increases mRNA and protein expression of MMP-9 in A375 cells, whereas the mRNA expression of *MMP-2* was significantly downregulated by HNK. Unfortunately, this study was not able to measure the protein expression of MMP-2 due to a lack of working primary antibody. In contrast to findings from previous studies, it has been indicated that HNK is able to decrease the protein levels of MMP-2 and MMP-9 by targeting various signalling pathways. For example, HNK was shown to inhibit tumour necrosis factor-α-induced MMP-2 and MMP-9 expression and activities by targeting extracellular signal-regulated kinase 1/2 signalling pathway in rat aortic smooth muscle cells (Zhu et al., 2014). HNK has also been found to reduce protein expression of MMP-2 and MMP-9 by targeting Janus kinase / STAT3 signal transduction pathways in human glioblastoma cells (Fan et al., 2018).

To the best of our knowledge, similar findings have not been reported in current literature and this may be the first study to indicate that HNK can upregulate MMP-9 expression in human cancer cells. This study trusts the data because qRT-PCR analyses have been conducted in five biological replicates and each single step has been conscientiously examined according to the minimum information for publication of quantitative real-time PCR experiments (MIQE) guidelines (Bustin et al., 2009). Immunoblotting data was also supported by three biological replicates. Nevertheless, this study will provide a possible hypothesis to explain why HNK may upregulate MMP-9 expression which will be discussed in **section 4.8.1** (Kp-10 upregulates mRNA expression of *NF-kB* and increases MMP-9 mRNA and protein expression in human A375 cells).

As to the MMP-2, this study has shown that HNK significantly reduced mRNA expression of *MMP-2* in A375 melanoma cells, similar results were found in human bladder cancer cells (Shen et al., 2017) and human glioblastoma cells (Fan et al., 2018). HNK has been shown to suppress *MMP-2* transcriptional regulation by targeting β-catenin signalling pathway in a variety of human cancer cells, such as melanoma cells (Chiu et al., 2019), oral squamous cell carcinoma cells (Yao et al., 2013) and non-small cell lung cancer cells (Singh and Katiyar, 2013). It was found that HNK increased the phosphorylation of β-catenin at certain key residues (Ser^{45}, Ser^{33}, Ser^{37} and Thr^{41}) and dose-dependently increased the expression of destruction complexes including: glycogen synthase kinase 3 and casein kinase 1α (Singh and Katiyar, 2013). Upon the phosphorylation of β-catenin by the destruction complexes, the phosphorylated β-catenin is ubiquitinated by β-transducin repeat-containing E3 ubiquitin protein ligases, which results in the protein degradation of cytosolic β-catenin and reduces nuclear accumulation of β-catenin (Yu et al., 2020, Stamos and Weis, 2013). Consequently, low levels of cytosolic β-catenin interact with T-cell factor and lymphoid enhancer factor transcription factors, and thereby reduce transcription activities of *MMP-2* in human cancer cells (Krishnamurthy and Kurzrock, 2018, Hlubek et al., 2004), such as A375 melanoma cells.

4.7.2. Honokiol increases mRNA expression of *TIMP-4*, whilst decreases detectable TIMP-4 protein levels in human A375 cells.

TIMPs are tissue inhibitor of MMPs and play a key role in regulating ECM remodelling during the metastatic process of tumour cells (Murphy, 2011). Therefore, this study has also measured TIMP-4 expression in HNK-treated A375 cells, it was found that the mRNA expression of *TIMP-4* (4.70±0.54) was upregulated by HNK (although, not statistically significant difference),

unexpectedly, detectable levels of TIMP-4 protein was significantly decreased. In previous studies, HNK has been shown to dose-dependently increase TIMP-4 expression in human renal carcinoma cells, however, the increase was observed at both the transcription and translation levels (Cheng et al., 2015). The results from this study therefore suggest that down-regulation of detectable TIMP-4 protein by HNK might be through disruption of TIMP-4 protein stability, instead of transcriptional suppression.

It has been demonstrated that when there is a poor correlation between mRNA and protein expression levels, one of the possible reasons is that polypeptide errors may occur during protein synthesis, such as misacylation of transfer RNA and amino acid misincorporation, which can induce protein misfolding and ultimately protein degradation (Perl et al., 2017, Payne, 2015, Koussounadis et al., 2015, Drummond and Wilke, 2009). Another possible reason is that some unknown microRNA may affect the efficiency of protein translation, for example, it has been shown that TIMP-4 protein expression in human prostate cancer cells was regulated by microRNA-200b-3p (Janiak et al., 2017).

However, similar results have been observed in other molecules. It was found that the mRNA expression of *MMP-9* and epidermal growth factor receptor (*EGFR*) was not affected by HNK treatment, whilst the protein expression was significantly reduced in human lung cancer cells (Pai et al., 2020, Liou et al., 2015). HNK has been shown to significantly reduce class I histone deacetylases (HDAC) expression, induce hyper-acetylation of heat shock proteins (Hsp) and reduce interaction between Hsp and its targeted proteins (Pai et al., 2020, Singh et al., 2013). This suggested that disruption of Hsp chaperone activities may direct misfolded or destabilised target proteins to be polyubiquitinated by E3 ubiquitin ligases and thereby degrading by proteasome (Trepel et al., 2010).

According to the results from previous studies, it is not excluded the possibility that the repression of TIMP-4 proteins in A375 cells by HNK is through downregulating HDAC expression that leads to the interruption of chaperone activities, which disrupts TIMP-4 protein maturation and ultimately induces ubiquitin-proteasome degradation (Pai et al., 2020). In order to clarify the TIMP-4 protein expression following HNK exposure, this study has further examined the TIMP-4 expression by HNK at various concentrations (10μM - 40μM), it was found that HNK dose-dependently reduced the detectable levels of TIMP-4 protein in human A375 melanoma cells (**Appendix D**). These results support the hypothesis that HNK might reduce TIMP-4 protein expression by ubiquitin-proteasome degradation rather than transcriptional inhibition in human A375 melanoma cells (**Figure 4.1**). However, further studies are needed to identify whether the repression of TIMP-4 protein in A375 cells is mediating by HNK only or is dependent upon HNK-mediated KISS1 / KISS1R signalling pathway.

4.7.3. The expression of NF-κB appears unchanged in honokiol-treated A375 cells.

NF-κB is a transcription factor which is responsible for regulating the cellular response to stress (Wang et al., 2017). NF-κB has been demonstrated to regulate the transcription of genes that are involved in tumour metastasis, such as *MMP-9* (Wang et al., 2017). Upon exposure to HNK, it was found that mRNA and protein expression of NF-κB appeared unchanged in A375 melanoma cells, suggesting that NF- κB protein may not be the major targeted molecule in HNK-modulated KISS1 / KISS1R signalling pathways. This result is in contrast with the observation that HNK can elicit inhibitory effects to suppress NF-κB transcriptional activities in various types of cancer cells, such as breast cancer (Wang and Zhang, 2017), colon cancer (Hua et al., 2013), non-small cell lung

cancer (Singh and Katiyar, 2013), lung adenocarcinoma and squamous cell carcinoma (Ahn et al., 2006).

HNK has been demonstrated to dose-dependently decrease the nuclear NF-κB levels together with increasing the cytoplasmic NF-κB expression in human pancreatic cancer cells (Arora et al., 2011). The activation of IKK-α and the degradation of IκB-α have also been found to be suppressed by HNK treatment in human non-small cell lung cancer (Singh and Katiyar, 2013, Ahn et al., 2006). These studies suggest that HNK may be able to suppress the activation of IKK-α and result in the inhibition of IκB-α degradation, which prevents nuclear translocation of p50/p65 subunits of NF-κB and thereby blocks the constitutive activation of NF-κB signalling pathways in human cancer cells (Singh and Katiyar, 2013, Arora et al., 2011).

However, one of the limitations of this study is that only the p65 form of the protein was measured from the whole cell, and it is unknown whether NF- κB signalling pathway has been actually activated or inhibited. Further studies should compare the p65 subunit protein levels between nuclear fraction and cytoplasmic fraction, the inhibition of NF-κB pathway is indicated by an increase level of cytoplasmic p65 expression and a reduction of nuclear p65 expression. Cellular distribution of p65 and p50 subunits of NF- κB are regulated by the phosphorylation of its biological inhibitor IκB-α, which can maintain p65 and p50 sequestered in an inactive complex in the cellular cytoplasm (Arora et al., 2011, Jiraviriyakul et al., 2019). Therefore, in further experiments, it is also important to measure the phosphorylation of IκB-α from the cytoplasmic extracts, in order to clarify whether the constitutive NF-κB activation is suppressed by blocking nuclear translocation of p65/p50.

4.7.4. Honokiol only slightly upregulates the mRNA expression of *VEGF-A* in human A375 cells.

Angiogenesis is defined as the formation of new blood vessels from pre-existing ones, and is one of the tissue remodelling effects associated with tumour progression (Yadav et al., 2015). Therefore, this study has measured the effects of HNK in VEGF-A expression of A375 cells. It was shown that the mRNA expression of *VEGF-A* (2.49±0.44) was only slightly upregulated by HNK and there was no statistically significant difference between HNK-treated group and vehicle control. Unfortunately, this study was not able to measure the protein expression of VEGF-A due to a lack of primary antibody. Consistent results have been reported in human renal cancer cells (Banerjee et al., 2013) and human ovarian cancer cells (Li et al., 2008), in which the expression of VEGF-A was significantly reduced by HNK.

It has been demonstrated that HNK is able to inhibit angiogenesis by modulating multiple signal transduction pathways, for example, HNK can prevent the binding of hypoxia- inducible-factor to hypoxia-response elements of the *VEGF-A* gene promoter and thus inhibit the secretion of VEGF-A proteins in human retinal pigment epithelial cells (Vavilala et al., 2014, Vavilala et al., 2013). These studies suggest that HNK may exert anti-angiogenic effects by reducing the secretion of VEGF-A proteins from human melanoma cells and simultaneously interfering the VEGF / VEGFR signalling pathways in human endothelial cells (Vavilala et al., 2014, Bai et al., 2003). However, one of the important limitations is that this study did not measure the expression of VEGF receptors (VEGFR-1, VEGFR-2 and VEGFR-3) and other VEGF family members including: VEGF-B, VEGF-C, VEGF-D and placental growth factor, which could be another key experiment to be carried out in further studies.

4.8. Kisspeptin-10 treatment with or without honokiol in human A375 melanoma cells.

Kp-10 has been demonstrated to be a physiological activator of KISS1 / KISS1R signalling pathway (Francis et al., 2014), therefore, modulation of kisspeptin signal transduction pathways by artificial Kp-10 in A375 melanoma cells was performed in this study. In addition to the Kp-10 treatment, A375 cells were also treated with Kp-10 and 30μM HNK together, in order to gain further insights into the molecular mechanism of KISS1 / KISS1R signalling upon HNK treatment. It was shown that treatment with Kp-10 alone upregulated mRNA expression of *KISS1*, *TIMP-4*, *VEGF-A*, *NF-κB* and downregulated *MMP-2* mRNA expression in A375 cells. The mRNA and protein expression of MMP-9 and KISS1R was increased by Kp-10. Compared with Kp-10 alone, combined treatment of Kp-10 and HNK weakly decreased mRNA expression of *KISS1* and *MMP-2*, weakly increased mRNA expression of *TIMP-4* and *VEGF-A*, and increased KISS1R and MMP-9 expression at both the transcript and protein level. The *NF-κB* mRNA expression appeared unchanged by the combined treatment of Kp-10 and HNK.

Following Kp-10 treatment, the mRNA expression of *KISS1* and KISS1R mRNA and protein expression was markedly increased in human A375 melanoma cells, consistent results have been shown in first trimester human trophoblasts (Francis et al., 2014) and trophoblast BeWo cells (Bilban et al., 2004), suggesting that KISS1 / KISS1R signalling pathway may be activated by Kp-10 in human A375 melanoma cells. Based on this result, this study will initially discuss the molecular mechanisms underlying Kp-10 treatment in human A375 melanoma cells.

4.8.1. Kp-10 upregulates mRNA expression of *NF-κB* and increases MMP-9 mRNA and protein expression in human A375 cells.

Exposure to Kp-10 in A375 cells has shown that the mRNA expression of *NF-κB* (vehicle control 1.0 vs Kp-10 2.1; n=1) was weakly upregulated, and MMP-9 expression was increased at both the transcript (vehicle control 1.0 vs Kp-10 1.9; n=1) and protein level (vehicle control 1.0 vs Kp-10 1.2; n=1). This result is in contrast to the reported literature, in that kisspeptin treatment can inhibit MMP-9 production and enzymatic activities by inhibiting NF-κB signalling pathway in human renal cell carcinoma cells (Yoshioka et al., 2008), human prostate cancer cells (Cho et al., 2009) and human bladder cancer cells (Takeda et al., 2012). These studies have demonstrated that kisspeptin treatment can increase the number of cytosolic inhibitors of NF-κB proteins, and thus prevent the nuclear translocation of the p50/p65 subunits, which inhibit the ability of NF-κB binding to the *MMP-9* promoter and thereby consequently reduce MMP-9 expression in tumour cells (Yan et al., 2001, Takeda et al., 2012). Although the results from this study are in contrast with findings in previous studies, two possible mechanisms may explain the increase of MMP-9 expression, which will be discussed below.

Among the KISS1 / KISS1R signal transduction pathways, PI3K and its downstream substrate Akt has been shown to positively regulate NF-κB signalling pathway, it has been found that the phosphorylation of PI3K and Akt upstream of NF-κB signalling, regulated p65/p50 DNA-binding activities in tumour cells (Lee et al., 2012a, Bai et al., 2009, Agarwal et al., 2005). However, as introduced in **section 1.5.3.3**, the effect of Kp upon KISS1R in the activation of PI3K and Akt signalling pathway is dependent on the type of human cancer cells (Lee et al., 2012a). Although this study has not measured the expression

of PI3K and Akt after exposure to Kp-10, it was found that the mRNA expression of *NF-κB* was slightly increased by Kp-10, implying that the PI3K and Akt signalling cascades might be activated by KISS1 / KISS1R signalling pathway in human A375 melanoma cells (**Figure 4.1**). Therefore, one of the possible mechanisms is that KISS1 / KISS1R signalling pathway may be activated by Kp-10 treatment, which may trigger PI3K and its downstream substrate Akt to regulate the DNA-binding activities of NF-κB and thus may promote transcriptional activities of *MMP-9* in A375 cells. However, this hypothesis is still required to be examined in further studies, as discussed in **section 4.7.3**. Only p65 protein levels from whole cell extracts have been measured and therefore it is unknown whether NF-κB signalling pathway has been activated or inhibited following Kp-10 treatment in A375 cells.

Another possible mechanism is that following Kp-10 treatment, the activation of KISS1 / KISS1R signalling pathway may transactive other receptor kinase activities to promote the *MMP-9* transcription in A375 cells. In previous studies, Kp-10 treatment has been demonstrated to increase the secretion and activation of MMP-9 in human umbilical vein endothelial cells and breast cancer cells (Sato et al., 2017, Zajac et al., 2011). Zajac et al. (2011) indicated that KISS1R could directly transactivate epidermal growth factor receptor (EGFR) *via* β-arrestin 2-dependent mechanisms (internalisation of G protein-coupled receptors signalling). It is proposed that following the transactivation of EGFR by KISS1R, β-arrestin's scaffold proteins together with effector proteins Src can activate Ras/Raf/MEK/ERK pathway (Luttrell et al., 2001, Ranjan et al., 2016). Subsequently, β-arrestin 1 translocates into the nucleus in order to promote transcription by recruiting E2 factor, which has been shown previously to increase the expression of MMP-9 in human cancer cells (Dasgupta et al., 2011,

Cortes-Reynosa et al., 2008, Guerrero et al., 2004). Although this study did not examine the expression of EGFR, previous studies have demonstrated that human A375 melanoma cell line is expressing EGFR (Sweeny et al., 2016, Pietraszek-Gremplewicz et al., 2019). Based on the above discussion, one of the possible mechanisms is that, HNK (answering question in **section 4.7.1**) or Kp-10-modulated KISS1 / KISS1R signalling pathway can transactivate EGFR *via* internalisation of KISS1R, which contributes to the activation of Ras/Raf/MEK/ERK pathway and translocation of β-arrestin 1 into the nucleus for recruiting E2 factor, and ultimately promote the transcription activities of *MMP-9* in human A375 melanoma cells (**Figure 4.1**).

4.8.2. Kp-10 downregulates mRNA expression of *MMP-2* and upregulates *TIMP-4* mRNA expression in human A375 cells.

As to MMP-2, it was observed that Kp-10 treatment slightly reduced mRNA expression of *MMP-2* (vehicle control 1.0 vs Kp-10 0.59; n=1) in human A375 cells, similar results have been found in human colorectal cancer cells (Ji et al., 2014), human first trimester trophoblast cells (Francis et al., 2014) and human malignant mesothelioma cells (Ciaramella et al., 2018b). Among the KISS1 / KISS1R signal transduction pathways, JNK pathway has been demonstrated to be one of the key signals to mediate *MMP-2* transcription by phosphorylating the oncoprotein c-Jun (Li et al., 2017). c-Jun can regulate JunB-FosB heterodimers of activator protein 1 (AP-1) transcription factors, in order to bind to the target regulatory elements in the *MMP-2* gene promoter, and ultimately initiate the transcriptional activities of *MMP-2* (Li et al., 2017, Song et al., 2006, Ispanovic and Haas, 2006, Bergman et al., 2003, Yan et al., 2008).

The phosphorylation of JNK signal transduction pathway has been shown to be suppressed by KISS1 / KISS1R signalling pathway in Chinese hamster ovary

cells (Kotani et al., 2001). This suggests that Kp-10 modulated kisspeptin signalling pathway might inhibit the phosphorylation of JNK/c-Jun/AP-1 pathway, and thereby lead to the reduction of transcriptional activities of *MMP-2* in A375 melanoma cells (**Figure 4.1**). However, it has been suggested that where *MMP-2* gene promoters lack a conserved proximal AP-1 binding site due to the absence of a TATA box, *MMP-2* transcriptional activities might be differentially regulated in distinct cell types (Fanjul-Fernandez et al., 2010, Staun-Ram et al., 2009). The *MMP-2* gene promoter has a GC box at approximately −90 base pair, which is a binding site for AP-2 and Sp1 transcription factors (Fanjul-Fernandez et al., 2010, Staun-Ram et al., 2009). Therefore, a follow-up investigation should measure DNA-binding activities of AP-2 and Sp1 transcription factors in Kp-10-treated A375 cells, such as, using chromatin immunoprecipitation assay or DNA electrophoretic mobility shift assay.

In addition, it was shown that Kp-10 upregulated mRNA expression of *TIMP-4* (vehicle control 1.0 vs Kp-10 2.7; n=1) in human A375 cells, consistent results have been found in human renal cell carcinoma cells (Cheng et al., 2015) and human first trimester trophoblast cells (Francis et al., 2014). As introduced in **section 1.8.2**, TIMP-4 can bind to the carboxy-terminal hemopexin domain of the pro-MMP-2, and thus suppresses activation of pro-MMP-2 in the complex form (Melendez-Zajgla et al., 2008, Bigg et al., 2001). TIMP-4 has also been shown to competitively abolish pro-MMP-2 activation when *TIMP-2* is overexpressed in monkey kidney epithelial cells (Hernandez-Barrantes et al., 2001). This could be another important mechanism to reduce MMP-2 expression upon Kp-10 treatment by inhibiting the activation of pro-MMP-2 in human A375 melanoma cells.

4.8.3. Kp-10 weakly upregulates the mRNA expression of *VEGF-A* in human A375 cells.

When A375 cells were treated with Kp-10 for 24 hours, the mRNA expression of *VEGF-A* (vehicle control 1.0 vs Kp-10 1.4; n=1) was weakly upregulated, but not statistically significant. Unfortunately, this study did not measure the protein expression of VEGF-A due to a lack of primary antibody. Previous studies have indicated that Kp-10 treatment significantly reduced mRNA and protein expression of VEGF-A in human primary trophoblast cells (Francis et al., 2014) and human umbilical vein endothelial cells (Cho et al., 2009). Kp-10 has also been shown to reduce vessel sprouting in the placental artery *ex vivo* angiogenesis model, suppress blood vessel formation in chicken embryonic model and inhibit tumour angiogenesis in xenograft mouse models with human prostate cancer cells, indicating the inhibitory effects of Kp-10 in angiogenesis (Ramaesh et al., 2010, Cho et al., 2009). It has been demonstrated that Kp-10 mediated kisspeptin signalling pathway decreased binding activities of Sp1 transcription factors to a GC-rich core promoter region of *VEGF-A* (Cho et al., 2009, Zhang et al., 2007), suggesting that Kp-10-mediated KISS1 / KISS1R signalling might inhibit the initiation step of tumour angiogenesis *via* suppressing the transcriptional process of *VEGF-A* in human A375 melanoma cells (**Figure 4.1**).

As introduced in **section 1.1.1.2**, when metastatic melanoma cells secret VEGF-A interact with VEGF receptor-2 in endothelial cells, the VEGF receptor-2-binding c-Src protein recruits and activates focal adhesion kinase (FAK), in order to activate VEGF-mediated downstream signalling pathways in endothelial cells and contribute to the process of angiogenesis (Rudge et al., 2007). Interestingly, Kp-10 treatment has been found to suppress migration abilities and reduce tube

formation in human umbilical vein endothelial cells (HUVEC) (Usui et al., 2014, Cho et al., 2009). In agreement, in an *in vitro* migration assay, melanoma cells were used to act as a chemoattractant for HUVEC, in which Kp-10 treatment showed a significant inhibitory effect on migration of HUVEC (Golzar and Javanmard, 2015). Similarly, in human endothelial cells, KISS1 / KISS1R signalling pathway has been indicated to suppress VEGF-mediated angiogenesis by targeting the formation of c-Src/FAK signalling complexes, in order to inhibit the activation of Ras-related C3 botulinum toxin substrate 1 (Rac1) / cell division control protein 42 (Cdc42) GTPases and thus leading to the suppression of angiogenesis (Zahra et al., 2019, Wu et al., 2019, Caron et al., 2016, Cho et al., 2009).

Taken together, these results suggested that Kp-10 modulated KISS1 / KISS1R signalling pathway not only reduce VEGF-A production from A375 melanoma cells, but also decrease migratory capacities and inhibit the formation of capillary-like tubes in human endothelial cells, and thereby contribute to the suppression of angiogenesis (Golzar and Javanmard, 2015, Cho et al., 2009).

4.8.4. Combined treatment of Kp-10 and honokiol in human A375 melanoma cells.

To the best of our knowledge, this is the first study to investigate the molecular mechanisms underlying the combined treatment of Kp-10 and HNK in human A375 melanoma cells, and therefore, there is no literature to compare and contrast. However, based on the information from **section 4.8.1** to **section 4.8.3**, this study will only be offering a brief discussion. Compared to Kp-10 treatment alone, firstly, *KISS1* mRNA expression was only slightly reduced and KISS1R expression was markedly increased at both the transcript and protein level, implying that KISS1 / KISS1R signalling pathway may be activated in A375

cells. Secondly, the *NF-κB* mRNA expression remained relatively unchanged following combined treatment with Kp-10 and HNK, this may support the hypothesis in **section 4.7.3** in that, NF-κB proteins may not be the major targeted molecule in HNK-mediated kisspeptin signalling pathway. However, one of the limitations of this study is that only the transcript level was measured from the whole cell, and it is unknown whether NF-κB signalling pathway has been actually activated or inhibited. Therefore, further studies are required to investigate the activation of NF-κB signalling pathway upon combined treatment with Kp-10 and HNK in human A375 cells.

Thirdly, treatment with Kp-10 alone had no major effects in MMP-9 mRNA and protein expression, whilst the expression of MMP-9 was dramatically increased by the combined treatment of Kp-10 and HNK, suggesting that HNK may interact with Kp-10 to generate synergistic effects and which can notably stimulate the activation of KISS1 / KISS1R signalling pathway, contribute to the transactivation of EGFR by KISS1R and thereby promoting transcriptional activities of *MMP-9* in A375 cells.

Fourthly, compared to Kp-10 alone, treatment with Kp-10 and HNK only weakly upregulated *TIMP-4* and *VEGF-A* mRNA expression, suggesting that the synergistic effects might be limited under these conditions. Finally, Kp-10 treatment slightly reduced mRNA expression of *MMP-2*, and combined treatment with Kp-10 and HNK markedly decreased *MMP-2* expression, suggesting that HNK might target KISS1 / KISS1R signalling and other signal transductions, such as β-catenin signalling pathway (**section 4.7.1**) together to inhibit *MMP-2* transcription activities in human A375 cells.

There are some limitations of this experiment that only one biological replicate was conducted and lack of immunoblotting analyses to examine the protein expression, however, the data is still valuable because the results provide the fundamental outline for further studies to investigate the molecular mechanisms underlying the Kp-10 and HNK-modulated KISS1 / KISS1R signalling pathway in human A375 melanoma cells. Based on the discussion in **section 4.7** and **section 4.8**, a proposed molecule mechanism of Kp-10 and HNK-modulated KISS1 / KISS1R signalling pathway in human melanoma A375 cancer cells is summarised in **Figure 4.1.**

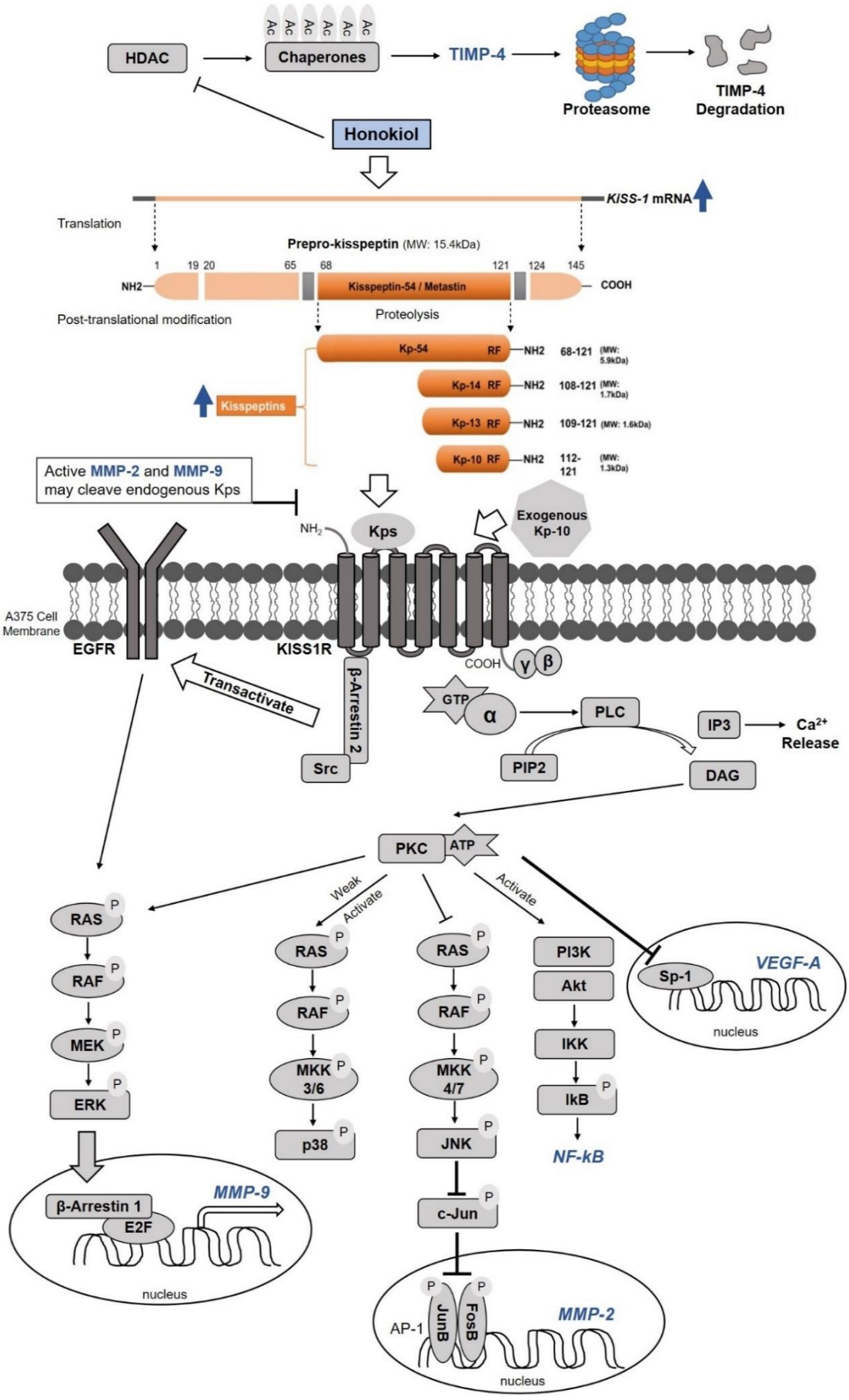

Figure 4.1. The proposed molecular mechanisms underlying the involvement of kisspeptin-10 and honokiol-modulated kisspeptin

signalling pathway in the inhibition of melanoma cancer metastasis. **HDAC**: histone deacetylases. **Ac**: acetyl groups. **Kps**: kisspeptins. **PLC**: phospholipase C. **PIP2**: phosphatidylinositol 4,5-bisphosphate. **IP3**: inositol trisphosphate. **DAG**: diacylglycerol. **Ca^{2+}**: calcium ion. **PKC**: protein kinase C. **MEK** / **MKK**: mitogen-activated protein kinases. **PI3K**: phosphatidylinositol-3-kinases. **Akt**: protein kinase B. **p38**: stress-activated protein kinases. **JNK**: c-Jun N-terminal kinases. **ERK**: extracellular signal-regulated kinase. **RAS**: small guanosine triphosphate. **RAF**: proto-oncogene serine/threonine-protein. **ATP**: adenosine triphosphate. **GTP**: guanosine triphosphate. **P**: phosphorylated. **NH_2**: azanide. **COOH**: carboxylic acid. **TIMP-4**: tissue inhibitors of matrix metalloproteinase 4. **MMP-2**: matrix metalloproteinase 2. **MMP-9**: matrix metalloproteinase 9. **KISS1**: kisspeptin. **KISS1R**: kisspeptin receptors. **NF-κB**: nuclear factor kappa-light-chain-enhancer of activated B cells. **IkB**: inhibitor of nuclear factor-κB. **IKK**: inhibitor of NF-κB kinase. **VEGF-A**: vascular endothelial growth factor A. **EGFR**: epidermal growth factor receptor. **E2F**: E2 factor family of transcription factors. **Sp-1**: Sp1 transcription factor. The activator protein 1 (**AP-1**) family is a group related JUN (**c-Jun**, **JunB**, and JunD) and FOS [c-FOS, **FosB**, Fos-related antigen 1 (FRA1), and FRA2] transcription factors. **kDa**: kilodalton. **MW**: molecular weight (Adapted from: Pai et al., 2020, Hu et al., 2017, Zajac et al., 2011, Cho et al., 2009b, Castano et al., 2009, Bergman et al., 2003).

Chapter 5. General discussion and conclusion

5.1. Hypothesis: honokiol might inhibit proliferation of human A375 melanoma cells by upregulating *KISS1* expression.

Previous studies have demonstrated that treatment with Kp-10 in human malignant pleural mesothelioma cells inhibited cellular proliferation in a dose-dependent manner (Ciaramella et al., 2018b). Similarly, *KISS1* overexpression in human gastric carcinoma cells and human osteosarcoma cells has been shown to suppress cellular proliferation in a time-dependent manner, suggesting that an increase expression of *KISS1* in tumours might contribute to the inhibition of cellular proliferation (Li et al., 2012, Zhang et al., 2013).

In contrast, no changes of cellular proliferation were found in human renal cell carcinoma Caki-1 cells (Shoji et al., 2009) and human pancreatic cancer PANC-1 cells (Wang et al., 2016, Masui et al., 2004) in response to Kp-54 treatment. Similarly, overexpression of *KISS1* in human breast cancer MDA MB 231 cells (Martin et al., 2005) and ovarian cancer SKOV3 cells (Jiang et al., 2005) has been shown not to generate any effects on cellular proliferation, however, it is important to note that low levels of the endogenous *KISS1R* are detected in these cell lines. These studies suggested that the controversial results on the influence of *KISS1* on cellular proliferation might be associated with cancer cell lines and the expression of endogenous *KISS1R*. Indeed, in human breast cancer HCC 1806 and MCF-7 cells with low endogenous *KISS1R* expression, it was found that there were no changes to cellular proliferation in response to Kp-10 treatment (Ziegler et al., 2013). However, the inhibition effect was observed in an artificial system of cells transfected with *KISS1R*. Ziegler et al. (2013) suggested that the antiproliferative effect of *KISS1* might depend on the nature of *KISS1R* expression in cellular plasma membrane.

This study has found a significant upregulation of *KISS1R* and *KISS1* mRNA expression in A375 cells treated with HNK. This suggested that inhibitory effects of HNK on the cellular proliferation might be associated with the upregulation of *KISS1R* expression, which in turn increases *KISS1*-mediated antiproliferative effects in human A375 melanoma cells. However, further experiments are required to assess this hypothesis, for instance, measuring cell viability followed by overexpression of *KISS1* and *KISS1R* in A375 cells individually.

Interestingly, intracardiac injection with human C8161.9 melanoma cells expressing *KISS1* into multiple organs (bone, eyes, kidney and lung) of mice has been found to completely block metastasis to multiple sites (Nash et al., 2007). It has also been shown that the cells persisted in mouse lungs for over 120 days without growth (mass) and proliferation (cell division), suggesting that *KISS1* could maintain the disseminated melanoma cells in a state of dormancy, and contribute to the suppression of cellular proliferation and metastatic colonisation to multiple sites (Nash et al., 2007).

To the best of our knowledge, this is the only published article indicating that *KISS1* can induce dormant state in malignant tumour cells. It is unknown whether this function is mediating by kisspeptin signalling pathway, since the lack of reliable, specific antibodies that recognise the KISS1 receptor in the Nash et al. (2007) study. Based on the findings from Nash et al. (2007) study, in that expressing *KISS1* in melanoma cells can maintain tumour dormancy. However, this study hypothesises that HNK-mediated upregulation of *KISS1* may induce dormancy in human A375 melanoma cells *via* autocrine kisspeptin signalling, and thus contribute to the suppression of cellular proliferation. Further studies should assess the stimulation of intracellular calcium mobilisation following HNK treatment, in order to support the hypothesis of autocrine kisspeptin signalling.

5.2. Further direction: RNA interference experiments.

This study had initially incorporated RNA interference of both *KISS1* and *KISS1R* transcripts, in order to investigate whether the effect of HNK in A375 cells is dependent on both or either KISS1 or KISS1R. A number of experimental parameters were attempted to optimise the transfection conditions, for instance, comparing different transfection reagents (Lipofectamine™ 2000 reagent vs. Oligofectamine™ reagent) and testing various working concentrations (**section 2.14**). Unfortunately, there was insufficient time to complete the RNA interference experiments due to the pandemic circumstances, follow-up studies can continue the RNA interference experiment in order to clarify whether the inhibitory effects of HNK in A375 cells is dependent on both or either KISS1 or KISS1R.

5.3. Study limitations and future perspectives.

Defective placentation has been suggested to be associated with various diseases of pregnancy, for example, failure of the trophoblasts to invade the uterus and failure to convert spiral arteries have been demonstrated to become the important causes in the placental pathology of pre-eclampsia (Goldman-Wohl and Yagel, 2002, Guo et al., 2016). As introduced in **section 1.2**, early stage trophoblast implantation strongly resembles melanoma metastasis (Soundararajan and Rao, 2004). This study has indicated that HNK may regulate melanoma metastasis by targeting KISS1 / KISS1R signalling pathways, and therefore, it is plausible that HNK may be a potential phytochemical to regulate the progress of pre-eclampsia. Indeed, a recent study has shown that HNK (200 μg/kg, 600 μg/kg and 2000 μg/kg; daily intake for one week *via* intragastric administration) dose-dependently reduced levels of urinary protein, decreased systolic blood pressure, increased VEGF-A levels and

exhibited anti-inflammatory activities (reduced the levels of IL-1β, IL-6 and TNF-α) in pregnancy-induced hypertension rats (Wang et al., 2020). An upregulation of VEGF-A expression was found to promote abilities of migration and tube formation in human trophoblast cells, indicating that HNK may generate pro-angiogenic property in pregnancy-induced hypertension rats (Wang et al., 2020, Guo et al., 2016). Therefore, these studies suggested that HNK may improve adaptive ability of pregnant patients with pre-eclampsia by increasing vasodilatory and eliciting pro-angiogenic activities, however, this hypothesis is still required to be explored in further studies (Wang et al., 2020, Guo et al., 2016).

Metastatic melanoma is a complex and molecularly heterogeneous disease, which is composed of a diverse collection of melanoma cell populations showing distinct molecular profiles and different responses to anti-cancer treatments (Dagogo-Jack and Shaw, 2018). There are several factors contributing to the development of melanoma, such as genetic, environmental and acquired factors. It has been discovered that approximately 40% to 60% of melanoma patients show an activating mutation in the gene encoding for the *BRAF* (Si et al., 2012, Curtin et al., 2005, Davies et al., 2002). The most common result of BRAF mutation is to cause a single base substitution of valine for glutamic acid at amino acid position 600 (V600E), which triggers the constitutive activation of MAPK pathways and thereby stimulates oncogenic activities of melanoma cells (Bucheit et al., 2013, Flaherty et al., 2010). KISS1 / KISS1R signalling has been indicated to regulate MAPK pathways, such as ERK1/2 and p38 (Castano et al., 2009). However, under these circumstances, it is unknown whether $BRAF^{V600E}$ mutation-mediated MAPK pathways will contribute to a positive or negative regulation to KISS1 / KISS1R signalling pathway in suppressing oncogenic

activities of BRAF mutant melanoma, which could be one of the research directions to investigate in further studies.

The active peptides of kisspeptin (Kp-54, Kp-14, Kp-13 and Kp-10) are secreted proteins, suggesting a possible therapeutic option where administration of Kp in a patient's body to reach a systemic distribution and ultimately access tumour cells through the bloodstream (Prague and Dhillo, 2015). It was reported that subcutaneous administration of a single dose of one picomole Kp-54 did not cause any reportable adverse effects in male adult rats, indicating that the administration of Kp in human body is strongly feasible (Patterson et al., 2006). In fact, the systemic administration of Kp for therapeutic applications has already been verified as safe in humans. One kisspeptin analogue (TAK-448) has been reported to be used in healthy human males and in those with prostate cancer (a single subcutaneous bolus injection between 0.01mg and 1mg per day for healthy subjects, 14 days; one-month depot injection in prostate cancer patients dosed with either 6mg, 12mg or 24mg), it was shown that the TAK-448 was effective and well tolerated in both healthy human and cancer patients (MacLean et al., 2014). In patients with prostate cancer, TAK-488 was found to reduce levels of testosterone and thus contribute to prostate-specific antigen responses (MacLean et al., 2014). However, based on the single one-month depot injection, it is unclear whether TAK-448 can elicit inhibitory effects in prostate tumour cells, suggesting that longer-term studies are still needed to investigate the potential anti-metastatic activities of TAK-448 (Matsui et al., 2014, MacLean et al., 2014).

One of the key limitations for using Kp as treatment in humans is that, chronic administration of Kp-54 in rats has been indicated to affect the physiological endocrine function and stimulate puberty, which result from the release of

gonadotropin-releasing hormone (Dhillo et al., 2007, Dhillo et al., 2005, Navarro et al., 2004). Theoretically, Kp treatment in tumour cells would be simple and straightforward if the cells express kisspeptin receptors, but the challenge is that some tumour cells do not express KISS1R (Ciaramella et al., 2018a, Nash et al., 2007). However, it is argued that KISS1-mediated antimetastatic effects do not require the expression of KISS1R, suggesting the existence of an intracrine signalling loop for KISS1 (Wang et al., 2016, Nash et al., 2007). If this hypothesis were to prove correct, it is theoretically possible to transfer *KISS1* gene by viral or non-viral gene delivery systems, and thereby initiating KISS1-mediated antimetastatic effects in the absence of the KISS1 receptors (Wirth and Yla-Herttuala, 2014).

This study has provided further evidence to support the possible therapeutic option for use of HNK as an agent to target KISS1 / KISS1R signalling pathway directly or indirectly in human melanoma cancer cells. Nevertheless, it is important to consider pharmacokinetic implications of HNK movement within the body (Ong et al., 2019). HNK has been demonstrated to undergo *in vivo* biotransformation through glucuronidation and sulfation in rat and human liver, which converts HNK into monoglucuronide HNK and sulphated hydroxy HNK before elimination (Bohmdorfer et al., 2011). However, it is unknown whether the process of biotransformation of HNK would reduce its bioavailability, and whether the metabolites of HNK still retain the anticancer properties to process biological activities. Additionally, it was reported that the presence of rhubarb and immature orange fruit extract in decoction form can influence the absorption, distribution and elimination of HNK (Su et al., 2008), suggesting that further studies are still required to clarify the pharmacokinetics of HNK.

Of note, this study has conducted *in vitro* research by growing A375 melanoma cells in monoculture on plastic cell culture dishes. Under these conditions, it is not able to accurately reflect the complexity of the microenvironment that involves structural heterogeneities and chemical gradients on tumour migration and invasion within a body (Talkenberger et al., 2017, Villanueva and Herlyn, 2008). New technologies have been developed for three-dimensional (3D) modelling of the tumour microenvironment, such as spheroid culture, biopolymer scaffolds, cancer-on-a-chip platform and 3D bioprinting (Wan et al., 2020, Datta et al., 2020, Brancato et al., 2017, Campbell et al., 2017). These *in vitro* tumour models aim to mimic the natural cancer microenvironment, in order to indicate the interactions between cell and cell, cell and matrix signalling pathways, and other important heterogeneous components such as tumour stroma (Asghar et al., 2015). Such technologies could be used in future research to expand *in vitro* findings of this study, which provides an exciting opportunity to improve the current understanding of molecular mechanisms of HNK-mediated KISS1 / KISS1R signalling pathway in the *in vivo* systems.

In spite of the limitations, *in vitro* findings still remain valuable to uncover the underlying molecular mechanisms and physiological effects in a given cell type. There are many variable factors that are not present in a cell line models and therefore allow characterisation of the mechanisms of HNK-mediated kisspeptin signalling pathway in a controlled environment. These *in vitro* results can function as the foundation for contributing to the translation of research findings of this study into a more complex microenvironment.

5.4. Conclusion

In conclusion, this study demonstrated that honokiol is a promising chemotherapeutic agent in the inhibition of metastatic cascade including: proliferation, metabolic activities and migration, but also induces apoptosis and morphological alterations in human melanoma cells. It has also provided insights into the molecular mechanism underlying honokiol-induced anti-metastasis, which may be through targeting KISS1 / KISS1R signalling pathway. It was revealed that honokiol-mediated KISS1 / KISS1R signalling pathway downregulate *VEGF-A* and *MMP-2* transcription, upregulate MMP-9 expression at both the transcript and protein level, upregulate *TIMP-4* transcription but detectable protein levels were decreased. The NF-κB mRNA and protein expression appear unchanged. This study suggests that KISS1 / KISS1R signalling pathway may be utilised as a potential therapeutic target for treating cancer and honokiol may become a promising anti-metastasis drug. The present results thus provide a foundation for further research studies and clinical development of honokiol against skin cancer.

References

ABBADY, A. Q., TWAIR, A., ALI, B. & MURAD, H. 2017. Characterization of Annexin V Fusion with the Superfolder GFP in Liposomes Binding and Apoptosis Detection. *Front Physiol,* 8**,** 317.

AGARWAL, A., DAS, K., LERNER, N., SATHE, S., CICEK, M., CASEY, G. & SIZEMORE, N. 2005. The AKT/I kappa B kinase pathway promotes angiogenic/metastatic gene expression in colorectal cancer by activating nuclear factor-kappa B and beta-catenin. *Oncogene,* 24**,** 1021-31.

AHN, K. S., SETHI, G., SHISHODIA, S., SUNG, B., ARBISER, J. L. & AGGARWAL, B. B. 2006. Honokiol potentiates apoptosis, suppresses osteoclastogenesis, and inhibits invasion through modulation of nuclear factor-kappaB activation pathway. *Mol Cancer Res,* 4**,** 621-33.

ALADOWICZ, E., FERRO, L., VITALI, G. C., VENDITTI, E., FORNASARI, L. & LANFRANCONE, L. 2013. Molecular networks in melanoma invasion and metastasis. *Future Oncol,* 9**,** 713-26.

ALONSO, S. R., ORTIZ, P., POLLAN, M., PEREZ-GOMEZ, B., SANCHEZ, L., ACUNA, M. J., PAJARES, R., MARTINEZ-TELLO, F. J., HORTELANO, C. M., PIRIS, M. A. & RODRIGUEZ-PERALTO, J. L. 2004. Progression in cutaneous malignant melanoma is associated with distinct expression profiles: a tissue microarray-based study. *Am J Pathol,* 164**,** 193-203.

AMARAL, C. L., FREITAS, L. B., TAMURA, R. E., TAVARES, M. R., PAVAN, I. C., BAJGELMAN, M. C. & SIMABUCO, F. M. 2016. S6Ks isoforms contribute to viability, migration, docetaxel resistance and tumor formation of prostate cancer cells. *BMC Cancer,* 16**,** 602.

ANDRE, T., KOTELEVETS, L., VAILLANT, J. C., COUDRAY, A. M., WEBER, L., PREVOT, S., PARC, R., GESPACH, C. & CHASTRE, E. 2000. Vegf, Vegf-B, Vegf-C and their receptors KDR, FLT-1 and FLT-4 during the neoplastic progression of human colonic mucosa. *Int J Cancer,* 86**,** 174-81.

ANTEBY, E. Y., GREENFIELD, C., NATANSON-YARON, S., GOLDMAN-WOHL, D., HAMANI, Y., KHUDYAK, V., ARIEL, I. & YAGEL, S. 2004. Vascular endothelial growth factor, epidermal growth factor and fibroblast growth factor-4 and -10 stimulate trophoblast plasminogen activator system and metalloproteinase-9. *Mol Hum Reprod,* 10**,** 229-35.

ANTICO ARCIUCH, V. G., ELGUERO, M. E., PODEROSO, J. J. & CARRERAS, M. C. 2012. Mitochondrial regulation of cell cycle and proliferation. *Antioxid Redox Signal,* 16**,** 1150-80.

APALLA, Z., NASHAN, D., WELLER, R. B. & CASTELLSAGUE, X. 2017. Skin Cancer: Epidemiology, Disease Burden, Pathophysiology, Diagnosis, and Therapeutic Approaches. *Dermatol Ther (Heidelb),* 7**,** 5-19.

ARORA, S., BHARDWAJ, A., SRIVASTAVA, S. K., SINGH, S., MCCLELLAN, S., WANG, B. & SINGH, A. P. 2011. Honokiol arrests cell cycle, induces apoptosis, and potentiates the cytotoxic effect of gemcitabine in human pancreatic cancer cells. *PLoS One,* 6**,** e21573.

ASGHAR, W., EL ASSAL, R., SHAFIEE, H., PITTERI, S., PAULMURUGAN, R. & DEMIRCI, U. 2015. Engineering cancer microenvironments for in vitro 3-D tumor models. *Mater Today (Kidlington),* 18**,** 539-553.

ATKINS, M. B., HODI, F. S., THOMPSON, J. A., MCDERMOTT, D. F., HWU, W. J., LAWRENCE, D. P., DAWSON, N. A., WONG, D. J., BHATIA, S., JAMES, M., JAIN, L., ROBEY, S., SHU, X., HOMET MORENO, B., PERINI, R. F., CHOUEIRI, T. K. & RIBAS, A. 2018. Pembrolizumab Plus Pegylated Interferon alfa-2b or Ipilimumab for Advanced Melanoma or Renal Cell Carcinoma: Dose-Finding Results from the Phase Ib KEYNOTE-029 Study. *Clin Cancer Res,* 24**,** 1805-1815.

AVTANSKI, D. B., NAGALINGAM, A., BONNER, M. Y., ARBISER, J. L., SAXENA, N. K. & SHARMA, D. 2014. Honokiol inhibits epithelial-mesenchymal transition in breast cancer cells by targeting signal transducer and activator of transcription 3/Zeb1/E-cadherin axis. *Mol Oncol,* 8**,** 565-80.

BAI, D., UENO, L. & VOGT, P. K. 2009. Akt-mediated regulation of NFkappaB and the essentialness of NFkappaB for the oncogenicity of PI3K and Akt. *Int J Cancer,* 125**,** 2863-70.

BAI, X., CERIMELE, F., USHIO-FUKAI, M., WAQAS, M., CAMPBELL, P. M., GOVINDARAJAN, B., DER, C. J., BATTLE, T., FRANK, D. A., YE, K., MURAD, E., DUBIEL, W., SOFF, G. & ARBISER, J. L. 2003. Honokiol, a small molecular weight natural product, inhibits angiogenesis in vitro and tumor growth in vivo. *J Biol Chem,* 278**,** 35501-7.

BANERJEE, P., BASU, A., ARBISER, J. L. & PAL, S. 2013. The natural product honokiol inhibits calcineurin inhibitor-induced and Ras-mediated tumor promoting pathways. *Cancer Lett,* 338**,** 292-9.

BEAUMONT, K. A., MOHANA-KUMARAN, N. & HAASS, N. K. 2013. Modeling Melanoma In Vitro and In Vivo. *Healthcare (Basel),* 2**,** 27-46.

BECKER, J. A., MIRJOLET, J. F., BERNARD, J., BURGEON, E., SIMONS, M. J., VASSART, G., PARMENTIER, M. & LIBERT, F. 2005. Activation of GPR54 promotes cell cycle arrest and apoptosis of human tumor cells through a specific transcriptional program not shared by other Gq-coupled receptors. *Biochem Biophys Res Commun,* 326**,** 677-86.

BERGMAN, M. R., CHENG, S., HONBO, N., PIACENTINI, L., KARLINER, J. S. & LOVETT, D. H. 2003. A functional activating protein 1 (AP-1) site regulates matrix metalloproteinase 2 (MMP-2) transcription by cardiac cells through interactions with JunB-Fra1 and JunB-FosB heterodimers. *Biochem J,* 369**,** 485-96.

BIGG, H. F., MORRISON, C. J., BUTLER, G. S., BOGOYEVITCH, M. A., WANG, Z., SOLOWAY, P. D. & OVERALL, C. M. 2001. Tissue inhibitor of metalloproteinases-4 inhibits but does not support the activation of gelatinase A via efficient inhibition of membrane type 1-matrix metalloproteinase. *Cancer Res,* 61**,** 3610-8.

BILBAN, M., GHAFFARI-TABRIZI, N., HINTERMANN, E., BAUER, S., MOLZER, S., ZORATTI, C., MALLI, R., SHARABI, A., HIDEN, U., GRAIER, W., KNOFLER, M., ANDREAE, F., WAGNER, O., QUARANTA, V. & DESOYE, G. 2004. Kisspeptin-10, a KiSS-1/metastin-derived decapeptide, is a physiological invasion inhibitor of primary human trophoblasts. *J Cell Sci,* 117**,** 1319-28.

BOHMDORFER, M., MAIER-SALAMON, A., TAFERNER, B., REZNICEK, G., THALHAMMER, T., HERING, S., HUFNER, A., SCHUHLY, W. & JAGER, W. 2011. In vitro metabolism and disposition of honokiol in rat and human livers. *J Pharm Sci,* 100**,** 3506-3516.

BORGHAEI, R. C., RAWLINGS, P. L., JR., JAVADI, M. & WOLOSHIN, J. 2004. NF-kappaB binds to a polymorphic repressor element in the MMP-3 promoter. *Biochem Biophys Res Commun,* 316**,** 182-8.

BRANCATO, V., COMUNANZA, V., IMPARATO, G., CORA, D., URCIUOLO, F., NOGHERO, A., BUSSOLINO, F. & NETTI, P. A. 2017. Bioengineered tumoral microtissues recapitulate desmoplastic reaction of pancreatic cancer. *Acta Biomater,* 49**,** 152-166.

BRAY, F., FERLAY, J., SOERJOMATARAM, I., SIEGEL, R. L., TORRE, L. A. & JEMAL, A. 2018. Global cancer statistics 2018: GLOBOCAN estimates of incidence and mortality worldwide for 36 cancers in 185 countries. *CA Cancer J Clin,* 68**,** 394-424.

BREW, K. & NAGASE, H. 2010. The tissue inhibitors of metalloproteinases (TIMPs): an ancient family with structural and functional diversity. *Biochim Biophys Acta,* 1803**,** 55-71.

BUCHEIT, A. D., SYKLAWER, E., JAKOB, J. A., BASSETT, R. L., JR., CURRY, J. L., GERSHENWALD, J. E., KIM, K. B., HWU, P., LAZAR, A. J. & DAVIES, M. A. 2013. Clinical characteristics and outcomes with specific BRAF and NRAS mutations in patients with metastatic melanoma. *Cancer,* 119**,** 3821-9.

BUSTIN, S. A., BENES, V., GARSON, J. A., HELLEMANS, J., HUGGETT, J., KUBISTA, M., MUELLER, R., NOLAN, T., PFAFFL, M. W., SHIPLEY, G. L., VANDESOMPELE, J. & WITTWER, C. T.

2009. The MIQE guidelines: minimum information for publication of quantitative real-time PCR experiments. *Clin Chem,* 55**,** 611-22.

CAMPBELL, J. J., HUSMANN, A., HUME, R. D., WATSON, C. J. & CAMERON, R. E. 2017. Development of three-dimensional collagen scaffolds with controlled architecture for cell migration studies using breast cancer cell lines. *Biomaterials,* 114**,** 34-43.

CARON, C., DEGEER, J., FOURNIER, P., DUQUETTE, P. M., LUANGRATH, V., ISHII, H., KARIMZADEH, F., LAMARCHE-VANE, N. & ROYAL, I. 2016. CdGAP/ARHGAP31, a Cdc42/Rac1 GTPase regulator, is critical for vascular development and VEGF-mediated angiogenesis. *Sci Rep,* 6**,** 27485.

CASTANO, J. P., MARTINEZ-FUENTES, A. J., GUTIERREZ-PASCUAL, E., VAUDRY, H., TENA-SEMPERE, M. & MALAGON, M. M. 2009. Intracellular signaling pathways activated by kisspeptins through GPR54: do multiple signals underlie function diversity? *Peptides,* 30**,** 10-5.

CEN, M., YAO, Y., CUI, L., YANG, G., LU, G., FANG, L., BAO, Z. & ZHOU, J. 2018. Honokiol induces apoptosis of lung squamous cell carcinoma by targeting FGF2-FGFR1 autocrine loop. *Cancer Med,* 7**,** 6205-6218.

CANCER RESEARCH UK. 2016. Melanoma skin cancer statistics. Retrieved from:https://www.cancerresearchuk.org/health-professional/cancer-statistics/statistics-by-cancer-type/melanoma-skin-cancer

CHEN, S., CHEN, W., ZHANG, X., LIN, S. & CHEN, Z. 2016. Overexpression of KiSS-1 reduces colorectal cancer cell invasion by downregulating MMP-9 via blocking PI3K/Akt/NF-kappaB signal pathway. *Int J Oncol,* 48**,** 1391-8.

CHEN, Y. J., WU, C. L., LIU, J. F., FONG, Y. C., HSU, S. F., LI, T. M., SU, Y. C., LIU, S. H. & TANG, C. H. 2010. Honokiol induces cell apoptosis in human chondrosarcoma cells through mitochondrial dysfunction and endoplasmic reticulum stress. *Cancer Lett,* 291**,** 20-30.

CHENG, S., CASTILLO, V., ELIAZ, I. & SLIVA, D. 2015. Honokiol suppresses metastasis of renal cell carcinoma by targeting KISS1/KISS1R signaling. *Int J Oncol,* 46**,** 2293-8.

CHENG, S., CASTILLO, V., WELTY, M., ELIAZ, I. & SLIVA, D. 2016. Honokiol inhibits migration of renal cell carcinoma through activation of RhoA/ROCK/MLC signaling pathway. *Int J Oncol,* 49**,** 1525-1530.

CHILAMPALLI, S., ZHANG, X., FAHMY, H., KAUSHIK, R. S., ZEMAN, D., HILDRETH, M. B. & DWIVEDI, C. 2010. Chemopreventive effects of honokiol on UVB-induced skin cancer development. *Anticancer Res,* 30**,** 777-83.

CHIU, C. S., TSAI, C. H., HSIEH, M. S., TSAI, S. C., JAN, Y. J., LIN, W. Y., LAI, D. W., WU, S. M., HSING, H. Y., ARBISER, J. L. & SHEU, M. L. 2019. Exploiting Honokiol-induced ER stress CHOP activation inhibits the growth and metastasis of melanoma by suppressing the MITF and beta-catenin pathways. *Cancer Lett,* 442**,** 113-125.

CHO, S. G., YI, Z., PANG, X., YI, T., WANG, Y., LUO, J., WU, Z., LI, D. & LIU, M. 2009. Kisspeptin-10, a KISS1-derived decapeptide, inhibits tumor angiogenesis by suppressing Sp1-mediated VEGF expression and FAK/Rho GTPase activation. *Cancer Res,* 69**,** 7062-70.

CIARAMELLA, V., DELLA CORTE, C. M., CIARDIELLO, F. & MORGILLO, F. 2018a. Kisspeptin and Cancer: Molecular Interaction, Biological Functions, and Future Perspectives. *Front Endocrinol (Lausanne),* 9**,** 115.

CIARAMELLA, V., DELLA CORTE, C. M., DI MAURO, C., TOMASSI, S., DI MARO, S., TROIANI, T., MARTINELLI, E., BIANCO, R., COSCONATI, S., PIERANTONI, R., MECCARIELLO, R., CHIANESE, R., CIARDIELLO, F. & MORGILLO, F. 2018b. Antitumor efficacy of Kisspeptin in human malignant mesothelioma cells. *Oncotarget,* 9**,** 19273-19282.

CORTES-REYNOSA, P., ROBLEDO, T., MACIAS-SILVA, M., WU, S. V. & SALAZAR, E. P. 2008. Src kinase regulates metalloproteinase-9 secretion induced by type IV collagen in MCF-7 human breast cancer cells. *Matrix Biol,* 27**,** 220-31.

CURTIN, J. A., FRIDLYAND, J., KAGESHITA, T., PATEL, H. N., BUSAM, K. J., KUTZNER, H., CHO, K. H., AIBA, S., BROCKER, E. B., LEBOIT, P. E., PINKEL, D. & BASTIAN, B. C. 2005. Distinct sets of genetic alterations in melanoma. *N Engl J Med,* 353**,** 2135-47.

DAGOGO-JACK, I. & SHAW, A. T. 2018. Tumour heterogeneity and resistance to cancer therapies. *Nat Rev Clin Oncol,* 15**,** 81-94.

DAI, X., LI, R. Z., JIANG, Z. B., WEI, C. L., LUO, L. X., YAO, X. J., LI, G. P. & LEUNG, E. L. 2018. Honokiol Inhibits Proliferation, Invasion and Induces Apoptosis Through Targeting Lyn Kinase in Human Lung Adenocarcinoma Cells. *Front Pharmacol,* 9**,** 558.

DASGUPTA, P., RIZWANI, W., PILLAI, S., DAVIS, R., BANERJEE, S., HUG, K., LLOYD, M., COPPOLA, D., HAURA, E. & CHELLAPPAN, S. P. 2011. ARRB1-mediated regulation of E2F target genes in nicotine-induced growth of lung tumors. *J Natl Cancer Inst,* 103**,** 317-33.

DATTA, P., DEY, M., ATAIE, Z., UNUTMAZ, D. & OZBOLAT, I. T. 2020. 3D bioprinting for reconstituting the cancer microenvironment. *NPJ Precis Oncol,* 4**,** 18.

DAVIES, H., BIGNELL, G. R., COX, C., STEPHENS, P., EDKINS, S., CLEGG, S., TEAGUE, J., WOFFENDIN, H., GARNETT, M. J., BOTTOMLEY, W., DAVIS, N., DICKS, E., EWING, R., FLOYD, Y., GRAY, K., HALL, S., HAWES, R., HUGHES, J., KOSMIDOU, V., MENZIES, A., MOULD, C., PARKER, A., STEVENS, C., WATT, S., HOOPER, S., WILSON, R., JAYATILAKE, H., GUSTERSON, B. A., COOPER, C., SHIPLEY, J., HARGRAVE, D., PRITCHARD-JONES, K., MAITLAND, N., CHENEVIX-TRENCH, G., RIGGINS, G. J., BIGNER, D. D., PALMIERI, G., COSSU, A., FLANAGAN, A., NICHOLSON, A., HO, J. W., LEUNG, S. Y., YUEN, S. T., WEBER, B. L., SEIGLER, H. F., DARROW, T. L., PATERSON, H., MARAIS, R., MARSHALL, C. J., WOOSTER, R., STRATTON, M. R. & FUTREAL, P. A. 2002. Mutations of the BRAF gene in human cancer. *Nature,* 417**,** 949-54.

DESJARDINS, P. & CONKLIN, D. 2010. NanoDrop microvolume quantitation of nucleic acids. *J Vis Exp*.

DHILLO, W. S., CHAUDHRI, O. B., PATTERSON, M., THOMPSON, E. L., MURPHY, K. G., BADMAN, M. K., MCGOWAN, B. M., AMBER, V., PATEL, S., GHATEI, M. A. & BLOOM, S. R. 2005. Kisspeptin-54 stimulates the hypothalamic-pituitary gonadal axis in human males. *J Clin Endocrinol Metab,* 90**,** 6609-15.

DHILLO, W. S., CHAUDHRI, O. B., THOMPSON, E. L., MURPHY, K. G., PATTERSON, M., RAMACHANDRAN, R., NIJHER, G. K., AMBER, V., KOKKINOS, A., DONALDSON, M., GHATEI, M. A. & BLOOM, S. R. 2007. Kisspeptin-54 stimulates gonadotropin release most potently during the preovulatory phase of the menstrual cycle in women. *J Clin Endocrinol Metab,* 92**,** 3958-66.

DRUMMOND, D. A. & WILKE, C. O. 2009. The evolutionary consequences of erroneous protein synthesis. *Nat Rev Genet,* 10**,** 715-24.

EGGERMONT, A. M., SUCIU, S., SANTINAMI, M., TESTORI, A., KRUIT, W. H., MARSDEN, J., PUNT, C. J., SALES, F., GORE, M., MACKIE, R., KUSIC, Z., DUMMER, R., HAUSCHILD, A., MUSAT, E., SPATZ, A., KEILHOLZ, U. & GROUP, E. M. 2008. Adjuvant therapy with pegylated interferon alfa-2b versus observation alone in resected stage III melanoma: final results of EORTC 18991, a randomised phase III trial. *Lancet,* 372**,** 117-26.

EIGENTLER, T. K., GUTZMER, R., HAUSCHILD, A., HEINZERLING, L., SCHADENDORF, D., NASHAN, D., HOLZLE, E., KIECKER, F., BECKER, J., SUNDERKOTTER, C., MOLL, I., RICHTIG, E., PONITZSCH, I., PEHAMBERGER, H., KAUFMANN, R., PFOHLER, C., VOGT, T., BERKING, C., PRAXMARER, M., GARBE, C. & DERMATOLOGIC COOPERATIVE ONCOLOGY, G. 2016. Adjuvant treatment with pegylated interferon alpha-2a versus low-dose interferon alpha-2a in patients with high-risk melanoma: a randomized phase III DeCOG trial. *Ann Oncol,* 27**,** 1625-32.

ELLISON, G., KLINOWSKA, T., WESTWOOD, R. F., DOCTER, E., FRENCH, T. & FOX, J. C. 2002. Further evidence to support the melanocytic origin of MDA-MB-435. *Mol Pathol,* 55**,** 294-9.

ESUMI, T., MAKADO, G., ZHAI, H., SHIMIZU, Y., MITSUMOTO, Y. & FUKUYAMA, Y. 2004. Efficient synthesis and structure-activity relationship of honokiol, a neurotrophic biphenyl-type neolignan. *Bioorg Med Chem Lett,* 14**,** 2621-5.

FAN, Y., XUE, W., SCHACHNER, M. & ZHAO, W. 2018. Honokiol Eliminates Glioma/Glioblastoma Stem Cell-Like Cells Via JAK-STAT3 Signaling and Inhibits Tumor Progression by Targeting Epidermal Growth Factor Receptor. *Cancers (Basel),* 11.

FERREIRA, T. & RASBAND, W. 2012. ImageJ User Guide. Retrieved from: https://imagej.nih.gov/ij/docs/guide/

FANJUL-FERNANDEZ, M., FOLGUERAS, A. R., CABRERA, S. & LOPEZ-OTIN, C. 2010. Matrix metalloproteinases: evolution, gene regulation and functional analysis in mouse models. *Biochim Biophys Acta,* 1803**,** 3-19.

FENG, Q., LIU, K., LIU, Y. X., BYRNE, S. & OCKLEFORD, C. D. 2001. Plasminogen activators and inhibitors are transcribed during early macaque implantation. *Placenta,* 22**,** 186-99.

FLAHERTY, K. T., PUZANOV, I., KIM, K. B., RIBAS, A., MCARTHUR, G. A., SOSMAN, J. A., O'DWYER, P. J., LEE, R. J., GRIPPO, J. F., NOLOP, K. & CHAPMAN, P. B. 2010. Inhibition of mutated, activated BRAF in metastatic melanoma. *N Engl J Med,* 363**,** 809-19.

FLAHERTY, K. T., ROBERT, C., HERSEY, P., NATHAN, P., GARBE, C., MILHEM, M., DEMIDOV, L. V., HASSEL, J. C., RUTKOWSKI, P., MOHR, P., DUMMER, R., TREFZER, U., LARKIN, J. M., UTIKAL, J., DRENO, B., NYAKAS, M., MIDDLETON, M. R., BECKER, J. C., CASEY, M., SHERMAN, L. J., WU, F. S., OUELLET, D., MARTIN, A. M., PATEL, K., SCHADENDORF, D. & GROUP, M. S. 2012. Improved survival with MEK inhibition in BRAF-mutated melanoma. *N Engl J Med,* 367**,** 107-14.

FLEIGE, S. & PFAFFL, M. W. 2006. RNA integrity and the effect on the real-time qRT-PCR performance. *Mol Aspects Med,* 27**,** 126-39.

FRANCIS, V. A., ABERA, A. B., MATJILA, M., MILLAR, R. P. & KATZ, A. A. 2014. Kisspeptin regulation of genes involved in cell invasion and angiogenesis in first trimester human trophoblast cells. *PLoS One,* 9**,** e99680.

FRASER, J. A., SUTTON, J. E., TAZAYONI, S., BRUCE, I. & POOLE, A. V. 2019. hASH1 nuclear localization persists in neuroendocrine transdifferentiated prostate cancer cells, even upon reintroduction of androgen. *Sci Rep,* 9**,** 19076.

GALVAO, J., DAVIS, B., TILLEY, M., NORMANDO, E., DUCHEN, M. R. & CORDEIRO, M. F. 2014. Unexpected low-dose toxicity of the universal solvent DMSO. *FASEB J,* 28**,** 1317-30.

GAO, D. Q., QIAN, S. & JU, T. 2016. Anticancer activity of Honokiol against lymphoid malignant cells via activation of ROS-JNK and attenuation of Nrf2 and NF-kappaB. *J BUON,* 21**,** 673-9.

GAO, K., DAI, D. L., MARTINKA, M. & LI, G. 2006. Prognostic significance of nuclear factor-kappaB p105/p50 in human melanoma and its role in cell migration. *Cancer Res,* 66**,** 8382-8.

GOERTZEN, C. G., DRAGAN, M., TURLEY, E., BABWAH, A. V. & BHATTACHARYA, M. 2016. KISS1R signaling promotes invadopodia formation in human breast cancer cell via beta-arrestin2/ERK. *Cell Signal,* 28**,** 165-176.

GOLDMAN-WOHL, D. & YAGEL, S. 2002. Regulation of trophoblast invasion: from normal implantation to pre-eclampsia. *Mol Cell Endocrinol,* 187**,** 233-8.

GOLZAR, F. & JAVANMARD, S. H. 2015. The effects of kisspeptin-10 on migration and proliferation of endothelial cell. *Adv Biomed Res,* 4**,** 41.

GUERRERO, J., SANTIBANEZ, J. F., GONZALEZ, A. & MARTINEZ, J. 2004. EGF receptor transactivation by urokinase receptor stimulus through a mechanism involving Src and matrix metalloproteinases. *Exp Cell Res,* 292**,** 201-8.

GUILLERMO-LAGAE, R., SANTHA, S., THOMAS, M., ZOELLE, E., STEVENS, J., KAUSHIK, R. S. & DWIVEDI, C. 2017. Antineoplastic Effects of Honokiol on Melanoma. *Biomed Res Int,* 2017**,** 5496398.

GUO, X., FENG, L., JIA, J., CHEN, R. & YU, J. 2016. Upregulation of VEGF by small activating RNA and its implications in preeclampsia. *Placenta,* 46**,** 38-44.

GUPTA, M. K. & QIN, R. Y. 2003. Mechanism and its regulation of tumor-induced angiogenesis. *World J Gastroenterol,* 9**,** 1144-55.

GUPTA, S. C., KIM, J. H., PRASAD, S. & AGGARWAL, B. B. 2010. Regulation of survival, proliferation, invasion, angiogenesis, and metastasis of tumor cells through modulation of inflammatory pathways by nutraceuticals. *Cancer Metastasis Rev,* 29**,** 405-34.

GUZMAN, S., BRACKSTONE, M., RADOVICK, S., BABWAH, A. V. & BHATTACHARYA, M. M. 2018. KISS1/KISS1R in Cancer: Friend or Foe? *Front Endocrinol (Lausanne),* 9**,** 437.

HAMID, O., ROBERT, C., DAUD, A., HODI, F. S., HWU, W. J., KEFFORD, R., WOLCHOK, J. D., HERSEY, P., JOSEPH, R., WEBER, J. S., DRONCA, R., MITCHELL, T. C., PATNAIK, A., ZAROUR, H. M., JOSHUA, A. M., ZHAO, Q., JENSEN, E., AHSAN, S., IBRAHIM, N. & RIBAS, A. 2019. Five-year survival outcomes for patients with advanced melanoma treated with pembrolizumab in KEYNOTE-001. *Ann Oncol,* 30**,** 582-588.

HANCHATE, N. K., PARKASH, J., BELLEFONTAINE, N., MAZUR, D., COLLEDGE, W. H., D'ANGLEMONT DE TASSIGNY, X. & PREVOT, V. 2012. Kisspeptin-GPR54 signaling in mouse NO-synthesizing neurons participates in the hypothalamic control of ovulation. *J Neurosci,* 32**,** 932-45.

HARIHAR, S., POUNDS, K. M., IWAKUMA, T., SEIDAH, N. G. & WELCH, D. R. 2014. Furin is the major proprotein convertase required for KISS1-to-Kisspeptin processing. *PLoS One,* 9**,** e84958.

HARLOZINSKA, A. 2005. Progress in molecular mechanisms of tumor metastasis and angiogenesis. *Anticancer Res,* 25**,** 3327-33.

HAUSCHILD, A., GROB, J. J., DEMIDOV, L. V., JOUARY, T., GUTZMER, R., MILLWARD, M., RUTKOWSKI, P., BLANK, C. U., MILLER, W. H., JR., KAEMPGEN, E., MARTIN-ALGARRA, S., KARASZEWSKA, B., MAUCH, C., CHIARION-SILENI, V., MARTIN, A. M., SWANN, S., HANEY, P., MIRAKHUR, B., GUCKERT, M. E., GOODMAN, V. & CHAPMAN, P. B. 2012. Dabrafenib in BRAF-mutated metastatic melanoma: a multicentre, open-label, phase 3 randomised controlled trial. *Lancet,* 380**,** 358-65.

HEBLING, J., BIANCHI, L., BASSO, F. G., SCHEFFEL, D. L., SOARES, D. G., CARRILHO, M. R., PASHLEY, D. H., TJADERHANE, L. & DE SOUZA COSTA, C. A. 2015. Cytotoxicity of dimethyl sulfoxide (DMSO) in direct contact with odontoblast-like cells. *Dent Mater,* 31**,** 399-405.

HERNANDEZ-BARRANTES, S., SHIMURA, Y., SOLOWAY, P. D., SANG, Q. A. & FRIDMAN, R. 2001. Differential roles of TIMP-4 and TIMP-2 in pro-MMP-2 activation by MT1-MMP. *Biochem Biophys Res Commun,* 281**,** 126-30.

HLUBEK, F., SPADERNA, S., JUNG, A., KIRCHNER, T. & BRABLETZ, T. 2004. Beta-catenin activates a coordinated expression of the proinvasive factors laminin-5 gamma2 chain and MT1-MMP in colorectal carcinomas. *Int J Cancer,* 108**,** 321-6.

HOFMANN, U. B., HOUBEN, R., BROCKER, E. B. & BECKER, J. C. 2005. Role of matrix metalloproteinases in melanoma cell invasion. *Biochimie,* 87**,** 307-14.

HOLMES, D. I. & ZACHARY, I. 2005. The vascular endothelial growth factor (VEGF) family: angiogenic factors in health and disease. *Genome Biol,* 6**,** 209.

HORIKOSHI, Y., MATSUMOTO, H., TAKATSU, Y., OHTAKI, T., KITADA, C., USUKI, S. & FUJINO, M. 2003. Dramatic elevation of plasma metastin concentrations in human pregnancy: metastin as a novel placenta-derived hormone in humans. *J Clin Endocrinol Metab,* 88**,** 914-9.

HSIAO, C. H., YAO, C. J., LAI, G. M., LEE, L. M., WHANG-PENG, J. & SHIH, P. H. 2019. Honokiol induces apoptotic cell death by oxidative burst and mitochondrial hyperpolarization of bladder cancer cells. *Exp Ther Med,* 17**,** 4213-4222.

HU, J., CHEN, L. J., LIU, L., CHEN, X., CHEN, P. L., YANG, G., HOU, W. L., TANG, M. H., ZHANG, F., WANG, X. H., ZHAO, X. & WEI, Y. Q. 2008. Liposomal honokiol, a potent anti-angiogenesis agent, in combination with radiotherapy produces a synergistic antitumor efficacy without increasing toxicity. *Exp Mol Med,* 40**,** 617-28.

HU, K. L., ZHAO, H., CHANG, H. M., YU, Y. & QIAO, J. 2017. Kisspeptin/Kisspeptin Receptor System in the Ovary. *Front Endocrinol (Lausanne),* 8**,** 365.

HUA, H., CHEN, W., SHEN, L., SHENG, Q. & TENG, L. 2013. Honokiol augments the anti-cancer effects of oxaliplatin in colon cancer cells. *Acta Biochim Biophys Sin (Shanghai),* 45**,** 773-9.

HUANG, H. 2018. Matrix Metalloproteinase-9 (MMP-9) as a Cancer Biomarker and MMP-9 Biosensors: Recent Advances. *Sensors (Basel),* 18.

HUANG, K., CHEN, Y., ZHANG, R., WU, Y., MA, Y., FANG, X. & SHEN, S. 2018a. Honokiol induces apoptosis and autophagy via the ROS/ERK1/2 signaling pathway in human osteosarcoma cells in vitro and in vivo. *Cell Death Dis,* 9**,** 157.

HUANG, K. J., KUO, C. H., CHEN, S. H., LIN, C. Y. & LEE, Y. R. 2018b. Honokiol inhibits in vitro and in vivo growth of oral squamous cell carcinoma through induction of apoptosis, cell cycle arrest and autophagy. *J Cell Mol Med,* 22**,** 1894-1908.

IP, C. K., CHEUNG, A. N., NGAN, H. Y. & WONG, A. S. 2011. p70 S6 kinase in the control of actin cytoskeleton dynamics and directed migration of ovarian cancer cells. *Oncogene,* 30**,** 2420-32.

ISPANOVIC, E. & HAAS, T. L. 2006. JNK and PI3K differentially regulate MMP-2 and MT1-MMP mRNA and protein in response to actin cytoskeleton reorganization in endothelial cells. *Am J Physiol Cell Physiol,* 291**,** C579-88.

JANIAK, M., PASKAL, W., RAK, B., GARBICZ, F., JAREMA, R., SIKORA, K. & WLODARSKI, P. 2017. TIMP4 expression is regulated by miR-200b-3p in prostate cancer cells. *APMIS,* 125**,** 101-105.

JANNEAU, J. L., MALDONADO-ESTRADA, J., TACHDJIAN, G., MIRAN, I., MOTTE, N., SAULNIER, P., SABOURIN, J. C., COTE, J. F., SIMON, B., FRYDMAN, R., CHAOUAT, G. & BELLET, D. 2002. Transcriptional expression of genes involved in cell invasion and migration by normal and tumoral trophoblast cells. *J Clin Endocrinol Metab,* 87**,** 5336-9.

JI, K., YE, L., RUGE, F., HARGEST, R., MASON, M. D. & JIANG, W. G. 2014. Implication of metastasis suppressor gene, Kiss-1 and its receptor Kiss-1R in colorectal cancer. *BMC Cancer,* 14**,** 723.

JIANG, W. G., SANDERS, A. J., KATOH, M., UNGEFROREN, H., GIESELER, F., PRINCE, M., THOMPSON, S. K., ZOLLO, M., SPANO, D., DHAWAN, P., SLIVA, D., SUBBARAYAN, P. R., SARKAR, M., HONOKI, K., FUJII, H., GEORGAKILAS, A. G., AMEDEI, A., NICCOLAI, E., AMIN, A., ASHRAF, S. S., YE, L., HELFERICH, W. G., YANG, X., BOOSANI, C. S., GUHA, G., CIRIOLO, M. R., AQUILANO, K., CHEN, S., AZMI, A. S., KEITH, W. N., BILSLAND, A., BHAKTA, D., HALICKA, D., NOWSHEEN, S., PANTANO, F. & SANTINI, D. 2015. Tissue invasion and metastasis: Molecular, biological and clinical perspectives. *Semin Cancer Biol,* 35 Suppl**,** S244-S275.

JIANG, Y., BERK, M., SINGH, L. S., TAN, H., YIN, L., POWELL, C. T. & XU, Y. 2005. KiSS1 suppresses metastasis in human ovarian cancer via inhibition of protein kinase C alpha. *Clin Exp Metastasis,* 22**,** 369-76.

JIAO, Y., FENG, X., ZHAN, Y., WANG, R., ZHENG, S., LIU, W. & ZENG, X. 2012. Matrix metalloproteinase-2 promotes alphavbeta3 integrin-mediated adhesion and migration of human melanoma cells by cleaving fibronectin. *PLoS One,* 7**,** e41591.

JIRAVIRIYAKUL, A., SONGJANG, W., KAEWTHET, P., TANAWATKITICHAI, P., BAYAN, P. & PONGCHAROEN, S. 2019. Honokiol-enhanced cytotoxic T lymphocyte activity against cholangiocarcinoma cells mediated by dendritic cells pulsed with damage-associated molecular patterns. *World J Gastroenterol,* 25**,** 3941-3955.

KAUSHIK, G., KWATRA, D., SUBRAMANIAM, D., JENSEN, R. A., ANANT, S. & MAMMEN, J. M. 2014. Honokiol affects melanoma cell growth by targeting the AMP-activated protein kinase signaling pathway. *Am J Surg,* 208**,** 995-1002; discussion 1001-2.

KAUSHIK, G., RAMALINGAM, S., SUBRAMANIAM, D., RANGARAJAN, P., PROTTI, P., RAMMAMOORTHY, P., ANANT, S. & MAMMEN, J. M. 2012. Honokiol induces cytotoxic and cytostatic effects in malignant melanoma cancer cells. *Am J Surg,* 204**,** 868-73.

KAUSHIK, G., VENUGOPAL, A., RAMAMOORTHY, P., STANDING, D., SUBRAMANIAM, D., UMAR, S., JENSEN, R. A., ANANT, S. & MAMMEN, J. M. 2015. Honokiol inhibits melanoma stem cells by targeting notch signaling. *Mol Carcinog,* 54**,** 1710-21.

KOTANI, M., DETHEUX, M., VANDENBOGAERDE, A., COMMUNI, D., VANDERWINDEN, J. M., LE POUL, E., BREZILLON, S., TYLDESLEY, R., SUAREZ-HUERTA, N., VANDEPUT, F., BLANPAIN, C., SCHIFFMANN, S. N., VASSART, G. & PARMENTIER, M. 2001. The metastasis suppressor gene KiSS-1 encodes kisspeptins, the natural ligands of the orphan G protein-coupled receptor GPR54. *J Biol Chem,* 276**,** 34631-6.

KOUSSOUNADIS, A., LANGDON, S. P., UM, I. H., HARRISON, D. J. & SMITH, V. A. 2015. Relationship between differentially expressed mRNA and mRNA-protein correlations in a xenograft model system. *Sci Rep,* 5**,** 10775.

KRISHNAMURTHY, N. & KURZROCK, R. 2018. Targeting the Wnt/beta-catenin pathway in cancer: Update on effectors and inhibitors. *Cancer Treat Rev,* 62**,** 50-60.

KUANG, J., YAN, X., GENDERS, A. J., GRANATA, C. & BISHOP, D. J. 2018. An overview of technical considerations when using quantitative real-time PCR analysis of gene expression in human exercise research. *PLoS One,* 13**,** e0196438.

LACAL, P. M., RUFFINI, F., PAGANI, E. & D'ATRI, S. 2005. An autocrine loop directed by the vascular endothelial growth factor promotes invasiveness of human melanoma cells. *Int J Oncol,* 27**,** 1625-32.

LIOU, S. F., HUA, K. T., HSU, C. Y., & WENG, M. S. 2015. Honokiol from Magnolia spp. induces G1 arrest via disruption of EGFR stability through repressing HDAC6 deacetylated Hsp90 function in lung cancer cells. *Journal of functional foods*, 15, 84-96.

LAI, I. C., SHIH, P. H., YAO, C. J., YEH, C. T., WANG-PENG, J., LUI, T. N., CHUANG, S. E., HU, T. S., LAI, T. Y. & LAI, G. M. 2015. Elimination of cancer stem-like cells and potentiation of temozolomide sensitivity by Honokiol in glioblastoma multiforme cells. *PLoS One,* 10**,** e0114830.

LAKSHMANAN, I. & BATRA, S. K. 2013. Protocol for Apoptosis Assay by Flow Cytometry Using Annexin V Staining Method. *Bio Protoc,* 3.

LANGLEY, R. R., CARLISLE, R., MA, L., SPECIAN, R. D., GERRITSEN, M. E. & GRANGER, D. N. 2001. Endothelial expression of vascular cell adhesion molecule-1 correlates with metastatic pattern in spontaneous melanoma. *Microcirculation,* 8**,** 335-45.

LEE, D. K., NGUYEN, T., O'NEILL, G. P., CHENG, R., LIU, Y., HOWARD, A. D., COULOMBE, N., TAN, C. P., TANG-NGUYEN, A. T., GEORGE, S. R. & O'DOWD, B. F. 1999. Discovery of a receptor related to the galanin receptors. *FEBS Lett,* 446**,** 103-7.

LEE, J. H., MIELE, M. E., HICKS, D. J., PHILLIPS, K. K., TRENT, J. M., WEISSMAN, B. E. & WELCH, D. R. 1996. KiSS-1, a novel human malignant melanoma metastasis-suppressor gene. *J Natl Cancer Inst,* 88**,** 1731-7.

LEE, J. H. & WELCH, D. R. 1997. Suppression of metastasis in human breast carcinoma MDA-MB-435 cells after transfection with the metastasis suppressor gene, KiSS-1. *Cancer Res,* 57**,** 2384-7.

LEE, J. S., SUL, J. Y., PARK, J. B., LEE, M. S., CHA, E. Y. & KO, Y. B. 2019. Honokiol induces apoptosis and suppresses migration and invasion of ovarian carcinoma cells via AMPK/mTOR signaling pathway. *Int J Mol Med,* 43**,** 1969-1978.

LEE, K. B., BYUN, H. J., PARK, S. H., PARK, C. Y., LEE, S. H. & RHO, S. B. 2012a. CYR61 controls p53 and NF-kappaB expression through PI3K/Akt/mTOR pathways in carboplatin-induced ovarian cancer cells. *Cancer Lett,* 315**,** 86-95.

LEE, P. Y., COSTUMBRADO, J., HSU, C. Y. & KIM, Y. H. 2012b. Agarose gel electrophoresis for the separation of DNA fragments. *J Vis Exp*.

LEVY, M. S., LOTFIAN, P., O'KENNEDY, R., LO-YIM, M. Y. & SHAMLOU, P. A. 2000. Quantitation of supercoiled circular content in plasmid DNA solutions using a fluorescence-based method. *Nucleic Acids Res,* 28**,** E57.

LI, L. H., WU, G. Y., LU, Y. Z., CHEN, X. H., LIU, B. Y., ZHENG, M. H. & CAI, J. C. 2017. p21-activated protein kinase 1 induces the invasion of gastric cancer cells through c-Jun

NH2-terminal kinase-mediated activation of matrix metalloproteinase-2. *Oncol Rep,* 38**,** 193-200.
LI, N., WANG, H. X., ZHANG, J., YE, Y. P. & HE, G. Y. 2012. KISS-1 inhibits the proliferation and invasion of gastric carcinoma cells. *World J Gastroenterol,* 18**,** 1827-33.
LI, T. H. & YAN, H. X. 2018. Antitumor and apoptosisinducing effects of pomolic acid against SKMEL2 human malignant melanoma cells are mediated via inhibition of cell migration and subG1 cell cycle arrest. *Mol Med Rep,* 17**,** 1035-1040.
LI, W., WANG, Q., SU, Q., MA, D., AN, C., MA, L. & LIANG, H. 2014. Honokiol suppresses renal cancer cells' metastasis via dual-blocking epithelial-mesenchymal transition and cancer stem cell properties through modulating miR-141/ZEB2 signaling. *Mol Cells,* 37**,** 383-8.
LI, Z., LIU, Y., ZHAO, X., PAN, X., YIN, R., HUANG, C., CHEN, L. & WEI, Y. 2008. Honokiol, a natural therapeutic candidate, induces apoptosis and inhibits angiogenesis of ovarian tumor cells. *Eur J Obstet Gynecol Reprod Biol,* 140**,** 95-102.
LIAN, L., LI, X. L., XU, M. D., LI, X. M., WU, M. Y., ZHANG, Y., TAO, M., LI, W., SHEN, X. M., ZHOU, C. & JIANG, M. 2019. VEGFR2 promotes tumorigenesis and metastasis in a pro-angiogenic-independent way in gastric cancer. *BMC Cancer,* 19**,** 183.
LIANG, W. Z., CHOU, C. T., CHANG, H. T., CHENG, J. S., KUO, D. H., KO, K. C., CHIANG, N. N., WU, R. F., SHIEH, P. & JAN, C. R. 2014. The mechanism of honokiol-induced intracellular Ca(2+) rises and apoptosis in human glioblastoma cells. *Chem Biol Interact,* 221**,** 13-23.
LIN, J. W., CHEN, J. T., HONG, C. Y., LIN, Y. L., WANG, K. T., YAO, C. J., LAI, G. M. & CHEN, R. M. 2012. Honokiol traverses the blood-brain barrier and induces apoptosis of neuroblastoma cells via an intrinsic bax-mitochondrion-cytochrome c-caspase protease pathway. *Neuro Oncol,* 14**,** 302-14.
LIOU, K. T., LIN, S. M., HUANG, S. S., CHIH, C. L. & TSAI, S. K. 2003. Honokiol ameliorates cerebral infarction from ischemia-reperfusion injury in rats. *Planta Med,* 69**,** 130-4.
LIU, T., ZHANG, L., JOO, D. & SUN, S. C. 2017. NF-kappaB signaling in inflammation. *Signal Transduct Target Ther,* 2.
LIU, Y. & SHEIKH, M. S. 2014. Melanoma: Molecular Pathogenesis and Therapeutic Management. *Mol Cell Pharmacol,* 6**,** 228.
LIVAK, K. J. & SCHMITTGEN, T. D. 2001. Analysis of relative gene expression data using real-time quantitative PCR and the 2(-Delta Delta C(T)) Method. *Methods,* 25**,** 402-8.
LU, C. H., CHEN, S. H., CHANG, Y. S., LIU, Y. W., WU, J. Y., LIM, Y. P., YU, H. I. & LEE, Y. R. 2017. Honokiol, a potential therapeutic agent, induces cell cycle arrest and program cell death in vitro and in vivo in human thyroid cancer cells. *Pharmacol Res,* 115**,** 288-298.
LUTTRELL, L. M., ROUDABUSH, F. L., CHOY, E. W., MILLER, W. E., FIELD, M. E., PIERCE, K. L. & LEFKOWITZ, R. J. 2001. Activation and targeting of extracellular signal-regulated kinases by beta-arrestin scaffolds. *Proc Natl Acad Sci U S A,* 98**,** 2449-54.
LV, X. Q., QIAO, X. R., SU, L. & CHEN, S. Z. 2016. Honokiol inhibits EMT-mediated motility and migration of human non-small cell lung cancer cells in vitro by targeting c-FLIP. *Acta Pharmacol Sin,* 37**,** 1574-1586.
MACLEAN, D. B., MATSUI, H., SURI, A., NEUWIRTH, R. & COLOMBEL, M. 2014. Sustained exposure to the investigational Kisspeptin analog, TAK-448, down-regulates testosterone into the castration range in healthy males and in patients with prostate cancer: results from two phase 1 studies. *J Clin Endocrinol Metab,* 99**,** E1445-53.
MADONNA, G., ULLMAN, C. D., GENTILCORE, G., PALMIERI, G. & ASCIERTO, P. A. 2012. NF-kappaB as potential target in the treatment of melanoma. *J Transl Med,* 10**,** 53.
MANNAL, P. W., SCHNEIDER, J., TANGADA, A., MCDONALD, D. & MCFADDEN, D. W. 2011. Honokiol produces anti-neoplastic effects on melanoma cells in vitro. *J Surg Oncol,* 104**,** 260-4.
MARTIN, T. A., WATKINS, G. & JIANG, W. G. 2005. KiSS-1 expression in human breast cancer. *Clin Exp Metastasis,* 22**,** 503-11.

MARTINEZ-FUENTES, A. J., MOLINA, M., VAZQUEZ-MARTINEZ, R., GAHETE, M. D., JIMENEZ-REINA, L., MORENO-FERNANDEZ, J., BENITO-LOPEZ, P., QUINTERO, A., DE LA RIVA, A., DIEGUEZ, C., SOTO, A., LEAL-CERRO, A., RESMINI, E., WEBB, S. M., ZATELLI, M. C., DEGLI UBERTI, E. C., MALAGON, M. M., LUQUE, R. M. & CASTANO, J. P. 2011. Expression of functional KISS1 and KISS1R system is altered in human pituitary adenomas: evidence for apoptotic action of kisspeptin-10. *Eur J Endocrinol,* 164**,** 355-62.

MASUI, T., DOI, R., MORI, T., TOYODA, E., KOIZUMI, M., KAMI, K., ITO, D., PEIPER, S. C., BROACH, J. R., OISHI, S., NIIDA, A., FUJII, N. & IMAMURA, M. 2004. Metastin and its variant forms suppress migration of pancreatic cancer cells. *Biochem Biophys Res Commun,* 315**,** 85-92.

MATSUI, H., MASAKI, T., AKINAGA, Y., KIBA, A., TAKATSU, Y., NAKATA, D., TANAKA, A., BAN, J., MATSUMOTO, S., KUMANO, S., SUZUKI, A., IKEDA, Y., YAMAGUCHI, M., WATANABE, T., OHTAKI, T. & KUSAKA, M. 2014. Pharmacologic profiles of investigational kisspeptin/metastin analogues, TAK-448 and TAK-683, in adult male rats in comparison to the GnRH analogue leuprolide. *Eur J Pharmacol,* 735**,** 77-85.

MELENDEZ-ZAJGLA, J., DEL POZO, L., CEBALLOS, G. & MALDONADO, V. 2008. Tissue inhibitor of metalloproteinases-4. The road less traveled. *Mol Cancer,* 7**,** 85.

MIELE, M. E., JEWETT, M. D., GOLDBERG, S. F., HYATT, D. L., MORELLI, C., GUALANDI, F., RIMESSI, P., HICKS, D. J., WEISSMAN, B. E., BARBANTI-BRODANO, G. & WELCH, D. R. 2000. A human melanoma metastasis-suppressor locus maps to 6q16.3-q23. *Int J Cancer,* 86**,** 524-8.

MORO, N., MAUCH, C. & ZIGRINO, P. 2014. Metalloproteinases in melanoma. *Eur J Cell Biol,* 93**,** 23-9.

MUIR, A. I., CHAMBERLAIN, L., ELSHOURBAGY, N. A., MICHALOVICH, D., MOORE, D. J., CALAMARI, A., SZEKERES, P. G., SARAU, H. M., CHAMBERS, J. K., MURDOCK, P., STEPLEWSKI, K., SHABON, U., MILLER, J. E., MIDDLETON, S. E., DARKER, J. G., LARMINIE, C. G., WILSON, S., BERGSMA, D. J., EMSON, P., FAULL, R., PHILPOTT, K. L. & HARRISON, D. C. 2001. AXOR12, a novel human G protein-coupled receptor, activated by the peptide KiSS-1. *J Biol Chem,* 276**,** 28969-75.

MURPHY, G. 2011. Tissue inhibitors of metalloproteinases. *Genome Biol,* 12**,** 233.

NATIONAL INSTITUTES OF HEALTH. 2020. Chromosome 1. Retrieved from: https://ghr.nlm.nih.gov/chromosome/1

NAGALINGAM, A., ARBISER, J. L., BONNER, M. Y., SAXENA, N. K. & SHARMA, D. 2012. Honokiol activates AMP-activated protein kinase in breast cancer cells via an LKB1-dependent pathway and inhibits breast carcinogenesis. *Breast Cancer Res,* 14**,** R35.

NASH, K. T., PHADKE, P. A., NAVENOT, J. M., HURST, D. R., ACCAVITTI-LOPER, M. A., SZTUL, E., VAIDYA, K. S., FROST, A. R., KAPPES, J. C., PEIPER, S. C. & WELCH, D. R. 2007. Requirement of KISS1 secretion for multiple organ metastasis suppression and maintenance of tumor dormancy. *J Natl Cancer Inst,* 99**,** 309-21.

NASH, K. T. & WELCH, D. R. 2006. The KISS1 metastasis suppressor: mechanistic insights and clinical utility. *Front Biosci,* 11**,** 647-59.

NAVARRO, V. M., FERNANDEZ-FERNANDEZ, R., CASTELLANO, J. M., ROA, J., MAYEN, A., BARREIRO, M. L., GAYTAN, F., AGUILAR, E., PINILLA, L., DIEGUEZ, C. & TENA-SEMPERE, M. 2004. Advanced vaginal opening and precocious activation of the reproductive axis by KiSS-1 peptide, the endogenous ligand of GPR54. *J Physiol,* 561**,** 379-86.

NAVENOT, J. M., WANG, Z., CHOPIN, M., FUJII, N. & PEIPER, S. C. 2005. Kisspeptin-10-induced signaling of GPR54 negatively regulates chemotactic responses mediated by CXCR4: a potential mechanism for the metastasis suppressor activity of kisspeptins. *Cancer Res,* 65**,** 10450-6.

OHTAKI, T., SHINTANI, Y., HONDA, S., MATSUMOTO, H., HORI, A., KANEHASHI, K., TERAO, Y., KUMANO, S., TAKATSU, Y., MASUDA, Y., ISHIBASHI, Y., WATANABE, T., ASADA, M., YAMADA, T., SUENAGA, M., KITADA, C., USUKI, S., KUROKAWA, T., ONDA, H.,

NISHIMURA, O. & FUJINO, M. 2001. Metastasis suppressor gene KiSS-1 encodes peptide ligand of a G-protein-coupled receptor. *Nature,* 411**,** 613-7.
OKUGAWA, Y., INOUE, Y., TANAKA, K., TOIYAMA, Y., SHIMURA, T., OKIGAMI, M., KAWAMOTO, A., HIRO, J., SAIGUSA, S., MOHRI, Y., UCHIDA, K. & KUSUNOKI, M. 2013. Loss of the metastasis suppressor gene KiSS1 is associated with lymph node metastasis and poor prognosis in human colorectal cancer. *Oncol Rep,* 30**,** 1449-54.
ONG, C. P., LEE, W. L., TANG, Y. Q. & YAP, W. H. 2019. Honokiol: A Review of Its Anticancer Potential and Mechanisms. *Cancers (Basel),* 12.
PACHMAYR, E., TREESE, C. & STEIN, U. 2017. Underlying Mechanisms for Distant Metastasis - Molecular Biology. *Visc Med,* 33**,** 11-20.
PAI, J. T., HSU, C. Y., HSIEH, Y. S., TSAI, T. Y., HUA, K. T. & WENG, M. S. 2020. Suppressing migration and invasion of H1299 lung cancer cells by honokiol through disrupting expression of an HDAC6-mediated matrix metalloproteinase 9. *Food Sci Nutr,* 8**,** 1534-1545.
PAMPILLO, M., CAMUSO, N., TAYLOR, J. E., SZERESZEWSKI, J. M., AHOW, M. R., ZAJAC, M., MILLAR, R. P., BHATTACHARYA, M. & BABWAH, A. V. 2009. Regulation of GPR54 signaling by GRK2 and {beta}-arrestin. *Mol Endocrinol,* 23**,** 2060-74.
PAN, J., ZHANG, Q., LIU, Q., KOMAS, S. M., KALYANARAMAN, B., LUBET, R. A., WANG, Y. & YOU, M. 2014. Honokiol inhibits lung tumorigenesis through inhibition of mitochondrial function. *Cancer Prev Res (Phila),* 7**,** 1149-59.
PARK, J., LEE, J., JUNG, E., PARK, Y., KIM, K., PARK, B., JUNG, K., PARK, E., KIM, J. & PARK, D. 2004. In vitro antibacterial and anti-inflammatory effects of honokiol and magnolol against Propionibacterium sp. *Eur J Pharmacol,* 496**,** 189-95.
PATTERSON, M., MURPHY, K. G., THOMPSON, E. L., PATEL, S., GHATEI, M. A. & BLOOM, S. R. 2006. Administration of kisspeptin-54 into discrete regions of the hypothalamus potently increases plasma luteinising hormone and testosterone in male adult rats. *J Neuroendocrinol,* 18**,** 349-54.
PAYNE, S. H. 2015. The utility of protein and mRNA correlation. *Trends Biochem Sci,* 40**,** 1-3.
PENG, J., TANG, M., ZHANG, B. P., ZHANG, P., ZHONG, T., ZONG, T., YANG, B. & KUANG, H. B. 2013. Kisspeptin stimulates progesterone secretion via the Erk1/2 mitogen-activated protein kinase signaling pathway in rat luteal cells. *Fertil Steril,* 99**,** 1436-1443 e1.
PERL, K., USHAKOV, K., POZNIAK, Y., YIZHAR-BARNEA, O., BHONKER, Y., SHIVATZKI, S., GEIGER, T., AVRAHAM, K. B. & SHAMIR, R. 2017. Reduced changes in protein compared to mRNA levels across non-proliferating tissues. *BMC Genomics,* 18**,** 305.
PIETRASZEK-GREMPLEWICZ, K., SIMICZYJEW, A., DRATKIEWICZ, E., PODGORSKA, M., STYCZEN, I., MATKOWSKI, R., ZIETEK, M. & NOWAK, D. 2019. Expression level of EGFR and MET receptors regulates invasiveness of melanoma cells. *J Cell Mol Med,* 23**,** 8453-8463.
PRAGUE, J. K. & DHILLO, W. S. 2015. Potential Clinical Use of Kisspeptin. *Neuroendocrinology,* 102**,** 238-45.
PRENTICE, L. M., KLAUSEN, C., KALLOGER, S., KOBEL, M., MCKINNEY, S., SANTOS, J. L., KENNEY, C., MEHL, E., GILKS, C. B., LEUNG, P., SWENERTON, K., HUNTSMAN, D. G. & APARICIO, S. A. 2007. Kisspeptin and GPR54 immunoreactivity in a cohort of 518 patients defines favourable prognosis and clear cell subtype in ovarian carcinoma. *BMC Med,* 5**,** 33.
RADISKY, E. S., RAEESZADEH-SARMAZDEH, M. & RADISKY, D. C. 2017. Therapeutic Potential of Matrix Metalloproteinase Inhibition in Breast Cancer. *J Cell Biochem,* 118**,** 3531-3548.
RAMAESH, T., LOGIE, J. J., ROSEWEIR, A. K., MILLAR, R. P., WALKER, B. R., HADOKE, P. W. & REYNOLDS, R. M. 2010. Kisspeptin-10 inhibits angiogenesis in human placental vessels ex vivo and endothelial cells in vitro. *Endocrinology,* 151**,** 5927-34.
RANJAN, R., GUPTA, P. & SHUKLA, A. K. 2016. GPCR Signaling: beta-arrestins Kiss and Remember. *Curr Biol,* 26**,** R285-8.
RIEGER, A. M., NELSON, K. L., KONOWALCHUK, J. D. & BARREDA, D. R. 2011. Modified annexin V/propidium iodide apoptosis assay for accurate assessment of cell death. *J Vis Exp*.

RIO, D. C., ARES, M., JR., HANNON, G. J. & NILSEN, T. W. 2010. Purification of RNA using TRIzol (TRI reagent). *Cold Spring Harb Protoc,* 2010**,** pdb prot5439.

RIQUELME, E., SURAOKAR, M., BEHRENS, C., LIN, H. Y., GIRARD, L., NILSSON, M. B., SIMON, G., WANG, J., COOMBES, K. R., LEE, J. J., HONG, W. K., HEYMACH, J., MINNA, J. D. & WISTUBA, II 2014. VEGF/VEGFR-2 upregulates EZH2 expression in lung adenocarcinoma cells and EZH2 depletion enhances the response to platinum-based and VEGFR-2-targeted therapy. *Clin Cancer Res,* 20**,** 3849-61.

ROBERT, C., SCHACHTER, J., LONG, G. V., ARANCE, A., GROB, J. J., MORTIER, L., DAUD, A., CARLINO, M. S., MCNEIL, C., LOTEM, M., LARKIN, J., LORIGAN, P., NEYNS, B., BLANK, C. U., HAMID, O., MATEUS, C., SHAPIRA-FROMMER, R., KOSH, M., ZHOU, H., IBRAHIM, N., EBBINGHAUS, S., RIBAS, A. & INVESTIGATORS, K.-. 2015. Pembrolizumab versus Ipilimumab in Advanced Melanoma. *N Engl J Med,* 372**,** 2521-32.

ROSS, D. T., SCHERF, U., EISEN, M. B., PEROU, C. M., REES, C., SPELLMAN, P., IYER, V., JEFFREY, S. S., VAN DE RIJN, M., WALTHAM, M., PERGAMENSCHIKOV, A., LEE, J. C., LASHKARI, D., SHALON, D., MYERS, T. G., WEINSTEIN, J. N., BOTSTEIN, D. & BROWN, P. O. 2000. Systematic variation in gene expression patterns in human cancer cell lines. *Nat Genet,* 24**,** 227-35.

RUDGE, J. S., HOLASH, J., HYLTON, D., RUSSELL, M., JIANG, S., LEIDICH, R., PAPADOPOULOS, N., PYLES, E. A., TORRI, A., WIEGAND, S. J., THURSTON, G., STAHL, N. & YANCOPOULOS, G. D. 2007. VEGF Trap complex formation measures production rates of VEGF, providing a biomarker for predicting efficacious angiogenic blockade. *Proc Natl Acad Sci U S A,* 104**,** 18363-70.

SATO, K., SHIRAI, R., HONTANI, M., SHINOOKA, R., HASEGAWA, A., KICHISE, T., YAMASHITA, T., YOSHIZAWA, H., WATANABE, R., MATSUYAMA, T. A., ISHIBASHI-UEDA, H., KOBA, S., KOBAYASHI, Y., HIRANO, T. & WATANABE, T. 2017. Potent Vasoconstrictor Kisspeptin-10 Induces Atherosclerotic Plaque Progression and Instability: Reversal by its Receptor GPR54 Antagonist. *J Am Heart Assoc,* 6.

SCHROEDER, A., MUELLER, O., STOCKER, S., SALOWSKY, R., LEIBER, M., GASSMANN, M., LIGHTFOOT, S., MENZEL, W., GRANZOW, M. & RAGG, T. 2006. The RIN: an RNA integrity number for assigning integrity values to RNA measurements. *BMC Mol Biol,* 7**,** 3.

SCHWALFENBERG, G. K. 2012. The alkaline diet: is there evidence that an alkaline pH diet benefits health? *J Environ Public Health,* 2012**,** 727630.

SENGUPTA, S., NAGALINGAM, A., MUNIRAJ, N., BONNER, M. Y., MISTRIOTIS, P., AFTHINOS, A., KUPPUSAMY, P., LANOUE, D., CHO, S., KORANGATH, P., SHRIVER, M., BEGUM, A., MERINO, V. F., HUANG, C. Y., ARBISER, J. L., MATSUI, W., GYORFFY, B., KONSTANTOPOULOS, K., SUKUMAR, S., MARIGNANI, P. A., SAXENA, N. K. & SHARMA, D. 2017. Activation of tumor suppressor LKB1 by honokiol abrogates cancer stem-like phenotype in breast cancer via inhibition of oncogenic Stat3. *Oncogene,* 36**,** 5709-5721.

SEYFRIED, T. N. & HUYSENTRUYT, L. C. 2013. On the origin of cancer metastasis. *Crit Rev Oncog,* 18**,** 43-73.

SHAMAS-DIN, A., KALE, J., LEBER, B. & ANDREWS, D. W. 2013. Mechanisms of action of Bcl-2 family proteins. *Cold Spring Harb Perspect Biol,* 5**,** a008714.

SHELLMAN, Y. G., MAKELA, M. & NORRIS, D. A. 2006. Induction of secreted matrix metalloproteinase-9 activity in human melanoma cells by extracellular matrix proteins and cytokines. *Melanoma Res,* 16**,** 207-11.

SHEN, L., ZHANG, F., HUANG, R., YAN, J. & SHEN, B. 2017. Honokiol inhibits bladder cancer cell invasion through repressing SRC-3 expression and epithelial-mesenchymal transition. *Oncol Lett,* 14**,** 4294-4300.

SHOJI, S., TANG, X. Y., UMEMURA, S., ITOH, J., TAKEKOSHI, S., SHIMA, M., USUI, Y., NAGATA, Y., UCHIDA, T., OSAMURA, R. Y. & TERACHI, T. 2009. Metastin inhibits migration and

invasion of renal cell carcinoma with overexpression of metastin receptor. *Eur Urol,* 55**,** 441-9.

SI, L., KONG, Y., XU, X., FLAHERTY, K. T., SHENG, X., CUI, C., CHI, Z., LI, S., MAO, L. & GUO, J. 2012. Prevalence of BRAF V600E mutation in Chinese melanoma patients: large scale analysis of BRAF and NRAS mutations in a 432-case cohort. *Eur J Cancer,* 48**,** 94-100.

SINGH, T. & KATIYAR, S. K. 2013. Honokiol inhibits non-small cell lung cancer cell migration by targeting PGE(2)-mediated activation of beta-catenin signaling. *PLoS One,* 8**,** e60749.

SINGH, T., PRASAD, R. & KATIYAR, S. K. 2013. Inhibition of class I histone deacetylases in non-small cell lung cancer by honokiol leads to suppression of cancer cell growth and induction of cell death in vitro and in vivo. *Epigenetics,* 8**,** 54-65.

SONG, H., KI, S. H., KIM, S. G. & MOON, A. 2006. Activating transcription factor 2 mediates matrix metalloproteinase-2 transcriptional activation induced by p38 in breast epithelial cells. *Cancer Res,* 66**,** 10487-96.

SOSMAN, J. A., KIM, K. B., SCHUCHTER, L., GONZALEZ, R., PAVLICK, A. C., WEBER, J. S., MCARTHUR, G. A., HUTSON, T. E., MOSCHOS, S. J., FLAHERTY, K. T., HERSEY, P., KEFFORD, R., LAWRENCE, D., PUZANOV, I., LEWIS, K. D., AMARAVADI, R. K., CHMIELOWSKI, B., LAWRENCE, H. J., SHYR, Y., YE, F., LI, J., NOLOP, K. B., LEE, R. J., JOE, A. K. & RIBAS, A. 2012. Survival in BRAF V600-mutant advanced melanoma treated with vemurafenib. *N Engl J Med,* 366**,** 707-14.

SOUNDARARAJAN, R. & RAO, A. J. 2004. Trophoblast 'pseudo-tumorigenesis': significance and contributory factors. *Reprod Biol Endocrinol,* 2**,** 15.

SPANDIDOS, A., WANG, X., WANG, H., DRAGNEV, S., THURBER, T. & SEED, B. 2008. A comprehensive collection of experimentally validated primers for Polymerase Chain Reaction quantitation of murine transcript abundance. *BMC Genomics,* 9**,** 633.

SPANDIDOS, A., WANG, X., WANG, H. & SEED, B. 2010. PrimerBank: a resource of human and mouse PCR primer pairs for gene expression detection and quantification. *Nucleic Acids Res,* 38**,** D792-9.

STAFFORD, L. J., XIA, C., MA, W., CAI, Y. & LIU, M. 2002. Identification and characterization of mouse metastasis-suppressor KiSS1 and its G-protein-coupled receptor. *Cancer Res,* 62**,** 5399-404.

STAMOS, J. L. & WEIS, W. I. 2013. The beta-catenin destruction complex. *Cold Spring Harb Perspect Biol,* 5**,** a007898.

STATHATOS, N., BOURDEAU, I., ESPINOSA, A. V., SAJI, M., VASKO, V. V., BURMAN, K. D., STRATAKIS, C. A. & RINGEL, M. D. 2005. KiSS-1/G protein-coupled receptor 54 metastasis suppressor pathway increases myocyte-enriched calcineurin interacting protein 1 expression and chronically inhibits calcineurin activity. *J Clin Endocrinol Metab,* 90**,** 5432-40.

STAUN-RAM, E., GOLDMAN, S., GABARIN, D. & SHALEV, E. 2004. Expression and importance of matrix metalloproteinase 2 and 9 (MMP-2 and -9) in human trophoblast invasion. *Reprod Biol Endocrinol,* 2**,** 59.

STAUN-RAM, E., GOLDMAN, S. & SHALEV, E. 2009. Ets-2 and p53 mediate cAMP-induced MMP-2 expression, activity and trophoblast invasion. *Reprod Biol Endocrinol,* 7**,** 135.

STRICKER, J., FALZONE, T. & GARDEL, M. L. 2010. Mechanics of the F-actin cytoskeleton. *J Biomech,* 43**,** 9-14.

SU, W. J., HUANG, X., QIN, E., JIANG, L. & REN, P. 2008. [Pharmacokinetics of honokiol in rat after oral administration of Cortex of Magnolia officinalis and its compound preparation Houpu Sanwu Decoction]. *Zhong Yao Cai,* 31**,** 255-8.

SUN, J. 2010. Matrix metalloproteinases and tissue inhibitor of metalloproteinases are essential for the inflammatory response in cancer cells. *J Signal Transduct,* 2010**,** 985132.

SUN, Y. B. & XU, S. 2013. Expression of KISS1 and KISS1R (GPR54) may be used as favorable prognostic markers for patients with non-small cell lung cancer. *Int J Oncol,* 43**,** 521-30.

SWEENY, L., PRINCE, A., PATEL, N., MOORE, L. S., ROSENTHAL, E. L., HUGHLEY, B. B. & WARRAM, J. M. 2016. Antiangiogenic antibody improves melanoma detection by fluorescently labeled therapeutic antibodies. *Laryngoscope,* 126**,** E387-E395.

SZERESZEWSKI, J. M., PAMPILLO, M., AHOW, M. R., OFFERMANNS, S., BHATTACHARYA, M. & BABWAH, A. V. 2010. GPR54 regulates ERK1/2 activity and hypothalamic gene expression in a Galpha(q/11) and beta-arrestin-dependent manner. *PLoS One,* 5**,** e12964.

TAKEDA, T., KIKUCHI, E., MIKAMI, S., SUZUKI, E., MATSUMOTO, K., MIYAJIMA, A., OKADA, Y. & OYA, M. 2012. Prognostic role of KiSS-1 and possibility of therapeutic modality of metastin, the final peptide of the KiSS-1 gene, in urothelial carcinoma. *Mol Cancer Ther,* 11**,** 853-63.

TALKENBERGER, K., CAVALCANTI-ADAM, E. A., VOSS-BOHME, A. & DEUTSCH, A. 2017. Amoeboid-mesenchymal migration plasticity promotes invasion only in complex heterogeneous microenvironments. *Sci Rep,* 7**,** 9237.

TAYLOR, S., WAKEM, M., DIJKMAN, G., ALSARRAJ, M. & NGUYEN, M. 2010. A practical approach to RT-qPCR-Publishing data that conform to the MIQE guidelines. *Methods,* 50**,** S1-5.

TOWBIN, H., STAEHELIN, T. & GORDON, J. 1992. Electrophoretic transfer of proteins from polyacrylamide gels to nitrocellulose sheets: procedure and some applications. 1979. *Biotechnology,* 24**,** 145-9.

TREPEL, J., MOLLAPOUR, M., GIACCONE, G. & NECKERS, L. 2010. Targeting the dynamic HSP90 complex in cancer. *Nat Rev Cancer,* 10**,** 537-49.

USACH, I., ALAIMO, A., FERNANDEZ, J., AMBROSINI, A., MOCINI, S., OCHIUZ, L. & PERIS, J. E. 2021. Magnolol and Honokiol: Two Natural Compounds with Similar Chemical Structure but Different Physicochemical and Stability Properties. *Pharmaceutics,* 13.

USUI, S., ISO, Y., SASAI, M., MIZUKAMI, T., MORI, H., WATANABE, T., SHIODA, S. & SUZUKI, H. 2014. Kisspeptin-10 induces endothelial cellular senescence and impaired endothelial cell growth. *Clin Sci (Lond),* 127**,** 47-55.

VALASTYAN, S. & WEINBERG, R. A. 2011. Tumor metastasis: molecular insights and evolving paradigms. *Cell,* 147**,** 275-92.

VAVILALA, D. T., O'BRYHIM, B. E., PONNALURI, V. K., WHITE, R. S., RADEL, J., SYMONS, R. C. & MUKHERJI, M. 2013. Honokiol inhibits pathological retinal neovascularization in oxygen-induced retinopathy mouse model. *Biochem Biophys Res Commun,* 438**,** 697-702.

VAVILALA, D. T., PONNALURI, V. K., KANJILAL, D. & MUKHERJI, M. 2014. Evaluation of anti-HIF and anti-angiogenic properties of honokiol for the treatment of ocular neovascular diseases. *PLoS One,* 9**,** e113717.

VILLANUEVA, J. & HERLYN, M. 2008. Melanoma and the tumor microenvironment. *Curr Oncol Rep,* 10**,** 439-46.

WALKER, C., MOJARES, E. & DEL RIO HERNANDEZ, A. 2018. Role of Extracellular Matrix in Development and Cancer Progression. *Int J Mol Sci,* 19.

WAN, L., NEUMANN, C. A. & LEDUC, P. R. 2020. Tumor-on-a-chip for integrating a 3D tumor microenvironment: chemical and mechanical factors. *Lab Chip,* 20**,** 873-888.

WANG, L., LIU, L., YING, L., & WANG, L. 2020. Honokiol inhibits inflammation and endoplasmic reticulum stress in a rat model of pregnancy-induced hypertension. Biotechnology & Biotechnological Equipment, 34(1), 11-17.

WANG, C. C., LIN, S. Y., LAI, Y. H., LIU, Y. J., HSU, Y. L. & CHEN, J. J. 2012a. Dimethyl sulfoxide promotes the multiple functions of the tumor suppressor HLJ1 through activator protein-1 activation in NSCLC cells. *PLoS One,* 7**,** e33772.

WANG, C. H., QIAO, C., WANG, R. C. & ZHOU, W. P. 2016. KiSS1mediated suppression of the invasive ability of human pancreatic carcinoma cells is not dependent on the level of KiSS1 receptor GPR54. *Mol Med Rep,* 13**,** 123-9.

WANG, H., JONES, J., TURNER, T., HE, Q. P., HARDY, S., GRIZZLE, W. E., WELCH, D. R. & YATES, C. 2012b. Clinical and biological significance of KISS1 expression in prostate cancer. *Am J Pathol,* 180**,** 1170-8.

WANG, T. J., LIU, H. T., LAI, Y. H., JAN, T. R., NOMURA, N., CHANG, H. W., CHOU, C. C., LEE, Y. J. & TSAI, P. J. 2018. Honokiol, a Polyphenol Natural Compound, Attenuates Cisplatin-Induced Acute Cytotoxicity in Renal Epithelial Cells Through Cellular Oxidative Stress and Cytoskeleton Modulations. *Front Pharmacol,* 9**,** 357.

WANG, X., DUAN, X., YANG, G., ZHANG, X., DENG, L., ZHENG, H., DENG, C., WEN, J., WANG, N., PENG, C., ZHAO, X., WEI, Y. & CHEN, L. 2011. Honokiol crosses BBB and BCSFB, and inhibits brain tumor growth in rat 9L intracerebral gliosarcoma model and human U251 xenograft glioma model. *PLoS One,* 6**,** e18490.

WANG, X. & SEED, B. 2003. A PCR primer bank for quantitative gene expression analysis. *Nucleic Acids Res,* 31**,** e154.

WANG, Z., ZHAI, Z. & DU, X. 2017. Celastrol inhibits migration and invasion through blocking the NF-kappaB pathway in ovarian cancer cells. *Exp Ther Med,* 14**,** 819-824.

WANG, Z. & ZHANG, X. 2017. Chemopreventive Activity of Honokiol against 7, 12 - Dimethylbenz[a]anthracene-Induced Mammary Cancer in Female Sprague Dawley Rats. *Front Pharmacol,* 8**,** 320.

WIRTH, T. & YLA-HERTTUALA, S. 2014. Gene Therapy Used in Cancer Treatment. *Biomedicines,* 2**,** 149-162.

WU, H. M., HUANG, H. Y., SOONG, Y. K., LEUNG, P. C. K. & WANG, H. S. 2019. Kisspeptin regulation of human decidual stromal cells motility via FAK-Src intracellular tyrosine kinases. *Hum Reprod,* 34**,** 1291-1301.

YADAV, L., PURI, N., RASTOGI, V., SATPUTE, P. & SHARMA, V. 2015. Tumour Angiogenesis and Angiogenic Inhibitors: A Review. *J Clin Diagn Res,* 9**,** XE01-XE05.

YAN, B. & PENG, Z. Y. 2015. Honokiol induces cell cycle arrest and apoptosis in human gastric carcinoma MGC-803 cell line. *Int J Clin Exp Med,* 8**,** 5454-61.

YAN, C., WANG, H. & BOYD, D. D. 2001. KiSS-1 represses 92-kDa type IV collagenase expression by down-regulating NF-kappa B binding to the promoter as a consequence of Ikappa Balpha -induced block of p65/p50 nuclear translocation. *J Biol Chem,* 276**,** 1164-72.

YAN, J., ERDEM, H., LI, R., CAI, Y., AYALA, G., ITTMANN, M., YU-LEE, L. Y., TSAI, S. Y. & TSAI, M. J. 2008. Steroid receptor coactivator-3/AIB1 promotes cell migration and invasiveness through focal adhesion turnover and matrix metalloproteinase expression. *Cancer Res,* 68**,** 5460-8.

YANG, S. E., HSIEH, M. T., TSAI, T. H. & HSU, S. L. 2002. Down-modulation of Bcl-XL, release of cytochrome c and sequential activation of caspases during honokiol-induced apoptosis in human squamous lung cancer CH27 cells. *Biochem Pharmacol,* 63**,** 1641-51.

YAO, C. J., LAI, G. M., YEH, C. T., LAI, M. T., SHIH, P. H., CHAO, W. J., WHANG-PENG, J., CHUANG, S. E. & LAI, T. Y. 2013. Honokiol Eliminates Human Oral Cancer Stem-Like Cells Accompanied with Suppression of Wnt/ beta -Catenin Signaling and Apoptosis Induction. *Evid Based Complement Alternat Med,* 2013**,** 146136.

YEH, P. S., WANG, W., CHANG, Y. A., LIN, C. J., WANG, J. J. & CHEN, R. M. 2016. Honokiol induces autophagy of neuroblastoma cells through activating the PI3K/Akt/mTOR and endoplasmic reticular stress/ERK1/2 signaling pathways and suppressing cell migration. *Cancer Lett,* 370**,** 66-77.

YOSHIOKA, K., OHNO, Y., HORIGUCHI, Y., OZU, C., NAMIKI, K. & TACHIBANA, M. 2008. Effects of a KiSS-1 peptide, a metastasis suppressor gene, on the invasive ability of renal cell carcinoma cells through a modulation of a matrix metalloproteinase 2 expression. *Life Sci,* 83**,** 332-8.

YU, W. K., XU, Z. Y., YUAN, L., MO, S., XU, B., CHENG, X. D. & QIN, J. J. 2020. Targeting beta-Catenin Signaling by Natural Products for Cancer Prevention and Therapy. *Front Pharmacol,* 11**,** 984.

YUAN, C., GAO, J., GUO, J., BAI, L., MARSHALL, C., CAI, Z., WANG, L. & XIAO, M. 2014. Dimethyl sulfoxide damages mitochondrial integrity and membrane potential in cultured astrocytes. *PLoS One,* 9**,** e107447.

ZAHRA, F. T., SAJIB, M. S., ICHIYAMA, Y., AKWII, R. G., TULLAR, P. E., COBOS, C., MINCHEW, S. A., DOCI, C. L., ZHENG, Y., KUBOTA, Y., GUTKIND, J. S. & MIKELIS, C. M. 2019. Endothelial RhoA GTPase is essential for in vitro endothelial functions but dispensable for physiological in vivo angiogenesis. *Sci Rep,* 9**,** 11666.

ZAJAC, M., LAW, J., CVETKOVIC, D. D., PAMPILLO, M., MCCOLL, L., PAPE, C., DI GUGLIELMO, G. M., POSTOVIT, L. M., BABWAH, A. V. & BHATTACHARYA, M. 2011. GPR54 (KISS1R) transactivates EGFR to promote breast cancer cell invasiveness. *PLoS One,* 6**,** e21599.

ZHANG, B., MANIATIS, T., SONG, Y., ZHANG, W., ZHANG, X., LI, N., CHEN, J., WONG, A. W. & ROBERTS, A. 2008. Evaluation of magnolia bark extract in chromosomal aberration assays. *Mutat Res,* 654**,** 133-7.

ZHANG, J., JIA, Z., LI, Q., WANG, L., RASHID, A., ZHU, Z., EVANS, D. B., VAUTHEY, J. N., XIE, K. & YAO, J. C. 2007. Elevated expression of vascular endothelial growth factor correlates with increased angiogenesis and decreased progression-free survival among patients with low-grade neuroendocrine tumors. *Cancer,* 109**,** 1478-86.

ZHANG, Y., TANG, Y. J., LI, Z. H., PAN, F., HUANG, K. & XU, G. H. 2013. KiSS1 inhibits growth and invasion of osteosarcoma cells through inhibition of the MAPK pathway. *Eur J Histochem,* 57**,** e30.

ZHENG, S., CHANG, Y., HODGES, K. B., SUN, Y., MA, X., XUE, Y., WILLIAMSON, S. R., LOPEZ-BELTRAN, A., MONTIRONI, R. & CHENG, L. 2010. Expression of KISS1 and MMP-9 in non-small cell lung cancer and their relations to metastasis and survival. *Anticancer Res,* 30**,** 713-8.

ZHU, J., LIANG, L., JIAO, Y., LIU, L. & ALLIANCE, U. S.-C. P. S.-O. 2015. Enhanced invasion of metastatic cancer cells via extracellular matrix interface. *PLoS One,* 10**,** e0118058.

ZHU, J., XU, S., GAO, W., FENG, J. & ZHAO, G. 2019. Honokiol induces endoplasmic reticulum stress-mediated apoptosis in human lung cancer cells. *Life Sci,* 221**,** 204-211.

ZHU, X., WANG, Z., HU, C., LI, Z. & HU, J. 2014. Honokiol suppresses TNF-alpha-induced migration and matrix metalloproteinase expression by blocking NF-kappaB activation via the ERK signaling pathway in rat aortic smooth muscle cells. *Acta Histochem,* 116**,** 588-95.

ZIEGLER, E., OLBRICH, T., EMONS, G. & GRUNDKER, C. 2013. Antiproliferative effects of kisspeptin10 depend on artificial GPR54 (KISS1R) expression levels. *Oncol Rep,* 29**,** 549-54.

Appendix.

Appendix A.

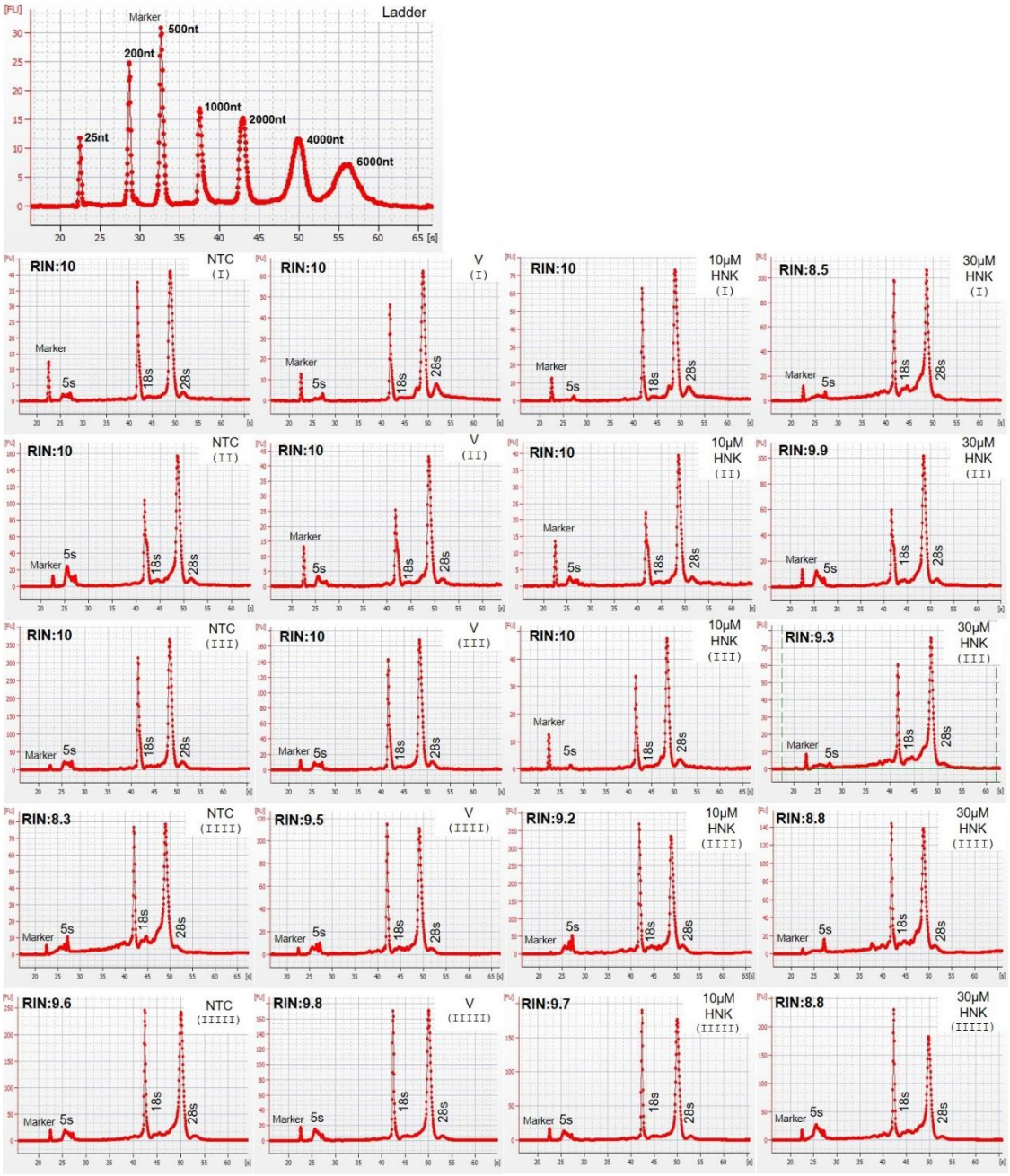

Figure A. Electropherograms of RNA samples from five independent replicates and the corresponding RNA integrity number. RNA integrity number (**RIN**) was calculated by Agilent 2100 Bioanalyzer according to the relative intensities of 18S and 28S ribosomal RNA to the marker.

Appendix B.

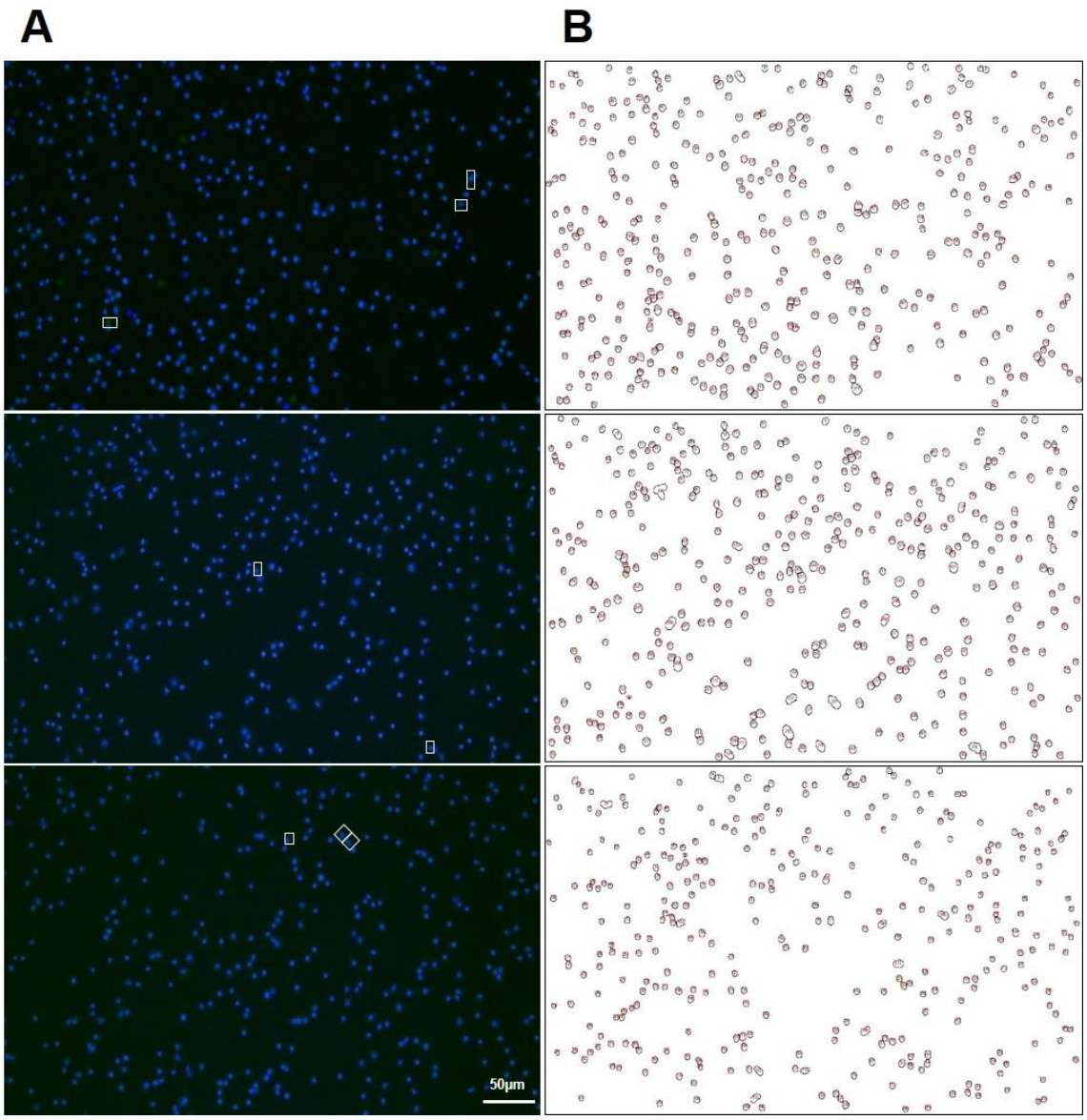

Figure B.1. **Images of three random fields in 500ng pmaxGFP plasmid group**. Cells were transfected by nucleofection with pmaxGFP plasmid (500ng) and incubation for 24 hours. Cells were mounted with DAPI (blue) to stain nuclear. (**A**) Images were merged by Image J and the number of transfected cells was counted (highlight by white square). (**B**) Total number of cells is quantified by Image J software.

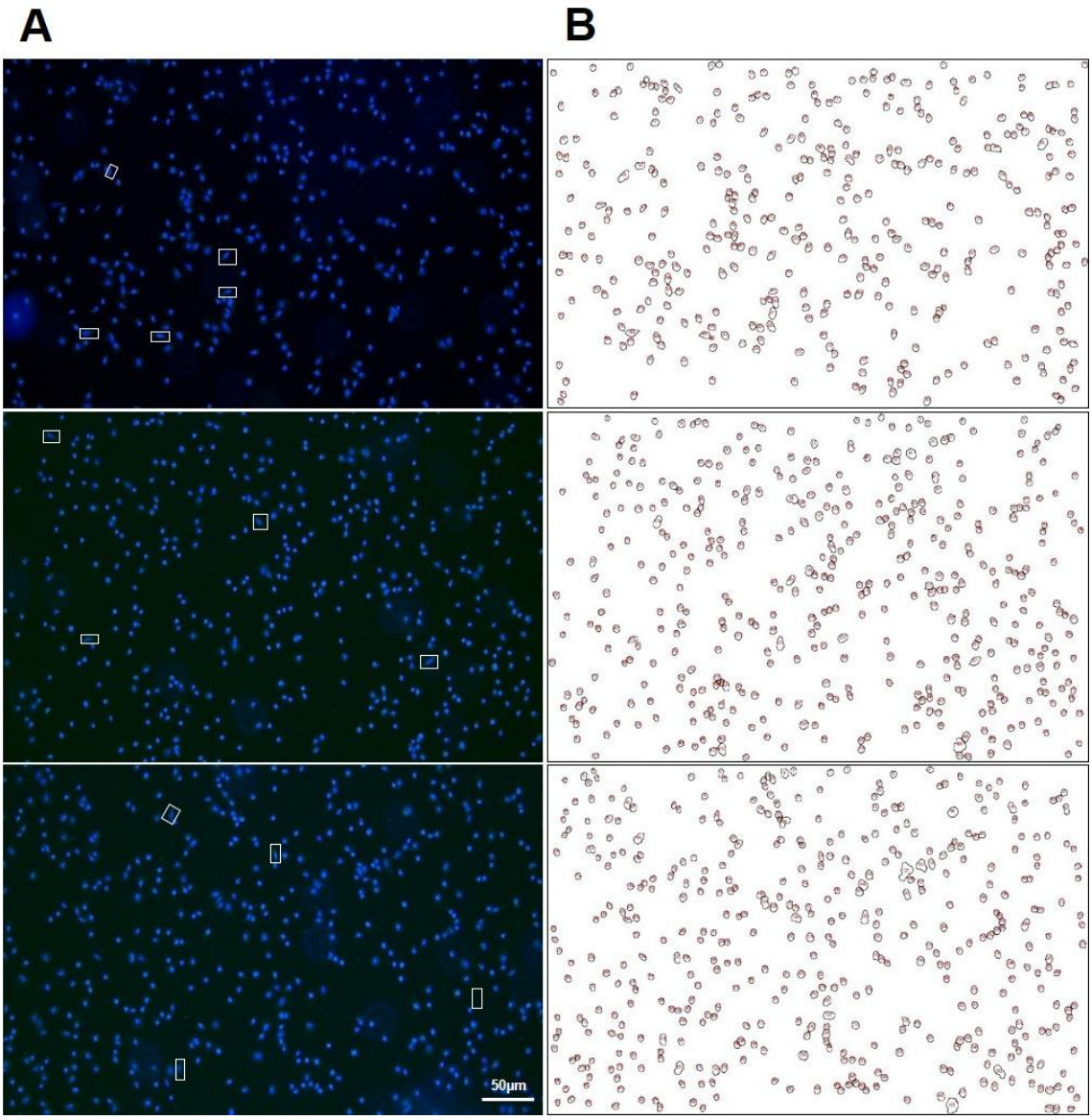

Figure B.2. Images of three random fields in 1µg pmaxGFP plasmid group. Cells were transfected by nucleofection with pmaxGFP plasmid (1µg) and incubation for 24 hours. Cells were mounted with DAPI (blue) to stain nuclear. (**A**) Images were merged by Image J and the number of transfected cells was counted (highlight by white square). (**B**) Total number of cells is quantified by Image J software.

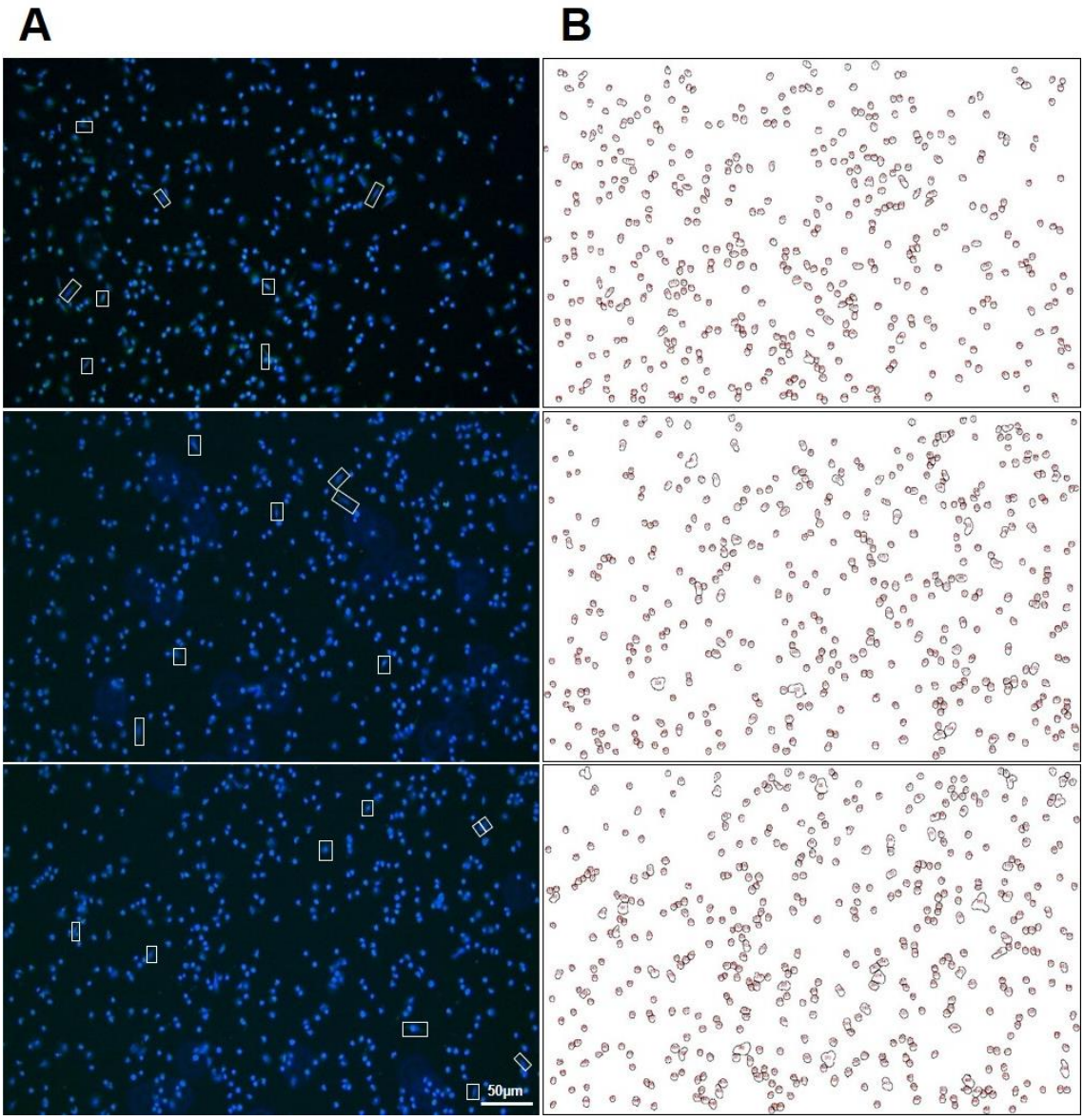

Figure B.3. Images of three random fields in 2µg pmaxGFP plasmid group. Cells were transfected by nucleofection with pmaxGFP plasmid (2µg) and incubation for 24 hours. Cells were mounted with DAPI (blue) to stain nuclear. (**A**) Images were merged by Image J and the number of transfected cells was counted (highlight by white square). (**B**) Total number of cells is quantified by Image J software.

Appendix C.

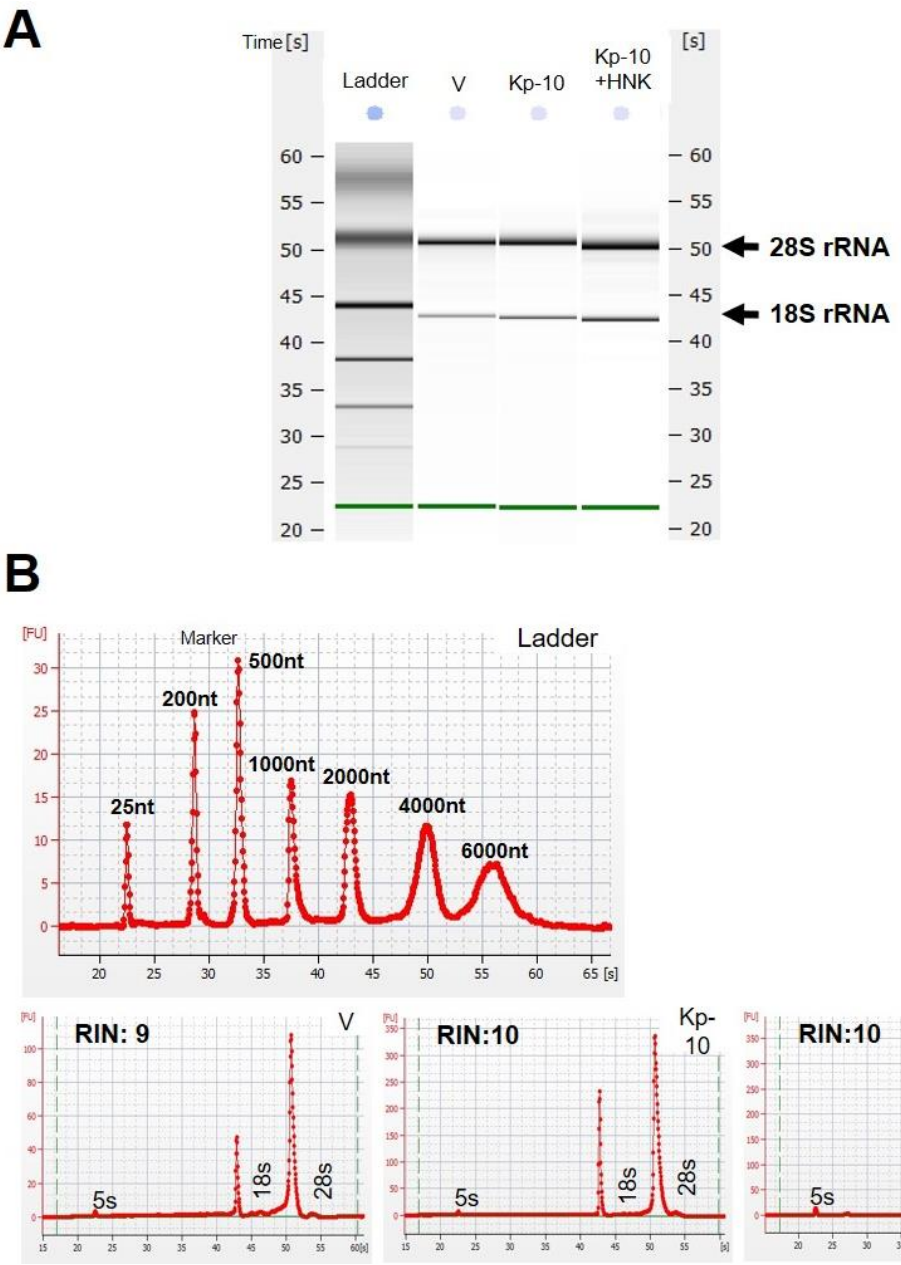

Figure C. RNA integrity. A375 cells were treated with 100nM kisspeptin-10 (**Kp-10**) with or without 30μM honokiol (**HNK**) for 24 hours. The percentage of DMSO as vehicle control (**V**) was 0.1%, since this reflected the maximum percentage of DMSO that cells were exposed to when treating with combination of 30μM honokiol and 100nM kisspeptin-10. (**A**) Total RNA was isolated by TRIzol reagent, RNA integrity was assessed by the digital gel obtained with the Agilent 2100 Bioanalyzer. (**B**) RNA integrity number (**RIN**) was calculated according to the relative intensities of 18S and 28S to the marker. **[s]**: seconds. **rRNA**: ribosomal RNA.

Appendix D.

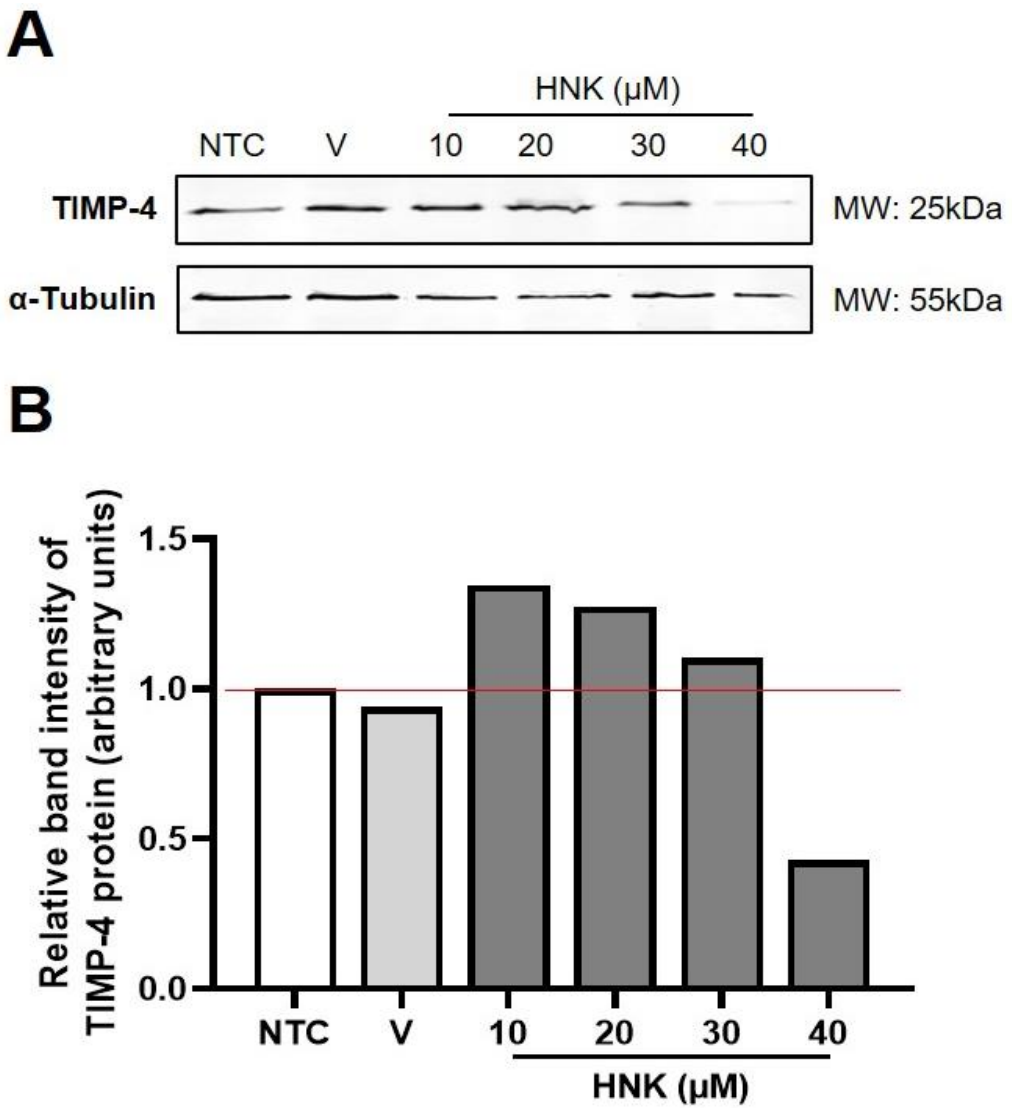

Figure D. Honokiol dose-dependently reduces protein expression of tissue inhibitors of metalloproteinase 4. A375 cells were non-treated (**NTC**) or treated with increasing concentrations of honokiol (**HNK**) (10μM, 20μM, 30μM and 40μM) for 24 hours. The percentage of DMSO as vehicle control (**V**) was 0.05%, since this reflects the maximum percentage of DMSO that cells were exposed to when treating with HNK at a concentration of 40μM. (**A**) Protein lysates separated on 12.5% SDS-page gel were immunoblotted for tissue inhibitors of metalloproteinase 4 (**TIMP-4**) and alpha tubulin (**α-Tubulin**). (**B**) Image J software was to analyse densitometry. TIMP-4 density normalised to alpha tubulin was quantified. Relative band intensity in treatment groups was calculated by multiplying the corresponding ratio of NTC respectively. Data is expressed as the mean (n = 1). **MW**: molecular weight. **kDa**: kilodalton.